EXPERIMENTAL AND 3D FINITE ELEMENT ANALYSES OF INVERT-REMOVED CIRCULAR CORRUGATED METAL PIPE CULVERTS RENEWED WITH POLYMER SPRAY-APPLIED PIPE LINING

by

SAMRAT RAUT

Presented to the Faculty of the Graduate School of

The University of Texas at Arlington in Partial Fulfillment

of the Requirements

for the Degree of

MASTER OF SCIENCE IN CIVIL ENGINEERING

THE UNIVERISTY OF TEXAS AT ARLINGTON

May 2020

ACKNOWLEDGEMENT

I would like to express my sincerest thanks and gratitude to my research advisor Dr. Xinbao Yu for providing me with this invaluable opportunity to work under his guidance. This research would never have been successful without his continuous guidance and support. I am very grateful for the opportunity to work under him and pursue my master's degree with his guidance.

I am also thankful to Dr. Mohammad Najafi for his guidance and support and making me the part of his research team at the Center for Underground Infrastructure Research and Education (CUIRE) at UTA and letting me work on the Spray Applied Pipe Lining (SAPL) project.

I would also like to thank Dr. Sahadat Hossain for his guidance in my Master's degree program and agreeing to be a part of my thesis committee.

Testing results presented in this thesis are joint efforts of several Ph.D. and Master's students working as graduate research assistants at CUIRE and shared in their theses and dissertations. Special thanks go to my colleagues Amin Darabnoush Tehrani, Hiramani Raj Chimauriya, Zahra Kohankar Kouchesfehani, Juhil Jitendra Makwana, and Shobhit Srivastav whose continuous effort and hard work for research had made the project successful. Amin Darabnoush Tehrani, Hiramani Raj Chimauriya, Zahra Kohankar Kouchesfehani were instrumental in testing setup and instrumentation at the CUIRE Laboratory. I would also like to thank my friend Kushal Raj Poudel for providing me the support in the CAD work for the FEM.

The presented research was funded by seven U.S. departments of transportation (DOTs) of Ohio DOT (project leader), DelDOT, FDOT, MnDOT, NCDOT, NYSDOT and PennDOT. The author would like to thank the DOTs for their support and participation in this research. Partner companies and consultants were LEO Consulting, LLC, Rehabilitation Resource Solutions, and American Structurepoint, Inc. In addition, many thanks to Sprayroq, Contech Engineering, Forterra Pipe and Precast, HVJ Associates, MTS Systems Corporation, and Micro-Measurement for providing us with various products and services that were most essential for these tests.

Last, but never the least, I am always grateful to my parents for their continuous inspiration and support. They have encouraged me through some of the toughest times, and I owe all I have achieved to them.

April 28, 2020

ABSTRACT

EXPERIMENTAL AND 3D FINITELEMENT ANALYSES OF INVERT-REMOVED CORRUGATED METAL PIPES REPAIRED WITH A SPRAY-APPLIED LINER

Samrat Raut

The University of Texas at Arlington, 2020

Supervising Professor: Dr. Xinbao Yu

Corrugated metal pipes (CMPs) are one of the widely used culvert structures in the American highway system. Compared to other types of culverts, CMPs have shorter design life, and many CMP culverts have reached or exceeded their design life. Therefore, renewal or replacement of those CMPs is needed to ensure the safety and service of the highways. Since replacements of these culverts are costly, renewalis less costly and has been on the focus in this decade. Different rehabilitation methods have been proposed by different DOTs and the researchers from open-cut methods to trenchless technology. Since open-cut methods disturb the operation of highways, rehabilitation with trenchless technology has been the preferred method. Several trenchless methods such as slip lining, cured-in-place pipe (CIPP), invert paving, and spray-applied pipe lining have been in existence. Although spray-applied lining has been in practice for several years, only limited research has been conducted to assess the structural capacity of these liners along with studies on the structural contribution of the host CMP. For this reason, a detailed study on the structural capacity gained by rehabilitating CMPs using spray-applied pipe liners (polymeric and cementitious) is undergoing at CUIRE, UTA. In this project, deterioration of CMPs is represented by the removal of an 18" wide piece of invert from the intact CMPs. Control tests were first performed on an intact CMP and an invert removed CMP in a soil box to determine the loss in capacity after invert removal. After completion of the control tests, another set of soil box test were carried on invert removed CMPs repaired with the spray-applied pipe liners (polymeric) with three different thicknesses: 0.25-in., 0.5-in., and 1-in. All the test results and the details of the experiment were performed as a team effort done at the Center for Underground Infrastructure Research and Education (CUIRE).

This thesis study presents the finite element analyses of the soil box tests performed at CURIE and the development of calibrated FEM models for future parametric studies. The soil box test procedure and results are first briefly presented, which include the plots of the load-displacement, earth pressure, and strains and were used to validate the FE results.

ABAQUS 6.14 FEA software was used to carry out FE analysis. The analysis was implicit and non-linear. A full 3D model was developed to represent the experimental setup. The boundary conditions were defined

similarly to the experimental setup. The restriction of the movement of the soil outside the soil-box due to end walls in their respective direction was defined by defining the boundary conditions which restrict the movement of the soil outside the soil-box system. Solid model was used to represent Soil, CMP, and liner; and C3D8R element type was used to define mesh elements. To determine the mesh sensitivity of the model, total energy, load-displacement for soil-CMP, and the Von Mises stress for the CMP were compared. The soil was model as Drucker Prager Model which represents the pressure-dependent soil model while CMP was represented by the non-linear elastic-plastic model. The properties of the liner as reported by Parades (2018) suggested it as a brittle material with a small plastic region. Since the model was implicit, cracking behavior could not be represented through FE model. The crack in the FE model was represented by the plastic strain developed in the liner. As the plastic region of the liner was very small, appearance of the first plastic strain in the FE model was compared with the appearance of the first crack in the test.

After the completion of the analysis the results obtained from the FE model were compared with the results from the experiment. The FE model for the intact CMP agreed closely with the test results, as seen in the comparisons of displacements, earth pressure, and bending moment. The FE model of invert cut CMP did not predict the behavior from the test well. There was excessive immediate deformation of soil and CMP during the removal of invert in the test, which could not be predicted by the FE model. While for the rehabilitated CMPs, the FE model predicted the compared parameters well with most parameters predicted within 10% discrepancy with measured values. The location and load of the first crack in the liner (appearance of first plastic strain in the FE model) were predicted by the FE model with significant accuracy. Although the model did not show the drop in the load, the model predicted the first crack load and ultimate load well. Thus, it was concluded that the model could be used to predict the behavior for other liner thicknesses and be used for future parametric studies although the model could be further improved if additional material tests for liners were performed to better define the material model.

Contents

List of Figures

Chapter 1: Introduction

1.1 Background

Culverts are underground structures constructed under roadways and railways as water conduits. Among the different types of culverts, metal culverts have been one of the most used type of culverts since their introduction in the late 19th century. With the ease of installation and relatively low cost for construction, use of metal culverts has been very pervasive especially in American highway network (Campbell, 2018). While metal pipes have lots of advantages over other types of culverts, one major disadvantage of metal pipes is their relatively short life span of 10 to 35 years (Rinker Materials ,1994). While all the culverts are exposed to the constant abrasion and corrosion from running water, metal culverts are particularly vulnerable to these factors.

Figure 1-01 Metal culverts in operation (Hartley, 2014)

American highways have now become old and along with it many of the metal culverts are nearing or have exceeded their service life and need rehabilitation and replacement. These failing culverts, if not reconstructed or replaced, pose a serious risk to public safety and highway operation. But the replacement of all highway culverts would pose a significant burden to the economy. Thus, the DOTs and the federal agency are shifting their attention from replacement to rehabilitation (Campbell, 2018).

Figure 1-2 Deteriorated Metal Culverts (Taher & Moore, 2011)

Deteriorated metal culverts can be rehabilitated by using both open cut methods and trenchless methods. Open cut methods are rarely used to rehabilitate culverts as they involve disrupting the traffic due to need for detouring and delaying (Najafi, 2013). Thus, trenchless methods are the preferred method in comparison to open cut methods.

Trenchless method such as sliplining, cured in place pipe (CIPP), invert lining, and spray applied pipe linings have been increasingly common methods for the culvert rehabilitation. The rehabilitation of the culvert means providing the new design life to the existing culverts (Darabnoush et al. 2019)). Details of the available methods are discussed later in Chapter 2. One of the newer methods of culvert rehabilitation is spray applied pipe lining method which has limited past research especially concerning the polymeric linerrenewal.

Figure 1-3 (left) Slip lining Method (Arizona DoT, 2014) (Right) Invert Paving ((Winconsin DOT, 2018)

Figure 1-4 Lining the culvert (Mandli, 2017)

Thus, to study the performance of the spray-applied pipe liner (SAPL), an extensive study is being carried at CUIRE, UTA. The project "Structural Design Methodology for Spray Applied Pipe Liners in Gravity Storm Water Conveyance Conduits" was possible with the research funding from 7 DOTs with the Ohio Department of Transportation (ODOT) being the main contributor.

1.2 Rationale of the study

The main aim of rehabilitation is to restore the full structural capacity and increase the design life of existing culverts. Various techniques used to rehabilitate the culverts have their advantages and disadvantages, and before their application in the field, a proper research is required to know how the rehabilitation will work. It is important to know whether the host pipe will add any contribution to the new rehabilitation technique. Especially for the case of the rehabilitation using spray-applied liners, it is vital to know the contribution of the host pipe. The host pipe may contribute significantly or may not contribute at all. The dependence is based on the deterioration level of the host pipe. Considering the worst-case scenario, the deterioration of the pipe was achieved by the complete removal of the invert. Moreover, for spray-applied pipe lining rehabilitation techniques, it is also essential to know the thickness required to fully restore the structural capacity of the pipe. Ideally, several lab tests with different thicknesses are required to determine the optimum thickness of liner needed for successful rehabilitation. However, performing multiple tests to satisfactorily address the issue is not always practical considering the time and funds required. A more economic approach can be to perform limited sets of tests and use the resulting data to calibrate a finite element model, which can then be used to generate the data for other thicknesses. Thus, this study includes the calibration of a three dimensional FE model using data from tests performed at CUIRE on intact CMP, Invert cut CMP, and three invert removed circular CMPs rehabilitated using polymeric spray applied pipe liners and thus prepared a base model to carry further parametric studies on CMPs lined with other thicknesses. All the test results and the details of the experiment presented in this study belong to the Center for Underground Infrastructure Research and Education (CUIRE).

1.3 Objectives

The specific objectives of the research are as follows:

1. Perform three-dimensional finite element analysis for the intact circular, invert removed circular and polymeric SAPL rehabilitated circular CMPs.
2. Compare and validate the obtained FEM results with the test data obtained from the lab testing carried at CUIRE.
3. Compare the load-carrying capacity of the lined CMPs with that of the unlined intact and invert removed CMPs through FEM results and analyze the performance of the liner.
4. Establish a base model through FEM for further research on various thickness of SAPL.

1.4 Thesis Organization

The thesis consists of five chapters.

Chapter 1 deals with brief introduction which provides the background for the study, rationale and the objective of the study.

Chapter 2 deals with the literature reviews performed during the research work. This chapter extensively talks on design procedures, form past and present, followed for the CMPs. It also talks about the deterioration and rehabilitation techniques along with related studies carried by various researchers. Finally, it gives an insight on the use of the finite element modeling techniques in analyzing the buried pipes in several studies over time.

Chapter 3 talks briefly on the experimental results for the intact circular, invert removed circular and three polymeric SAPL rehabilitated circular CMPs, which were later used to verify the FEM works.

Chapter 4 details the three-dimensional finite element modeling of the CMP tests described in chapter 3.

Chapter 5 presents the conclusion of the study and provides recommendation for future research.

Chapter 2: Literature Review

2.1 History of the design of the Corrugated Metal Pipe:

Corrugated Metal Pipe (CMP) were developed and came into use at the end of the 19th century at around 1886. (Campbell, 2018). Although the use of the CMP and buried pipes dated much earlier the pioneer work for design of flexible pipe was done by A. Marston (1913,1930) and M. Spangler (1941).Initially flexible pipe design was based on the calculation of the deflection caused by the load above the pipe. Since, Marston's design was based on the Marston load theory and was more appropriate for the rigid pipes, it was modified by Spangler, one of Marston's student, to make it apt for the flexible pipes. The Spangler's deflection formula was combination of design elastic ring theory and experimental work performed in the Iowa University, thus providing the name Iowa formula. Iowa formula is based on the assumption that the load is uniformly distributed over the bedding width of the pipe while the passive horizontal pressure is distributed parabolically over 100 degree arch (Muhannad, 2002) (Figure 2-5). This theory was further modified by Watkins and Spangler (1958) who related the passive horizontal pressure to the modulus of the soil reaction. They were able to establish the relation between the soil modulus and the horizontal pressure applied by the soil. The new formula for the calculation of the horizontal deflection was named as "Modified Iowa Formula" (Equation 2.1) and is given as:

$$\Delta x = \frac{D_L(KW_c r^3)}{EI + 0.061E^{'} r^3} \qquad 2.1$$

Where:

Δx = Horizontal deflection of pipe (in.)

D_L = Deflection lag factor (1.0 with 85% or greater compaction)

K = Bedding constant (0.1)

W_c = External Load per unit of pipe length (lb./linear in. of pipe) (Its calculated from the Marston formula)

r = Pipe Radius (inches)

EI = Pipe wall stiffness (lb.-in^2)

E = Modulus of elasticity (steel: 30,000,000 psi, cement mortar: 4,000,000 psi)

I = Transverse moment of inertia per unit length of pipe wall (in^4/in)

E' = Modulus of soil reaction (lb./in^2)

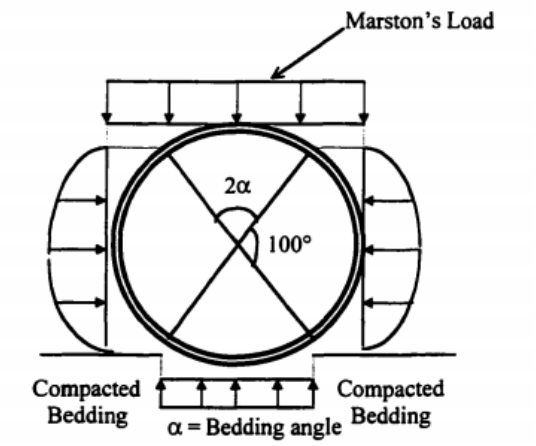

Figure 2-5 Assumed soil stress distribution on pipe

The modified Iowa formula only provided the horizontal deflection of the pipe and could not give the vertical deflection in the pipe. Later formula for the vertical deflection was developed by U.S Bureau of Reclamation using the Howard (1977) soil modification factor. The formula for the vertical deflection is given as: (Fuerst & Robertson J., 2013)

$$\Delta y = \frac{T_f 0.07\gamma h + 10W_L}{\frac{EI}{r^3} + 0.061F_d E'} \qquad 2.2$$

Where
$\Delta y =$ percent vertical deflection;
$T_f =$ Time lag factor(1.0 for initial condition);
$0.07 =$ combination of conversion factors and bedding constant, $\frac{ft^2}{in^2}$;
$\gamma =$ backfill unit weight, lb/ft^3 ;
$h =$ depth of the cover
$W_L =$ live load, lb/in^2;
$E' =$ modulus of soil reaction, lb/in^2; $F_d =$ design factor, dimensionless
$\frac{EI}{r^3} =$ pipe stiffness factor, $\frac{lb}{in^2}$, (obtained from manufacturer's literature)
*The equation is applicable for the 50 feet cover depth.

Both Iowa formula and the modified Iowa formula considered the Modulus of the soil reaction (E') as a constant parameter and neglected variation of the soil pressure with depth. This made difficult for obtaining the reliable estimate of the soil structure interaction. This disadvantage caused the formula to be obsolete (Campbell, 2018) which was later addressed by Burns and Richards (1964), from University of Arizona. They gave the closed form elastic solution which provided the idealized solution for the buried flexible pipes using conventional soil properties, modulus of soil (E') and Poisson ratio. Their solution, based on ring compression theory, not only provided the solution for deflection in the pipe but also provided the solution for the thrust and bending moments in pipe (Katona, 2018). On upcoming years and decade several advancements on the design criteria was made with the most notable one being the work of the Howard (1977) and McGrath (1998) who incorporated the variation of the soil pressure with the depth in their design criteria. However, Howard's (1977) estimation of the soil pressure with the depth works were basically based on the empirical values which was later improved by McGrath (1998) by provided the relationship for the theoretical stress and the Howard's values of soil Modulus (J. McGrath, 2014). This improved formula was adopted by AASTHO in their design criteria up to now. Although the adaptation by AASTHO for the calculation of the defection was based on the McGrath (1998) work's, they replaced the Modulus of the soil reaction (E') with the secant constrained soil modulus (M_s) because Modulus of the soil reaction (E') predicted was very high.

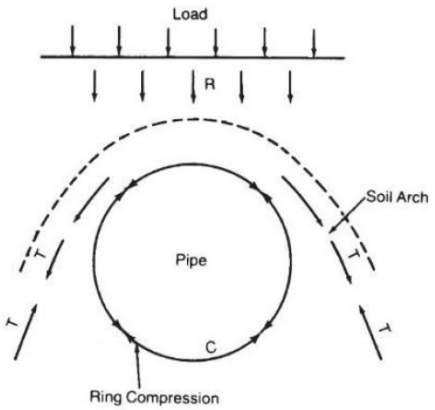

Figure 2-6 Ring Compression and Soil Arching in flexible pipe (Corrugated Steel Pipe Institute, 2009)

2.1.1 Design Procedure by AASTHO

Although lot of design factors and equations are considered before the design of flexible pipe, AASTHO mainly adopts 5% deflection criteria as the main structural design criteria along with factor of safety against local buckling, thrust and bending moment. For calculation of the diameter and thickness of pipe, it depends on hydraulic design.

For calculating deflection in flexible pipe, AASTHO adopts equation 2.3.

$$\Delta_t = \frac{K_B\left(D_L P_{sp} + C_L P_L\right)D_0}{1000\left(\frac{E_P I_P}{R^3} + 0.061 M_S\right)} + \varepsilon_{sc} D \qquad 2.3$$

Where,

ε_{sc} = service compressive strainas specified by AASTHO
D_L = deflection lag factor, a value of 1.5 is typical
K_B = Bedding constant, a value of 0.10 is typical
P_{sp} = Soil prism pressure evaluated at pipe spring line
C_L = live load coefficent
P_L = live load pressure
D_0 = outside diameter of the pipe
E_P = modulus of pipe
I_P = moment of inertia of the pipe per unit length
R = radius from center of the pipe to centroid of the pipe profile
D = Diameter to centroid of the pipe
M_s=secant constrained soil modulus

Beside the deflection factor, AASTHO also considers calculation of thrust force around the pipe for the structural stability of the Pipe in its design criteria. Thrust on the pipe can be defined as the stress around the pipe which implies load per unit length of the pipe. Thus, the designed pipe must be able to withstand the loads such as dead load of the soil, vehicular load and the hydrostatic load.

According to AASTHO the factored thrust in the flexible pipe is calculated as equation 2.4

$$T_L = \frac{P_{FD} S}{2} + \frac{P_{FL} C_L F_1}{2} \qquad 2.4$$

Where

T_L=factored thrust per unit length
P_{FD} = factored dead load vertical crown pressure

S = Culvert span or euivalent to outside diameter of the pipe for circular culvert
P_{FL} = factored live load vertical crown pressure
C_L = width of the culvert on which live laod is applied paralle to span (ft)
$F_1 = \frac{0.75S}{l_w} \geq$ Fmin (for corrugated metal pipe)
$\text{Fmin} = \frac{15}{12(S)} \geq 1$
l_w = Live laod patch length at depth H

This calculated factored thrust is compared with critical thrust. The design requires calculated factored thrust to be less than the critical thrust calculated by the equation (Siavkumar Babu, 2010):

$$T_{cr} = (f_u)(A_P)(\emptyset_P)$$

Where,
T_{cr} = critical thrust
A_P = area of pipe wall per unit length
$\emptyset_P$ = capacity modification factor for pipe (1.0)
(f_u) = Minimum Tensile strerngth of the material

Another important factor for the flexible pipe, is factor of safety against buckling. Since the flexible pipe are susceptible to buckle AASTHO requires pipe to have buckling pressure less than critical buckling pressure. From AASTHO LRFD design criteria the buckling pressure in the pipe is calculated as:

$$P_V = \frac{R_W H\gamma}{144} + \frac{\gamma_w H_w}{144} + \frac{W_L}{S} \qquad 2.6$$

Where,
P_V = actual buckling pressure, psi
R_W = water buoyancy factor, dimensionless, $(1 - 0.33\frac{H_w}{H})$

H = buried depth above the top of pipe
H_w = height of groundwater above top of pipe
W_L = live load
S = span of the pipe , or euivalent to outside diameter of the pipe for circular culvert

Thus, obtained buckling pressure is compared to the critical buckling pressure calculated as below:

$$P_{CR} = \frac{0.772}{SF}\left[\frac{M_s EI}{1-\nu^2}\right]^{\frac{1}{2}} \qquad 2.7$$

Where,

P_{CR} = critical buckling pressure
SF = factor of saftey
M_s = Modulus of the soil reaction
EI = Pipe stiffness factor
ν = poission ratio of the pipe

Thus, the design of the current flexible pipe includes following steps:

a. Determining the diameter and the thickness of the pipe based on the hydraulic capacity requirement.
b. Provide enough ring stiffness and soil strength required to resist excessive ring deflection
c. Provide enough ring stiffness and soil strength required to resist external pressure.
d. Provide enough ring stiffness and soil strength to resist the local buckling in the pipe.
e. Provide enough ring stiffness and soil strength to resist the critical thrust and bending moment provided by the applied load.

2.2 Soil Structure Interaction study:

Since culverts are buried underneath the soil, design of culvert not only considers the structure but also consider effects of soil on the culvert, subsequently making the design of the culvert as the soil-structure interaction. Lots of studies have been performed over the time to utilize the strength of the soil to increase the performance and life span of the buried culvert. According to Katona (G. Katona, 2018) culverts are unique in designing because the earth load distribution is not predicted prior but is dependent on how the culvert deforms. The earliest attempt for the study of the intact pipe and soil-pipe interaction was made by A. Marston (1913,1928) which was followed by M.G. Spangler and Watkins (1941,1958). These studies were based on both theory and experiment. After them, the most notable study was carried by Howard in 1972 AD.

Howard (1972) carried out the load test on buried flexible pipes, sponsored by the Bureau of Reclamations, to enhance the performance of the buried flexible pipes and lower the installation and construction costs. The pipes were buried in the steel container, with clay as the backfill material, compacted to the 90-100% proctor density which was then covered with the wooden plate. A large universal testing machine was used to apply the load on wooden plate which transfer uniform surcharge load to the system. The load was applied till the pressure reached 100 psi or pipe failed. From the ten pipes tested, five pipes had a 90% compacted backfill and remaining five pipes had 100% compacted backfill. After the test, four of the pipes failed through buckling at vertical deflection of 8% and remaining pipes were loaded to 100 psi loads.

Before Howard's study, Spangler and Watkins (1958) assumed the constant value of the passive resistance (E') to predict the deflection in the pipe and till that period no consideration of the soil compaction and depth was made to calculate the modulus of the soil. As of result vertical and horizontal deflection were assumed to be same. Previously the value of 700 psi was used for the value of E' (equation 2.1) while Howard through his test concluded the value of the E' depends on the compaction of the soils. He in his test has explained that the 90% compacted backfill had the average value of E' as 500 psi while the 100% compacted backfill had the average value of E' as 1200 psi. Also, he found that deflection of the pipe decreased by 50% when the soil compaction was increased from 90% to 100%. The study provided the first insight on the relation between soil pipe interaction and effect of well compacted soil on the structural performance of flexible pipe.

Since the value of the soil modulus, E', was determined experimentally and had no any theoretical relationships to address the effect of the different types of soils and soil at different depths, the soil modulus was later modified by M.C. Grath (1998). He with the help of Selig-Duncan soil model was able to provide the relationship between theoretical stress and Howard's soil modulus. The new soil modulus value was termed as constrained soil modulus and it has been adapted for the recent design criteria.

Bakht (1980) performed the experiment on the in-service culverts with the objective of determining the bending moment and the circumferential thrust around corrugated metal pipe due to live loads. The test was performed in Ontario, Canada. The pipes were of large diameter with diameter varying from 7 m to 7.5 m.

The instrumentation of the pipe included the displacement transducers and uniaxial strain gauges along the circumference in order to have the direct measurements of the displacement and bending moment and thrust of the pipe respectively. All the measurements were taken from the center of the pipe. The pipes were loaded using the tandem axel truck whose load could be varied. Bakht (1980) through the experiment figure out that the distribution of the circumferential thrust around the pipe was not uniform which at that time was supposed to be uniform. The assumptions of the uniform incremental circumferential thrust around the pipe had led to believe that friction between the pipe soil interface was negligible which was proved to be untrue.

Another study on the buried pipes was performed by M.C. Webb (Webb, 1995) to study the effect of proper compaction during the backfilling process. Different pipes such as reinforced concrete, corrugated and HDPE pipes were tested to study the change in the shape of the pipes during the process of backfilling. Almost all the test showed the peaking response of the pipe i.e. negative vertical deflection and positive horizontal deflection until before the cover backfill. The main finding of the experiment was: if the backfill soil in the sides were compacted using higher energy dissipating equipment, such as vibrating plate, it caused greater peaking which reduces the deflection at crown during the backfilling above the crown. This would enhance the performance of the buried pipe greatly.

(Arockiasamy, Chaalla, & Limpeteeprakarn, 2006) performed the full-scale study of different buried flexibles pipes for the determination of the soil-pipe system response under the live load applications. The tests were performed on 3 PVC pipes, 2 aluminum pipes and 1 metal pipes with the nominal diameter of 36 and 48 in. under burial depth of 0.5D, 1D and 2D. The standard highway designed axel load of 32 kips was modified to include the dynamic load allowance which increased the load depending on the burial depth and diameter of the pipe. The load applied was 34.6 kips, 38.6 kips and 40 kips respectively for 2D, 1D, and 0.5D burial depth for 36 in. diameter pipe while for 48 in. diameter pipe the load applied were 32 kips, 37.3 kips and 39.9 kips for 2D, 1D, and 0.5D burial depth respectively. The loads were applied through the FDOT dump truck whose load were varied using the concrete blocks. The experiment demonstrated that increase in the cover thickness of the pipe by about 6 in. would decrease the vertical soil pressure by 2 to 3 times for the larger diameter HDPE pipe (48 in.) compared to the 36 in. diameter HDPE pipe. Also, the study supported the 5% deflection criteria for the design of the corrugated metal pipes which is adopted by AASTHO.

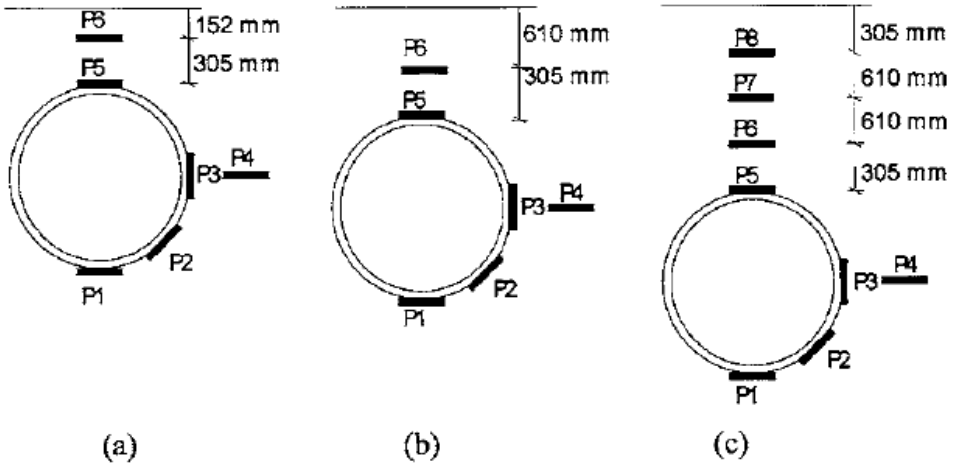

Figure 2-7 Buried pipe configuration (Arockiasamy, Chaalla, & Limpeteeprakarn, 2006)

(Barbato, Bowman, & Herbin, 2010) performed the study, sponsored by Louisiana Department of Transportation, to evaluate the effects of the mechanical and geometrical parameters such as excavation width, fill cover height, bedding height, ring stiffness, compaction etc. which are used to characterize the soil pipe interaction during the installation of buried flexible pipes. The study was performed exclusively using over 25000 FEM analysis which recommended that minimum cover height is to be expressed as a function of the pipe diameter, the width of the trench should be two times the diameter of the pipe for the flexible and semi flexible pipes. The study also found that performance of the soil pipe system crucially depends on the type of the road surface in which stiffer road pavement will decrease the load transferred to the pipe in significant amount as the load gets distributed evenly over the larger area of the soil.

2.3 CMP Deteriorations and need for replacement:

With the ease of the installation, short construction period and less cost, metal culverts have been widely used by the DOTs. But the biggest disadvantage of the metal culverts are its relatively less service life years, about 10 to 35 years before perforation ((Rinker Materials, 1994)), compared to the concrete culverts whose expected service life is 75 to 100 years (NCHRP Synthesis 474, 1998). The service life of the CMP largely depends on the quality of the installation, quality of water, types of soil, bedding condition etc. Hence, the cause of the deterioration and the replacement of the CMPs may be due to inadequate pipe capacity, structural failure due to excessive soil loading, erosion due to excessive water transport of sand and gravel, corrosion from acidic soil and water, poor bedding condition etc. (Winconsin Transportation Bulletin, 2015).

Thus, a culvert could be considered deteriorated if one or multiple of the following condition is present in it:

a. Invert loss or perforation of the invert.
b. Buckling of the pipe.
c. Separation of the joints and seams.
d. Shape distortion.
e. Piping of soil etc.

Figure 2-8 CMP with complete loss of invert (Colorado DOT, 2014)

Figure 2-9 Separation of the joints and seams in CMP (Tenbusch & Dorwart, 2009)

The deterioration in the pipe will cause the different modes of the failure in the pipes. Several DOTs and Federal Agency have studied the modes of the failure of the CMP due its deterioration and established the condition for the need of replacement. All the needs for the replacement or renewal of the CMP could be summarized as:

a. Loss in Structural capacity

The most common failure mode in the CMP and need for replacement of the CMP is inadequate structural capacity. The structural capacity in the pipe could be lost due to the complete corrosion of the invert, separation of the joints, damaged wall due to corrosion etc. (Chimauriya, 2019). But among all, the main factor for the loss of the structural capacity could be attributed to the invert loss in the pipe. With the loss in the invert in the pipe the hoop strength in the pipe gets broken as of the result the pipe starts to close in thus reducing the circumferential diameter in the pipe further buckling the pipe causing the loss in the load carrying capacity of the culvert. Also, this lost in the structural integrity in the pipe may cause the failure of the pavement by excessive settlement.

Figure 2-10 Failure of CMP due to buckling (Tenbusch & Dorwart, 2009)

b. Geotechnical Aspect of the failure
For the failure of the culvert always the loss in the strength capacity may not be the main factor. Sometime the failure of the culverts may be caused due to the geotechnical aspect of the CMP i.e. improper compaction of the backfill or piping in the soil. It is known that by now that the strength and the performance of the flexible pipe greatly depends on the properties of the side backfill soil. So, with the corrosion of the invert, the pipe diameter effectively gets reduced, this reduction in the pipe diameter causes the side-backfill, that was compacted, to loosen. This loosening of the compacted backfill will cause the pipe to lose its confinement from the soil thus losing the structural integrity of the pipe-soil interaction leading to the buckling of the pipe (Figure 2-10) (Tenbusch & Dorwart, 2009). Also, the corrosion of the invert causes the bedding of the culverts to get eroded. This erosion in the bedding cause range of the problems causing small depression in the pavement to the complete collapse of the system. Thus, deficiencies and failure in the geotechnical aspect may also lead to the need for the rehabilitation of the culverts.

c. Reduction in hydraulic capacity:
General the culverts are designed for certain hydraulic capacity but when the circumferential diameter gets reduced due to the loss of the invert, failure of joints and seams, corrosion of the wall, the hydraulic capacity gets reduced. When the hydraulic capacity gets reduced the hydrostatic pressure above the upstream channels get increased. When the hydrostatic pressure is increased it might start to erode the soil and from the flow channels through the structural backfill causing the piping in the soil. This piping and the erosion in the soil will remove the available side support for the pipe thus causing the failure of the pavements.

2.3.1 Study of the deteriorated corrugated metal pipe:

Mai et al. (2013) performed the experiment to compare the strength of the large intact steel culvert with the corroded steel culvert. The corroded steel pipe had 70% wall remaining on the west haunch while only 48% wall thickness was remaining in the east haunch side. The pipes had 1.8 m diameter and 3 m length and were tested at the shallow cover depth (0.9 m and 0.6 m) under the live load conditions. To simulate the actual field conditions the deteriorated pipe had loose backfill while the intact pipe had the compacted backfill but for both the pipes the top fill was compacted to same level. The soil material they used was classified as well graded sandy gravel (GW-SW). The live load was applied through the single steel pad

and two pads simulating the single axel loading and the load applied was based on the AASTHO design trucks. For 0.9 m burial depth the calculated single wheel pair load and the single axel load was 106 kN and 214 kN respectively. The findings of the tests can be summarized as:

- Both pipes behave similarly during side backfilling i.e. had equal amount of horizontal and vertical deflection but once the backfilling above the crown was done the deteriorated pipe deformed significantly compared to the intact pipe.
- While comparing the thrust force for the two pipes, it was found that the intact pipe had 71.6 % higher thrust force than the deteriorated pipe which were tested under 100 kN single wheel pair load with 0.9 m burial depth while it was only 27.2% higher when tested under 90 kN single wheel pair load with 0.6 m burial depth.
- Also, the change in the vertical diameter for the deteriorated pipe was found to be 400% and 257% more than the intact pipe when tested under 0.6 m burial depth with single-wheel pair load.

All this finding concluded that the deteriorated culvert could not withstand the AASTHO specified load.

Figure 2-11 Experimental setup (inside the pipe) (Mai, Hoult, & Moore, 2013)

Regier et al. (2018) carried the experiment in order to access the remaining capacity of the corroded pipe and find the deterioration level which then before was only based on the visual inspection and was not quantifiable. A series of the experiment with different corrosion level pipes buried under the shallow cover of 0.45 m and 0.9 m depth was carried out (Figure 2-12). The culvert specimens were subjected to the accelerated corrosion in order to obtain the different deterioration level of the pipe. The total number of the test culverts were 6 each 1.5 m long and 0.9 m diameter. The first pipe (P18, Figure 2-12) was corroded to worse level and had average remaining wall thickness was 18% along the invert. The second pipe (P 34, Figure 2-12) was corroded with average remaining wall thickness of 34% while two other pipes (P45 and P 47,Figure 2-12) had average remaining wall thickness of 44% and 50% respectively. Other remaining pipes were lightly corroded and were treated as the intact control pipe. The loading was applied using the 2000 kN actuator. Two load pads were used during the test, 600 mmX250 mm for service load and 950 mmX370 mm for ultimate load conditions. The applied loading rate was 25kN/min.

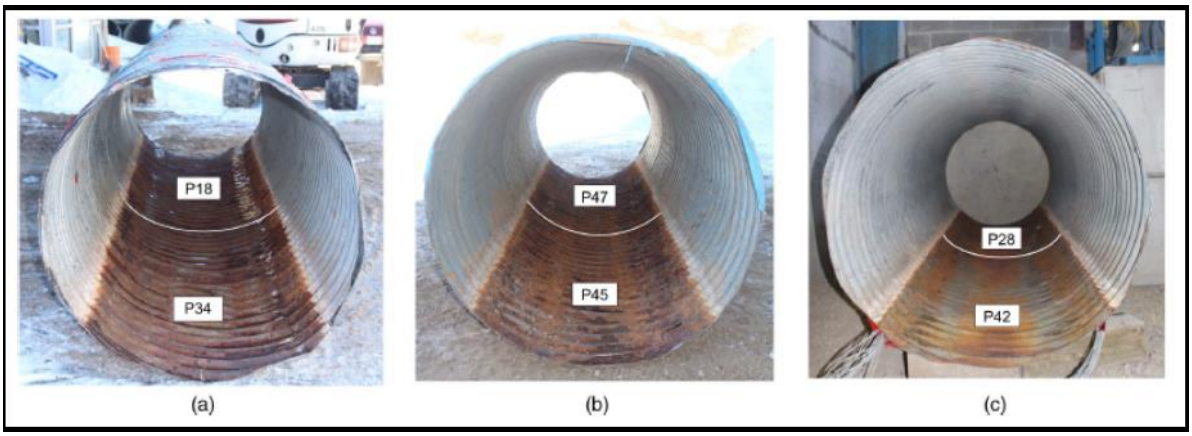

Figure 2-12 Corrugated steel pipes with different level of corrosion (Regier, Moore, & Hoult, 2018)

The findings of the test could be summarized as:

- During the backfilling process the pipe with severe corrosion (P18) experienced the largest vertical and horizontal deformation, which were believed to be caused by heavily corroded sections in haunch.
- It was found that culverts with worst corrosion (P18 and P34) failed at lower load because of local buckling of the remnants steel in the heavily corroded area while the culvert with the mild corrosion failed by bending in the upper half of the culvert from which it was concluded that the level of corrosion dictates the failure of the pipe.
- Through the test they also found that the intact pipe, for shallow cover depth, have different failure mechanism compared to the failure mechanism considered during designing. In the test the intact pipe failed through the local bending in the top rather than the thrust controlled failure from springline.

  The experiments could not quantify the critical level of the corrosion for dictating the failure mechanism.

(Sargand, Khoury, & Hussein, 2018) performed the experiment to find out the load capacity of the CMP culvert with extreme corrosion in the invert. The test was carried out in the real field culvert which was schedule to replacement due to its extreme degree of the corrosion. To rehabilitate the pipe, they used the method of the invert paving. For the test they paved half of the pipe with the concrete and leave the other half in the corroded condition. They applied the static load in order to replicate the rear axle of a truck parked over the crown of the culvert. Each pipe was tested under the load of 18 kips, 40 kip and 60 kip. From the testing it was found that despite having significant corrosion on the invert and the shallow cover the deteriorated culvert still could carry the significant amount of load (80 kips) which was three time larger than the legal load limit of 18 kips.

Figure 2-13 (a) Load Configuration for testing (b) Invert Deteriorated Pipe with instrumentation (Sargand, Khoury, & Hussein, 2018)

2.3.2 Repair, Rehabilitate or Replace Method:

The need of the renewal, rehabilitation and replacement of the pipe depends on the degree of deterioration of the pipe. Generally, replacing of the culvert will be costly and time consuming thus depending on the level of deterioration the repairment, and rehabilitation of the pipe would be more viable and economical option. There are several methods of pipe rehabilitation techniques which could be either trenchless or open cut method. But generally trenchless method is preferred to open-cut

method as with the use of trenchless method eliminates the blocking of the traffic in the highways. Some of the method for the repair and rehabilitation are (Meegoda, 2009):

a. Painting and cleaning
   For the initial level of the deterioration the painting and cleaning is the good option as its intervenes the corrosion process thus stopping the further deterioration of the pipe.

b. Invert Paving

Figure 2-14 Invert Paving (Masada, 2017)

   As we could see the corrosion of the pipe is mostly concentrated over the invert region of the culverts. Invert paving could be the good option if the other parts of the culvert are more or less intact (FHWA (1995)). Paving could be done using the asphalt and cement, cement mortar or concrete. The thickness of the pavement is recommended to be in the range of 3-6 inches. (FHWA (1995)).

c. Slip-lining:
   Slip Lining method is the process in which the deteriorated pipe is accesses through the strategic points and whole new pipe is slipped inside the old pipe. When trenching to repair pipes and culverts is not an option, trenchless slip lining technology can be a cost-effective solution. The slip lining could be done using plastic pipes, metal pipes, fiber glass reinforced cement. (Matthews, Simicevic, & Kestler, 2012).

Figure 2-15 Slip Lining Method of pipe rehabilitation (Terrafix Geosynthetics, 2011)

d. Spray applied liners

Lining the deteriorated pipe is the recent trenchless technology to rehabilitate the deteriorated pipe. The liner could be cementitious or polymeric. The use of the liner technology has been increasingly popular considering other method of rehabilitation as the installation cost is low. A lot of study has been conducted to see the increase in the structural capacity of the pipe rehabilitated with the application of the liner. The liner not only increases the structural capacity of the pipe but also prevents the corrosion and invert loss in the metal pipes.

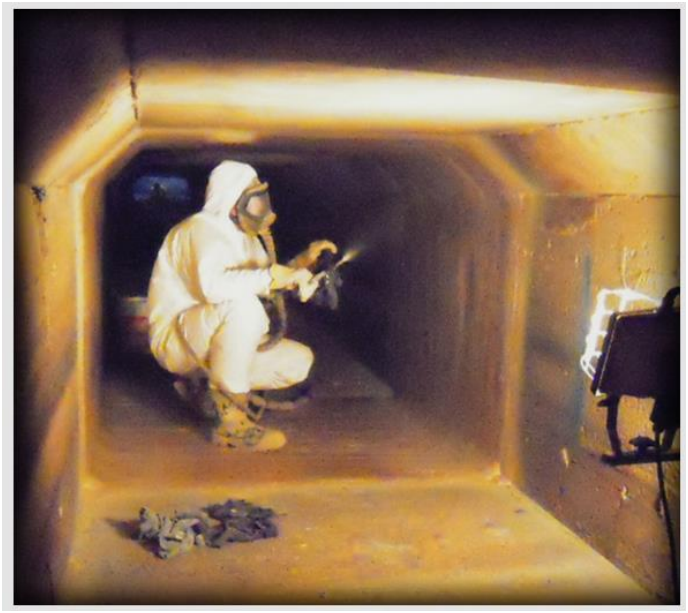

Figure 16 Box culvert being lined with the polymeric liner material through hand spraying (Sprayroq, 2020)

2.3.3 Study of the rehabilitated CMP

To find out the increase in the structural capacity of the CMP once it gets rehabilitated, a lot of the field and lab studies has been made recently. Summary and review of some of the recent studies relevant to our research has been made and is presented in this section.

Garcia & Moore (2015) conducted the experiment to find the increase in the strength of the deteriorated buried culverts rehabilitated with the spray applied cementitious liner. The deteriorations were concentrated on the invert and haunch regions for both pipes. A detail study on the various conditions of the two deteriorated pipes with diameter of 1.2 m were done. The pipes were first tested without liner with the cover thickness of 1.2 m. And those two pipes were rehabilitated with cementitious liner. Each of the pipe were lined with different thickness (76 mm and 51 mm) and these pipes were tested under the two different load conditions. First load condition was to simulate the single axel of Canadian design truck and other condition was to simulate the tandem axel of Canadian design truck. Also, the pipes were tested under two different cover thickness of 1.2 m and 2.1 m. Both the pipes were buried in the well graded sandy gravel (GW-SW) which was compacted to 95% proctor density.

The findings and the conclusion of the experiments can be summarized as:

- The study found that the deteriorated pipes were able to carry the service load as they could not see the signs of the failure of pipe up to 203 kN.
- With the application of the liners it was observed that the change in the vertical and horizontal diameter was minimal thus providing the semi rigid response of the pipe. Also, the change of curvature of the pipe was small for similar load conditions which indicated the increase in the circumferential bending stiffness. Thus, strengthening the fact of semi-rigid behavior of the pipe after the application of the liner.
- The study also concluded that the increase in the liner thickness increased the stiffness of the rehabilitated pipe.

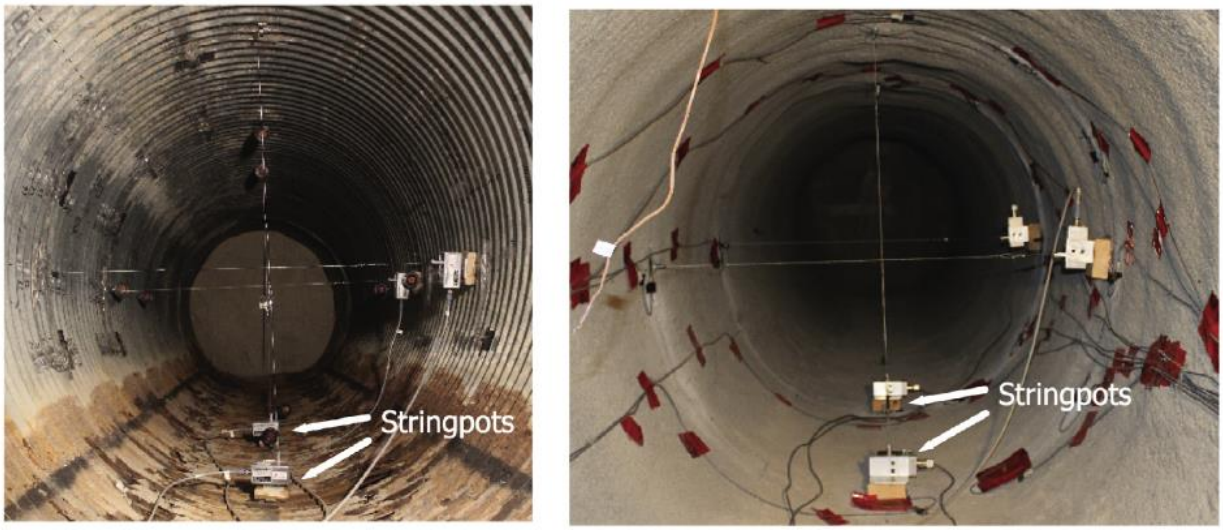

(a) (b)

Figure 2-17 (a) Pipe before the application of the liner (b) Pipe after the application of the liner (Garcia & Moore, 2015)

Another detail study of the rehabilitated pipe was made by Masada (2017) which was sponsored by Ohio department of transportation. The test was carried to find the increase in the structural capacity of the deteriorated pipe after the deteriorated pipe's invert was paved with the reinforced concrete according to the ODOT CMS item 611.11 standard field paving procedures. The pipes were new pipe and 60 in. in diameter with length of 16 ft. in which deterioration was simulated by removing large rectangular part from the invert. Total of three tests were carried out. The first test was done on the intact new pipe which could be the baseline structural capacity of the new CMP. And the large part of the invert was removed from the middle and then it was loaded to failure. Finally, the pipe whose invert was removed were paved with the

concrete pavement of 75 mm thickness and loaded to the failure. The results of the test of the repaired pipe could be summarized as:

- The load carrying capacity of the pipe, when the large portion of the invert is removed, was reduced by 73% of its original intact pipe capacity.
- Also, when the large portion of the invert gets removed, it was observed that CMP would experience more horizontal deflection than the vertical deflection and the failure mode of the pipe would be the seam splitting and excessive deflection (Figure 2-18.c).
- After the pipe had been rehabilitated through the concrete paving procedures it was observed that the capacity of the pipe would get increased up to 87% of the load capacity of the intact pipe when the paving procedures was as per the ODOT CMS item 611.11 standard field paving procedures. It was also observed that the pipe achieved 100% of the capacity compared to the original pipe when it was paved with concrete using #4 steel rebars.
- The failure mode of the rehabilitated pipe was buckling above the spring-lines.

a

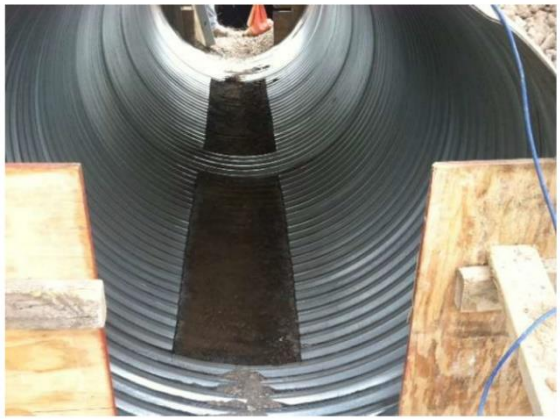

b

c

d

e

Figure 2-18 Invert removal and repair process (a)-(e) (Masada, 2017)

2.4 Study of the culverts through Finite element

Most of the times to develop the design equation lot of parametric studies are required and it does not seem viable option, considering time and economics, to perform all the experimental tests to get the results for the given parameters. So, for this reason people have been using the computer aided design analysis model to perform the parametric study in every field of engineering. Finite element method is the numerical technique which uses the partial differential equations to solve the given physical phenomena dividing whole model into certain finite elements.

The use of the finite elements analysis to study the soil-pipe interaction for the culverts started as early as in 1980s. One early study of the culvert soil interaction was made by Duane, Robinson, & Moore (1986). They had devlope the culvert soil intearction model using general finite element codes incoporating the Duncan Soil models and incremental construction model of the culvert via subroutines. Their model was validated with the results obtaiend form analytical and empirical procedures which was adopted for the culvert designs. They used the finite element codes like CANDE (Katona (1976)) and FINLIN to study the soil-pipe interaction. The study was performed for the 24 in. diameter flexible plain pipe with wall thickness of 0.31 in. The developed model was 2D symmetrical model about the vertical with restriction of the horizontal movement along the vertical boundary. They compared the deflection, thrust and bending moments of the pipe using the strains using different soil models. Different models predicted the soil-pipe interaction differently with certain descripancies but it was comparable with the theoretical solutions which provided the stepping stone in modeling the pipe soil interaction.

2.4.1 Representation of the CMP in Finite Element

Corrugated Metal Pipe (CMP) has an irregular geometry and are complex to be represented in ABAQUS models, which costs a significant amount of computational time. So, in order to reduce the computational time and make the model more efficient, equivalent models with simplified geometry are often used as the alternative. CMPs have unique values of the flexural rigidity (EI) and axial stiffness (EA) in the direction perpendicular and parallel to the direction of the corrugations due to directionally dependent geometric properties ($I_L < I_\theta$ and $A_L < A_\theta$) (Campbell, 2018). Thus, the complex geometry of the CMP is represented in simple rectangular geometry by converting to “equivalent” plain pipe, and the equivalent properties are calculated as follow:

$$E\,I_L = \bar{E}_L\bar{I} \text{ and } E\,I_\theta = \bar{E}_\theta\,\bar{I}$$
$$\bar{I}_L = \bar{I}_\theta = \bar{I}$$

where,

E= Young's Modulus of the CMP Pipe

$\bar{I}_L$ = Equivalent Moment of inertia in Longitudinal Direction

$\bar{I}_\theta$ = Equivalent Moment of inertia in Circumferential Direction

$\bar{I}$ = Equivalent Moment of inertia

I_L=Moment of Inertia in Longitudinal Direction

I_θ =Moment of Inertia in Circumferential Direction

$\bar{E}_L$= Equivalent Young's Modulus in Longitudinal Direction

$\bar{E}_\theta$ = Equivalent Young's Modulus in Circumferential Direction

A= Cross-Sectional Area of the CMP Pipe

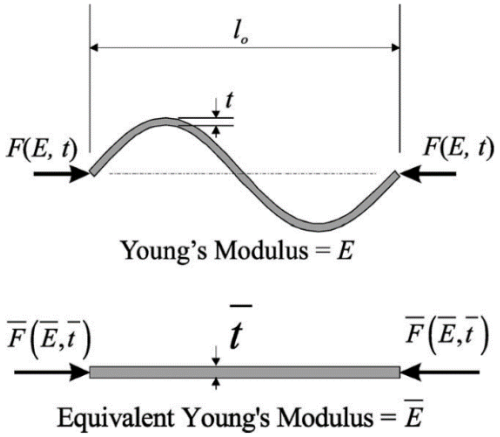

Figure 2-19: Actual geometry and equivalent geometry of the corrugated pipe (Elshmi T. M., 2011)

The following equations were used to calculate the equivalent properties of the CMP:

$$\bar{t} = \sqrt{\frac{12I}{A}}$$
$$\bar{E} = \frac{12E\,I}{t^3}$$

where,

$\bar{t}$ = Equivalent Thickness of the CMP pipe

E = Young's Modulus of the Pipe

I = Moment of "Inertia" of the CMP pipe

A = Cross-sectional Area of the CMP pipe

$\bar{E}$ = Equivalent Young's Modulus of the CMP pipe in circumferential direction

For orthotropic model, *Moore & Brachman (1994)* assumed that the Young's modulus in the longitudinal direction is 150 times less than the Young's modulus in the circumferential direction.

$$E_L = \frac{E_\theta}{150}.$$

Later, different methods were developed to calculate the longitudinal Young's modulus to more accurately represent the CMP geometry through equivalent geometry. The following equations was developed by Elshmi (2018) to calculate the circumferential and longitudinal Young's modulus (Elshmi T. M., 2011).

$$t = d\sqrt{\frac{3}{2(1+\frac{\pi^2 d^2}{4b^2})}} \tag{3.6}$$

$$E_\theta = \frac{3}{2}\left(1+\frac{\pi^2 d^2}{8b^2}\right)\frac{E_P t_p}{d}\left(\frac{2}{3}\left(1+\frac{\pi^2 d^2}{4b^2}\right)\right)^{\frac{3}{2}} \tag{3.7}$$

$$E_L = \frac{2}{3}E_P\left(\frac{t_p}{d}\right)^3\left(\sqrt{\frac{2}{3}}(1+\frac{\pi^2 d^2}{4b^2})^3\right) \tag{3.8}$$

Where,
d = depth of the corrugations
b = half the crest -crest to the length of the Corrugations
t = Equivalent Thickness
E_θ = Circumferential Young's Modulus
E_l = Longitudinal Young's Modulus

But nowadays with the more powerful computers the CMP is being represented with its original geometry only for studying the exact distribution of the stress and strain over the pipe.

2.4.2 Study of CMP through the Finite Element Method

Moore & Brachman (1994) carried out the three dimensional thoeretical finite element analysis of the culvert whoes results were compared to the results obtained by experiemental test carried by Bakht (1980) over the corrugated metal pipe. For modeling the culvert in three dimension, they used two dimensional finite element meshes in xy-plane and Fourier transform analysis in the z-direction. The corrugated metal was converted to equivalent geometry plain pipe in order to simply the analysis. The pipe was converted to equivalent model using both isotropic model (having same value of Young's modulus in the circumferential and longitudnal direction) and orthotropic model (having different value of Young's modulus in the circumferential and longitudnal direction). For the soil they reported that its modulus may differ from 30-80 MPa. The isotropic model predicted the general trend of the thrust distribution and circumferential bending strain successful but overestiamted both of it in the several places. The orthotropic model although decreased the value of the thrust distribution in the crown but it was not well comparable with the experimental thrust distribution. In contrast to the three dimensional model the two dimensional model predicted very small thrust value at the crown while the thrust at the springline and haunches was overestiamted which in overall concluded that the results obtained from the three dimensional modeling was far superior to the results obtained from the two dimensional modeling. As for the discrepancy for the three dimensional model Moore & Brachman (1994) attributed to their consideration of the culvert geometry to be infintely long.

The over estimation of the circumferential bending moment and thrust distribution was realized by El-Sawy (2003), and thus he again performed the 3D FEM analysis of the experiment performed by Bakht (1980).

A general FE package software called ANSYS was used to model the pipe. The culvert was represented using the shell element while the soil was modeled as the solid eements. The soil was meshed using the 20-noded isoparametric brick tetra hedral solid elements around the culvert while 10-noded isoparametric tetrahedral elements were used outside of the culvert perimeter. For the culvert 8 noded quadrilateral shell element was used. He, similar to Moore & Brachman (1994), also represented the culvert as isotropic plate and orthotropic plate. But unlike Moore & Brachman (1994) who considered the longitudnal Young's modulus to be 150 time less than the circumferential Young's modulus, equated the true longitudnal axial stiffness to equivalent axial stiffness and found that the longitudnal Young's modulus is 193 times less than the circumferential Young's modulus. Both the soil and the culvert was modeled as elastic model.

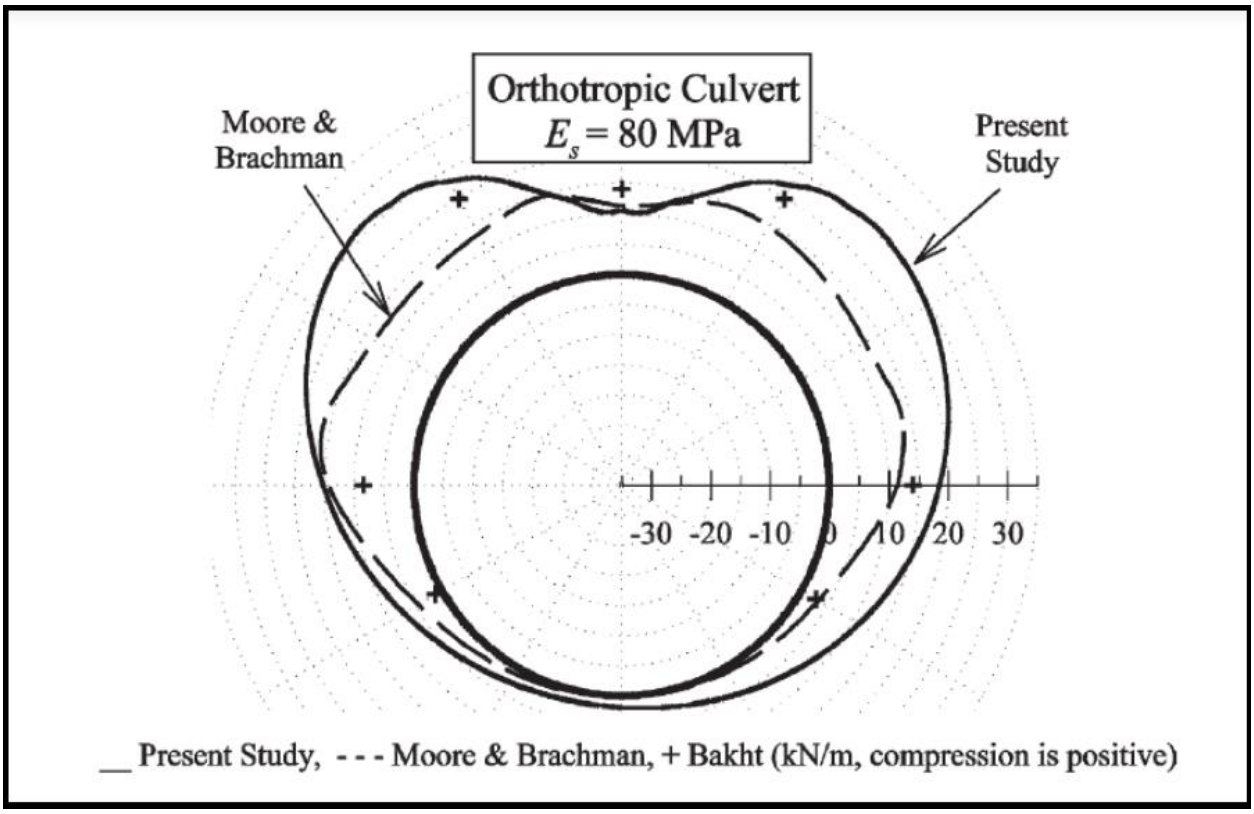

Figure 2-20 Prediction and Comparison of the circumferential thrust by (El-Sawy, 2003)

The Finite element study predicted the values of the circumferential thrust and bending moments around the pipe more closely than the Moore & Brachman (1994) ,using the orthotropic model, to the experiemental results. Although the prediction was better still discrpency between the experiemental value and the predicted value around the crown was around 30%. Through the analysis El Sawy (2003) concluded that circumferential thrust decreased within the short distance and hence simple prismatic model with constant overburden could be used to model the culvert in the embankment.

Kunecki & Kubica, (2004) studied the shallow covered (0.8 m) corrugated steel culverts under the standarized railway load through the experiemental and FEM analysis. For the verification of the test results the FEM analysis was carried out using the Cosmos/M software. The used software allowed the simulation of the live loads. The soil and culvert was modeled in 2D, the soil was modeled as 316 Plane 2D elements and culvert was modeled as 32 Beam2D elements. The FEM and experiement showed the discrepancy of 0.11 mm in the vertical dispalcement and the 0.08 mm in the horizontal displacment which showed the close agreement between the model and the experiement but while comparing the thrust around the pipe it

was significantly higher than the measured values around the pipe. The discrepancy may be due to the 2D representation of the model and the elastic model.

El-Taher & Moore (2008) used the Finite element analyis method to study the load carrying capacity of the deteriorated steel culverts. The study was pereformed to calculate the acceptable limits of the invert corrosion. Total of the five design cases were considered with different cover depth and spans. The culvert was modeled in the 2D with the equivalent geometry with the focus of the corrosion in the invert region only. To represent the corrossion in the culvert the reduction of the thickness was applied along the invert from haunch to haunch and from spring line to spring line. The reduction was applied according to the calculated reduced equivalent thickness. ABAQUS,version 6.5 was used to model the model considering only the linear elastic system behaviour. Both the soil and the pipe was meshed using CPE8 elements with full integration to eliminate the possibility of hourglassing. The thickness of the pipe was reduced by deactivating the elements along the invert. Since the study was based only on the computational analysis the obtained results were compared to the closed form solutions. Although the study found the reduction in factor of safety against buckling and yield due to the reduction in the wall thickness, the study concluded that due to good surrounding backfill material (well graded gravel) the effect of the reduction in the wall thickness, simulated condition of the corroded invert of the culvert, was minimal for the change of the thrust and moment around the pipe. Also the study did not considered the complete loss of the invert or the perforation in the invert. Thus the model was successful in providing the general idea of the behavior of the deteriorated culverts but it could not predict exactly the loss in the capcaity of the culvert due to the corrosion.

From the study of the soil pipe interaction, it is a proven fact that compaction of the backfill soil plays great role in determining the behavior of the flexible pipe. Experimental tests has been performed to study the effect of the compaction by Bhakt (1980), M.C. Webb (1995), J. McGrath (1999), Barbato, Bowman, & Herbin (2010) etc.

(Elshmi & Moore, 2014) made a study to consider the effect of backfilling during finite element modeling especially for the shallow covered culvert. Previously, Taleb and Moore (1999) tried to model the effect of backfilling by setting the lateral stress values to the passive values instead of the active values which then would increase the lateral stress significantly than the vertical stress causing the peaking of flexible pipe during the installation procedures. (Elshmi & Moore, 2014) tried to improve the model by introducing the kneading coefficient (K_n) which occurred during the compaction of the soil. This kneading coefficient is multiplied to lateral stress calculated. The research tried to find the value of the kneading coefficient empirically through finite element analysis in which they analyzed five different pipes made of different materials like HDPE, Corrugated Metal Pipe and Concrete. The behavior of the pipe was modeled in the two- dimension using the ABAQUS 6.5 software. Both the pipe and the soil were modeled using the six noded quadratic plane strain triangular elements. The soil in the modeled was placed in the layer of 200 mm. The corrugated metal pipe was modeled using the equivalent geometry. All the FEM results were compared to the experiment carried by J. Mc Grath (1999). Through the analysis they suggested the value of the kneading coefficeient to be 2.

(Mai, Hoult, & Moore, 2013) perform the two dimensional finite element analysis of the deteriorated metal culverts under the surface loading. The analysis was performed for the optimization of the rehabilitation of the deteriorated culverts. The culverts were analyzed using two finite element software: CANDE and ABAQUS and the results of the FEM are compared to the results obtained from the experiement of the deteriorated culverts. A linear-elastic model was employed for the Finite Element Analysis. The pipe was modeled as the equivalent plain shell element using the isotropic plate model for the conversion and the element type being the beam element while the soil was modeled using the Mohr Coulmb criteria using the CPE6M elements using the hourglass control. Also, the backfilling of the soil was modeled by activaiting

the soil up to the bedding and the culvert at first and then activating thr remaining soil layers. The interaction between the pipe and the soil in the model was cosidered as the fully bonded condition. To model the corrosion in the culverts, different properties were used in the upper part and the invert part of the culverts. For assigning the different properties around the the invert area, the area was divided into 8 areas whoes properties was reduced according to corrosion level while the upper part of the culvert was modeled using the intact pipe properties. After the analysis, the results obtained for deflection form the ABAQUS model was within the 6% of the measured diameter change and while since the linear elastic model was employed to get the results, non-linear beahviour was not captured by the model. From both the method, ABAQUS and CANDE, the thrust in the pipe was over estimated and among the two software the ABAQUS seemed to predict the thrust and the deflection more accurately than the CANDE. Similar to the previous other studies the study does not consider the complete corrosion or perforation of the invert condition.

Campbell,(2018) performed the FEM study in 3D to improve the 2D model of Mai et al.(2013). He performed the detail analysis of the intact pipe and deteriorated corrugated pipe along with the parametric studies using the Plaxis 3D software. For modeling the CMP he had used the orthotropic plate model while he had used different type of soil models ,such as linear elastic model, Mohr-Columb model and Hardeing soil model, to represent the soil in the analyis. The interaction between the pipe and soil was established as a fully bonded condition. Through the analysis he was able to improve the 2D model of Mai et. al (2013) successfully and was able to draw the number of the conculsions in his thesis. The major conclusions could be summaraized as:

- The non-linear models performed significantly better than linear model. Among the non-linera soil models Hardening soil model estimated the deflection, bending moments,and thrust better.
- For the intact pipe, maximum thrust due to dead load was found to be in the springline while in the live load conditions the maximum thrust shifted to the crown of the pipe
- The soil friction angle had the minimal effect while the secant modulus of the soil had the significant effect in the pipe force system.
- In case of the deteriorated pipe, it was found that corrosion significantly reduces the factor of safety against buckling and yielding but there was less reduction in the force carrying capacity of the CMP due to corrosion.

Elshimi (2011) performed the detailed finite element analysis for the deep corrugated metal arch culvert. He modeled the culvert as both the actual corrugated section and equivalent orthotropic plane section. From his analysis he found that the equivalent orthotropic model was able to predict most of the culvert behavior like the actual corrugated section except the ultimate load, which was predicted 24% more than the load predicted by the corrugated section model and the experiments. He attributed this discrepancy in the ultimate load to the exclusion of the geometric non-linearity in the equivalent pipe. The actual geometry model was found to predict the load within the 3% of the experimental results.

All of the above study is performed for comparing to the field results but most of the experimental tests are carried in the confined spaces such as soil box system which may have considerable effect on the experiemental results if not addressed properly. Regarding the issue, Mai et. al. (2018) studied the effects of proximity of pipe sample to rigid wall boundary and the effects of wall friction on load transferred to the CMP. They carried out numerical simulations for different sizes of soil box with different clearance between the pipe and the rigid wall. They found that even when the clearance between the pipe and rigid wall was only 0.3D, the pipe could be tested without significant impact from proximity to the rigid walls. Additionally, they also investigated the effects of wall friction on the test. The friction of the high-stiffness rigid wall will take a significant amount of the applied surface load. Hence, the wall surface roughness needs to be treated to reduce the wall friction. Mai et al. (2018) investigated different methods to reduce

wall friction. Among them, application of a double layer of thin polyethylene sheeting with silicon grease lubrication in between was found to provide the best results with approximately 5° friction angle which significantly reduces the effect of wall friction.

Chapter 3: Experimental Work

To study the structural capacity of liners applied on circular and arch corrugated metal pipe (CMP), a soil box system was setup at the CURIE lab. First, control tests were performed on bare intact and invert removed CMPs as a baseline study. After establishing the structural capacity of the intact CMP and the invert removed CMP, next set up test was carried out for three invert-removed circular CMPs and three invert-removed arch pipes rehabilitated by the polymeric liners. In this chapter, a discussion of experimental setup and test results of invert-removed circular CMPs rehabilitated with spray-applied polymeric liners is presented. These experimental tests were used to calibrate the finite element work which is later discussed in Chapter 4. All the test results and the details of the experiment belongs to Center for Underground Infrastructure Research and Education (CUIRE).

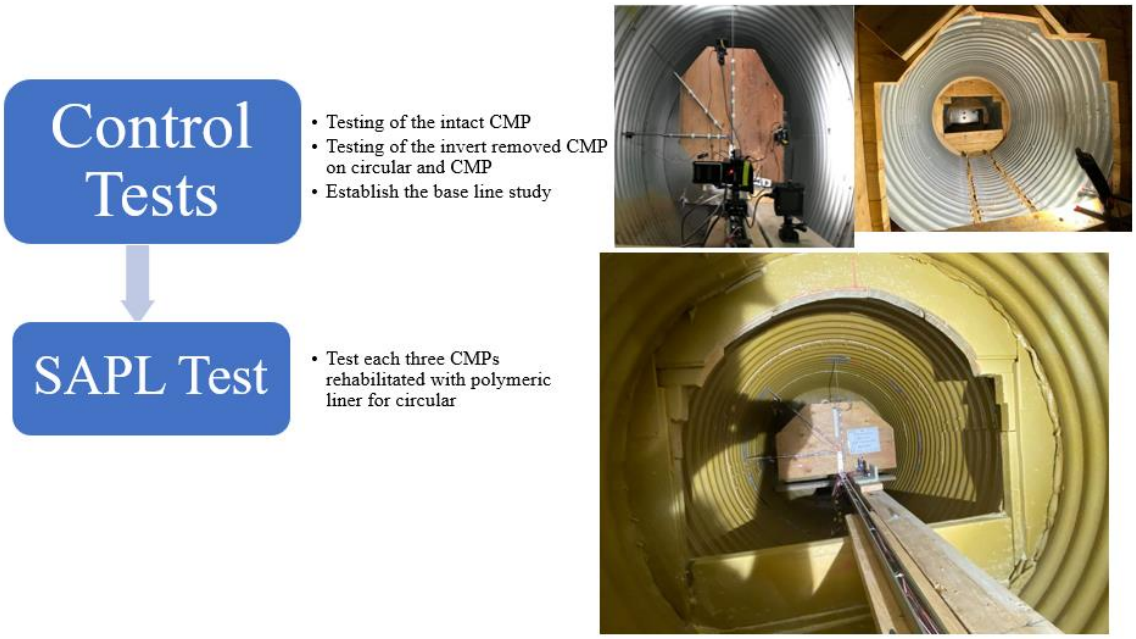

Figure 3-21 Experimental test plan (Source: CUIRE Laboratory)

3.1 Test Plan

3.1.1 Geometry of the soil box

A 25'x12' soil box, 10' depth was divided into three segments (Figure 3-22). Each of the segments were 6 ft. in length and were separated by 2 in. thick wooden partition walls. The wooden partition wall was braced at each end and its stability under the application of the load was checked through theoretical calculations and FEM method. The depth of foundation, embedment and soil cover was 2 ft., 5ft. and 2 ft. respectively.

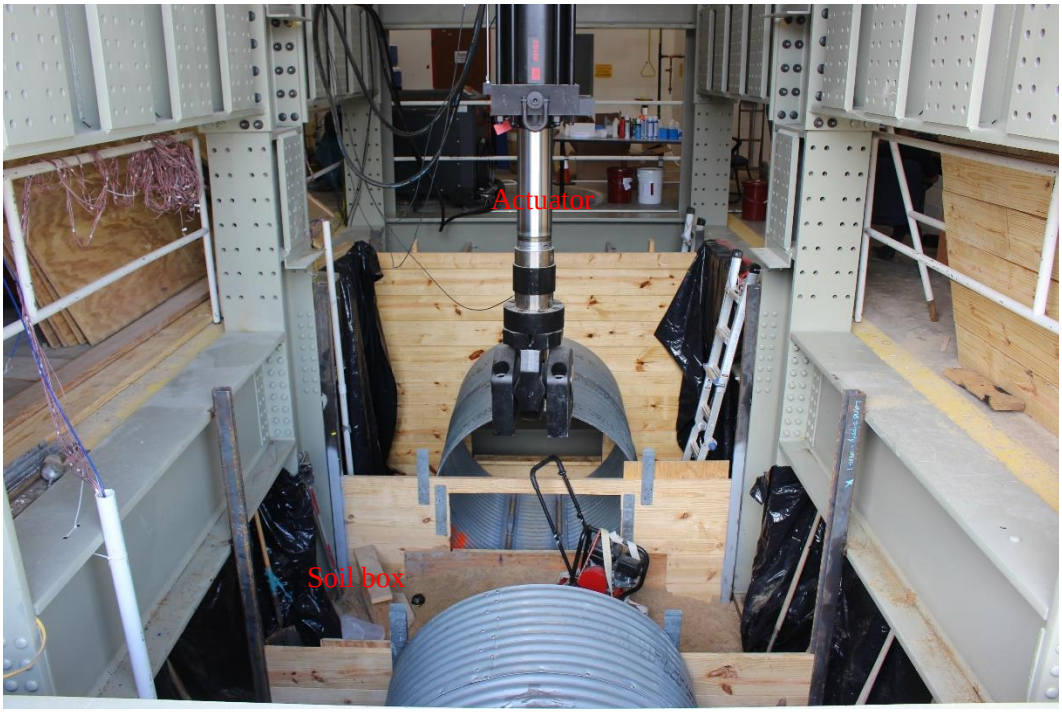

Figure 3-22 Lab setup (Source: CUIRE Laboratory)

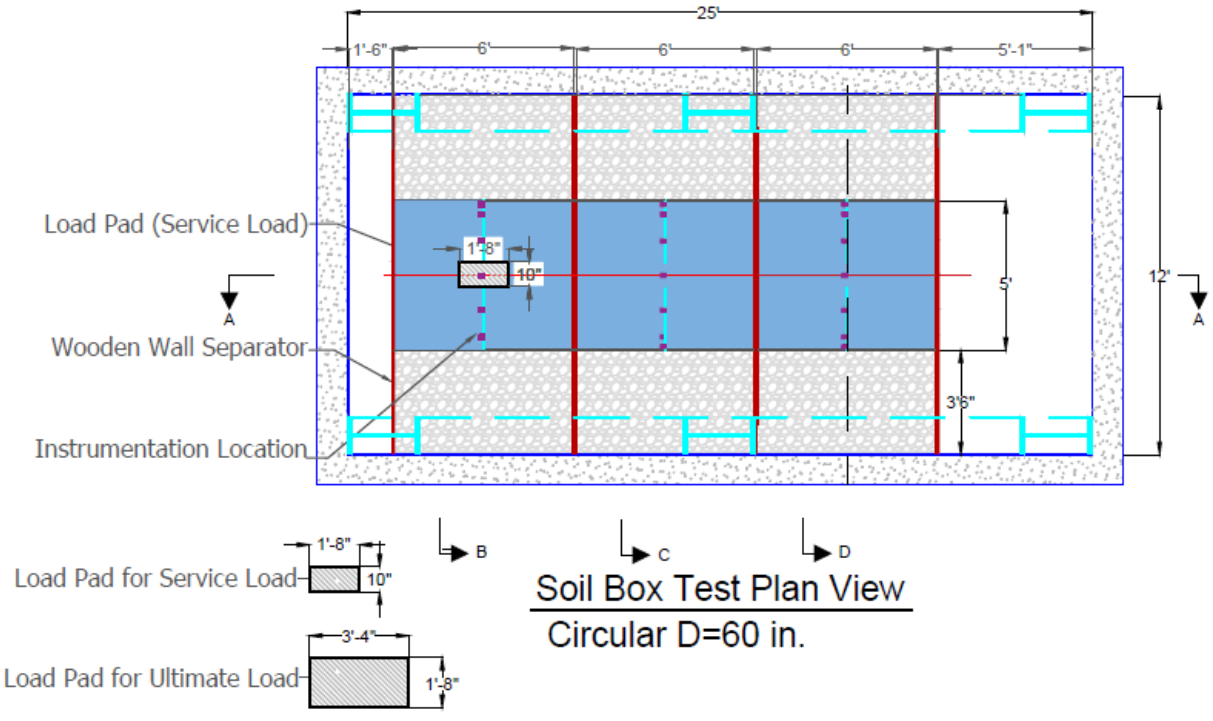

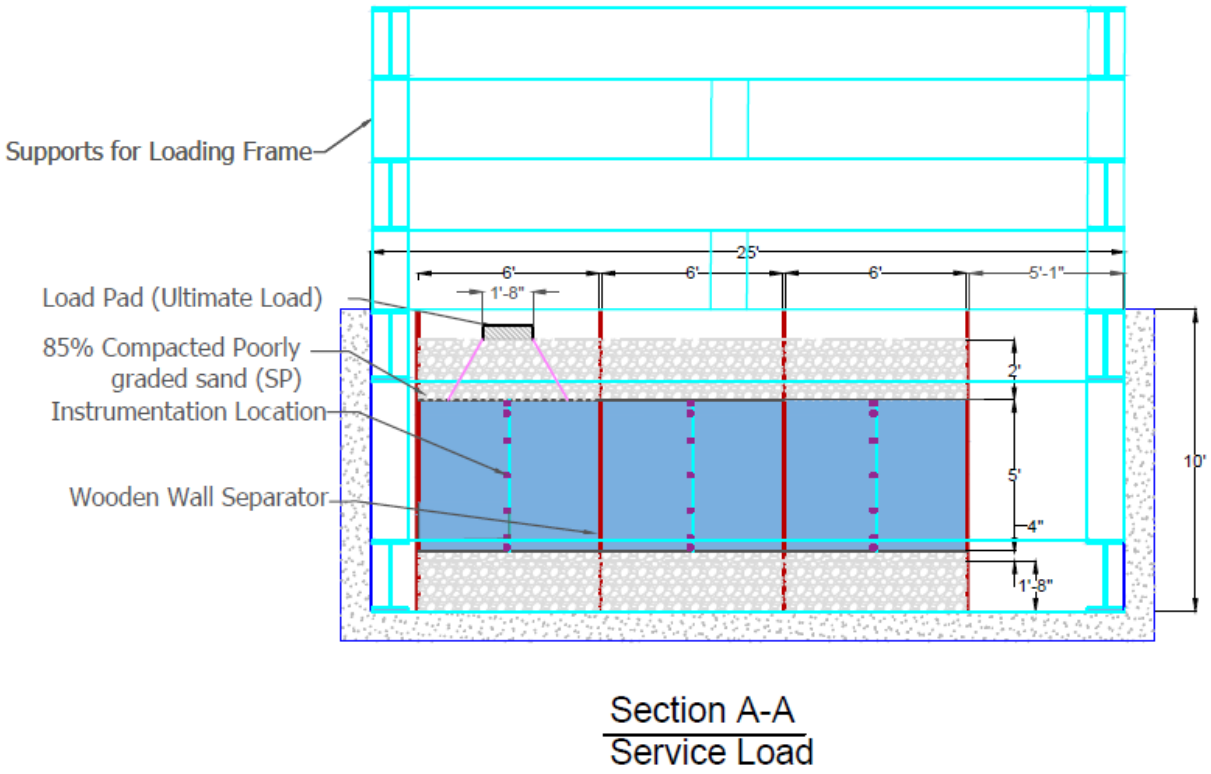

Figure 3-23 (a) Plan view of the soil box setup (b) Sectional view of the soil box for circular lined pipe

(Source: CUIRE Laboratory)

3.1.2. Pipe geometry

To check the application and performance of spray applied liners two types of the CMPs were used viz. arch and circular CMPs. Both CMPs had the same corrugation profile (2 2/3"x1/2"), length (6 ft) and thickness (0.109 in.) (Figure 3-24). The diameter of the circular pipe was 60 in. (Figure 3-25) while the arch pipe had 72 in. span and 47 in. rise.

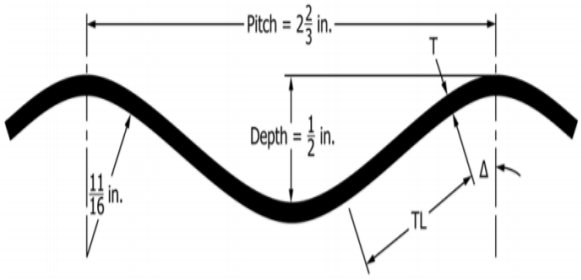

Figure 3-24 Corrugated profile section with dimension as per ASTM 796-17 a

To represent the deterioration in CMP, the CMPs were fabricated in such a way, 18 in. of the invert from the CMPs could be removed once it was buried in the soil (Figure 3-25).

Figure 3-25 (a) Intact CMP (b) CMP with invert removal arrangement

(Source: CUIRE Laboratory)

3.1.3 Foundation, Embedment and Backfill soil

Granular soils were chosen as backfill material to achieve higher degree of control over the soil properties as granular soils are less prone to change with the variation of the moisture content in the field (Chimauriya, 2019). It was found that past experimental studies on the buried culverts made by Mai, et al. (2013), Regier et al. (2018), Arockiasamy et.al (2006) used sandy gravel and sandy soils as the backfill materials. Also, according to study made by Drenvich & Evans (2007) granular soil would achieve the maximum density at either zero saturation or fully saturated state. Thus, addition of the moisture to achieve the maximum density during compaction was not required.

A total of three types of soil were used to backfill the soil box. For the foundation and embedment layers poorly graded sand (SP) was used. While for the top 1 ft. of the cover, poorly graded gravel (GP) was used for the control test. Although the use of the gravel prevented the early failure of the soil, the bearing capacity of the GP soil was not enough to prevent the failure of the soil before the failure of the liner and the CMP. Thus, to avoid the failure of soil prior to liner/CMP, in the 2nd test setup, the top 1 ft. layer of the soil was replaced by the TxDOT classified Grade D subbase layer which is also commonly referred as Recycled Concrete Aggregates (RCA).

Sieve analysis for the classification of sand and standard proctor test for determining the maximum dry density was carried out in the UTA Geotechnical lab.

a b

Figure 3-26 (a) Concrete Sand (b) Recycled Concrete Aggregates

(Source: CUIRE Laboratory)

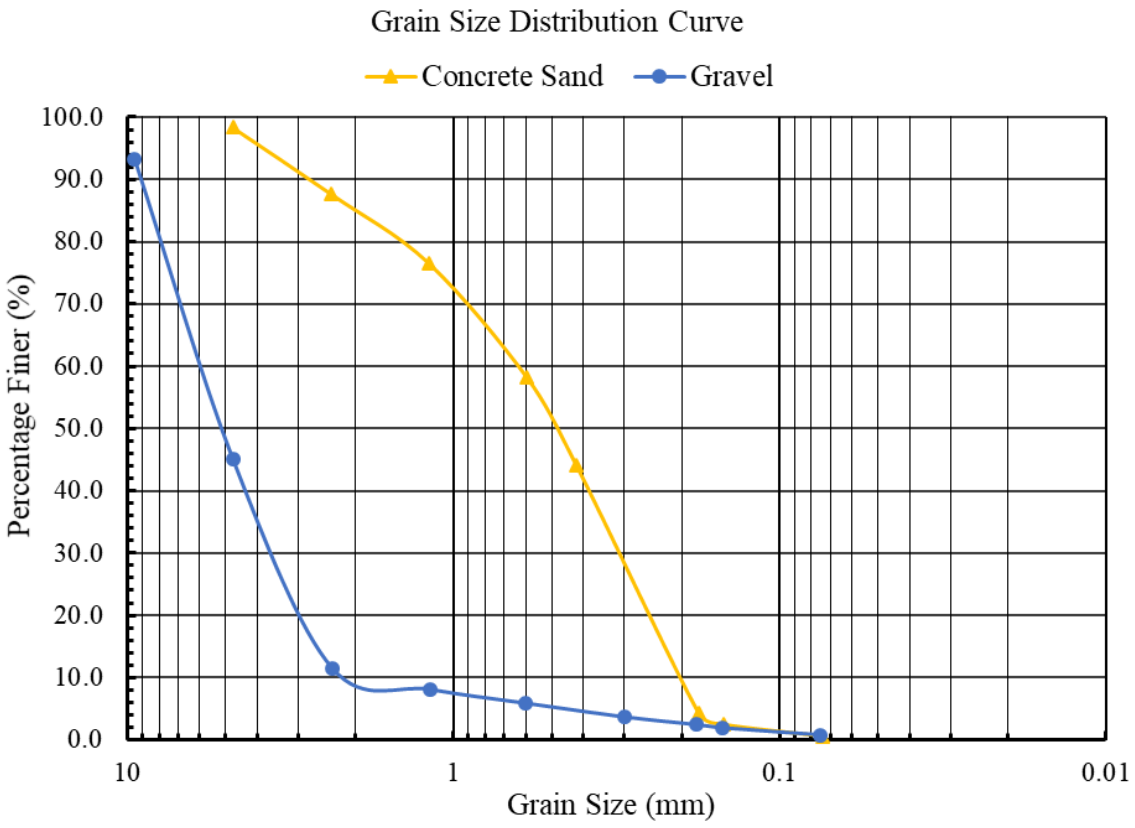

Figure 3-27 Sieve analysis results for the concrete (Chimauriya, 2019)

3.2 Installation Procedures

AASTHO construction specifications for buried culverts were followed for the installation of CMPs. AASTHO (2002) lists four types of construction specifications for buried culverts which are classified as Type 1 to Type 4 as shown in Figure 3-28. The type 1 construction specifies the highest quality of the

installation while the Type 4 installation specifies the least quality installation procedures. Among these installation criteria, for the critical load design, Type 3 installation procedure was adopted in our test plan. The installation procedures are shown in Figure 3-28,Figure 3-29Figure 3-29.

Installation type	Bedding Thickness	Haunch and outer Bedding	Lower side
Type 1	For soil foundation, use B_C/2.0 ft. minimum, not less than 3.0 in. For rock foundation use B_C ft. minimum, not less than 6.0 in.	95% SW	90% SW, 95% ML or 100% CL or natural soils of equal firmness
Type 2-Installation are available for horizontal elliptical, vertical elliptical and arch pipe	For soil foundation, use B_C/2.0 ft. minimum, not less than 3.0 in. For rock foundation use B_C ft. minimum, not less than 6.0 in.	90% SW, 95% ML	85% SW, 90% ML or 95% CL or natural soils of equal firmness
Type 3-Installation are available for horizontal elliptical, vertical elliptical and arch pipe	For soil foundation, use B_C/4.0 ft. minimum, not less than 3.0 in. For rock foundation use B_C ft. minimum, not less than 6.0 in.	85% SW, 90% ML or 95% CL	85% SW, 90% ML or 95% CL or natural soils of equal firmness
Type 4	For soil foundation no bedding required. For rock foundation use B_C ft. minimum, not less than 6.0 in.	No compaction required except if CL, use 85% CL	85% SW, 90% ML or 95% CL or natural soils of equal firmness

Figure 3-28 Installation Procedures requirements specified by AASTHO (2002)

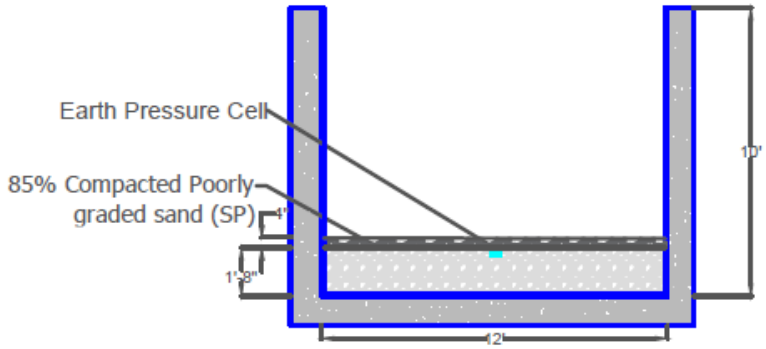

Step 1. Placing Foundation and Bedding

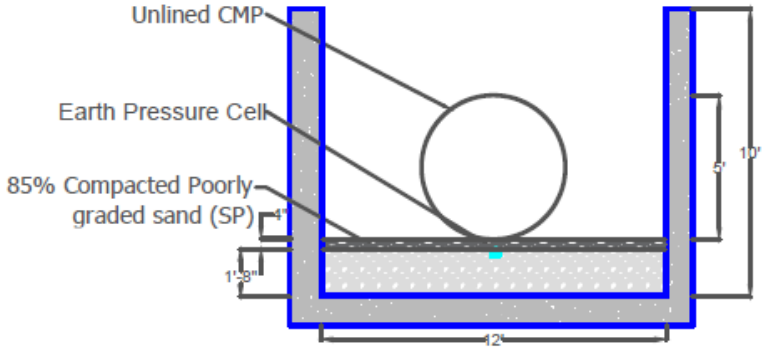

Step 2. Placing Bare CMP

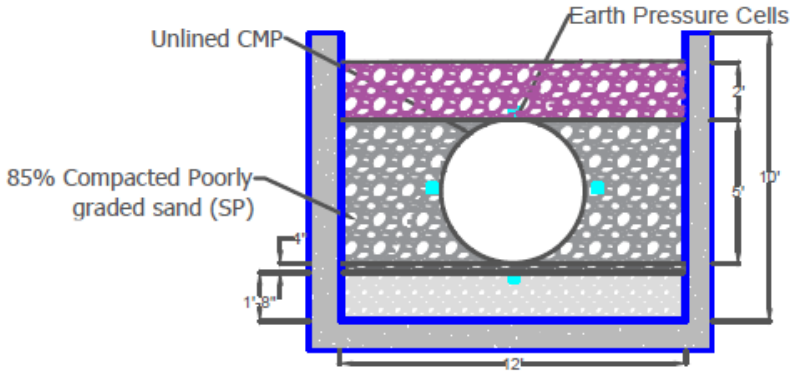

Step 3. Embedment and Backfilling

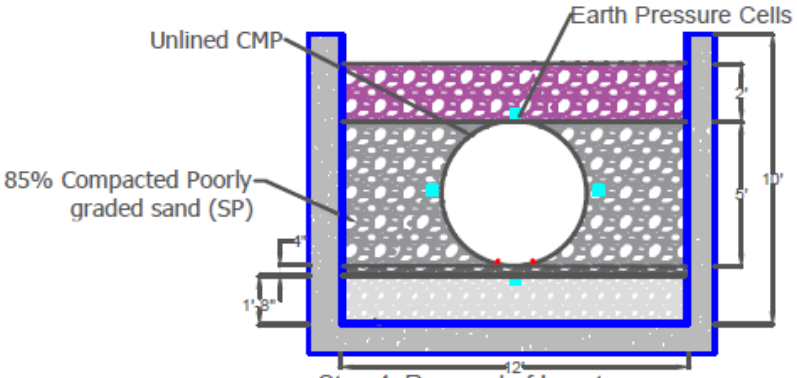

Step 4. Removal of Invert

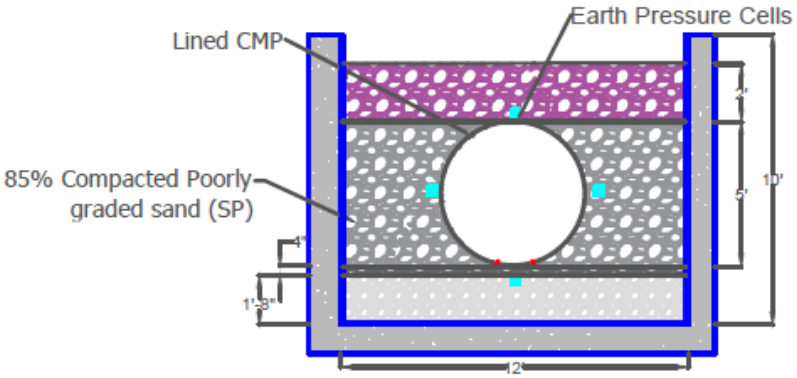

Step 5. Lining the CMP

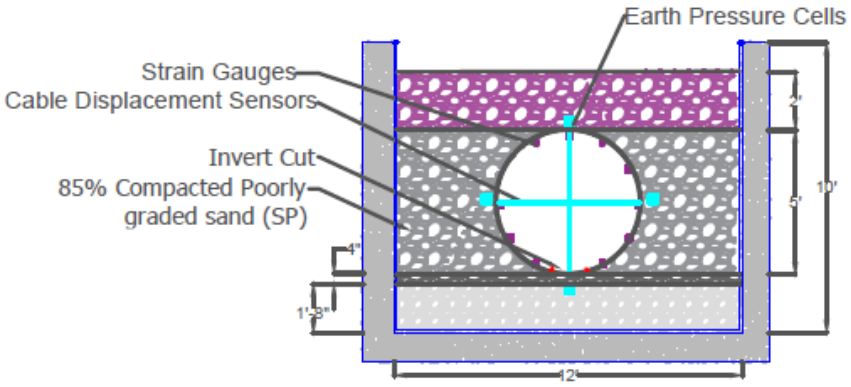

Step 6: Installing Strain Gauges and Cable Displacement Sensors

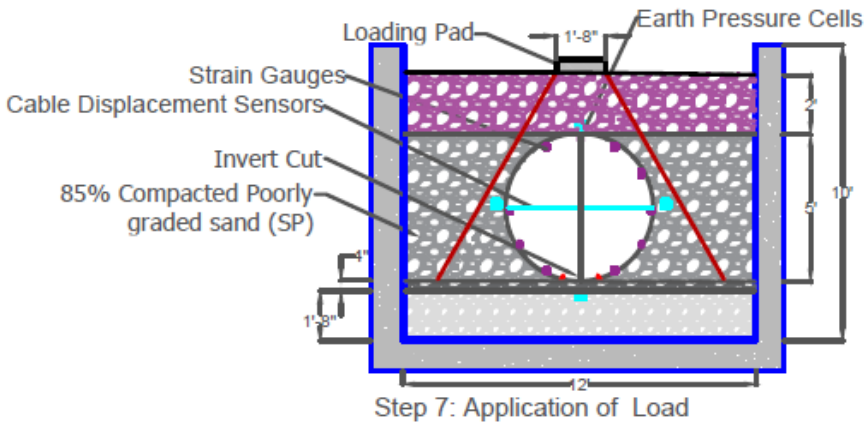

Figure 3-29 Installation steps in the soil box (CUIRE, 2018)

3.2.1 Burial Configuration

(a) (b)

(c)

Figure 3-30 (a) and (b) Placing of the soil (c) Measurement of the density via Nuclear density gage (Source: CUIRE Laboratory)

The depth of the soil box is 9 ft. The depth of the foundation layer is 2 ft. compacted to 95% of proctor density using two passes of vibratory plate compactor. The density measurements were taken using nuclear density gage, courtesy of HVJ Associates, and Braun Intertec. After the placement of foundation, a 6 in. bedding is placed in which the middle one third is loosely placed as per the recommendation from AASTHO's installation guide (Figure 3-29). Once the bedding is prepared, CMPs are placed and backfilling of embedment is done. The embedment is backfilled with lift thickness of 8 in. and no compaction is applied on the embedment because just placing the SP gravel, the compaction level of more than 85% was achieved. The average measurements of the density of the placed fill is shown in the Figure 3-31. Fill height of the embedment is 5 ft. The same process is followed for backfilling the 1 ft. cover. Remaining 1 ft. of cover is backfilled using poorly graded gravel (GP) for control test and for circular liner test, it was replaced with TxDOT specified Grade D sub-base layer.

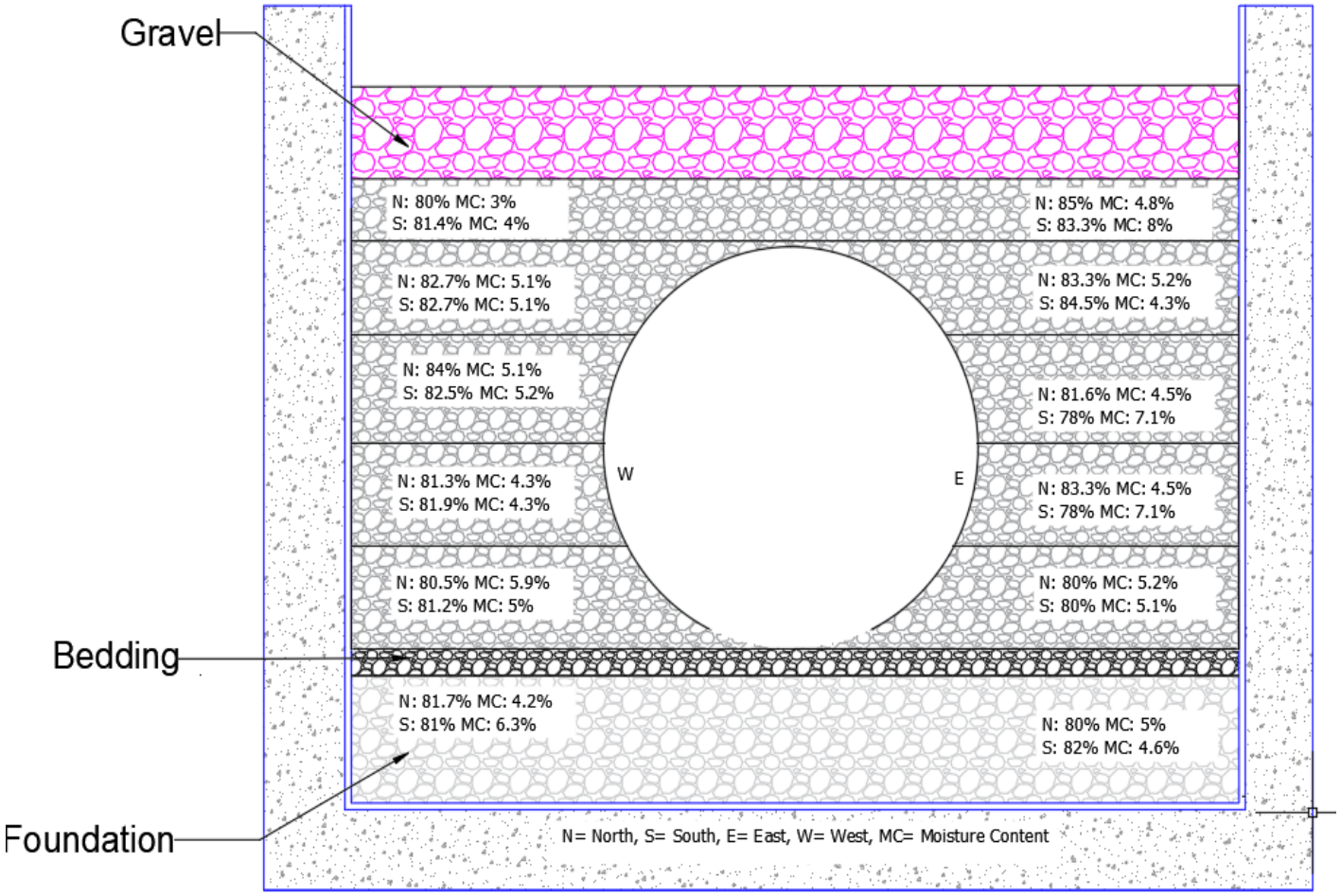

Figure 3-31 Compaction value around the soil (Darabnoush Tehrani, et al., 2020)

(Source: CUIRE Laboratory)

3.2.2 Instrumentation

The CMPs were instrumented thoroughly using the different types of the instruments such as LVDTs, Cable Displacement Sensors (CDS), Uniaxial Strain Gauges and Earth Pressure Cells. Three cameras were placed inside the pipe during testing in order to monitor the continuous change in the CMP profile during the application of the load.

Three LD620-150 LVDTs from OMEGA were placed inside the CMP to record the horizontal and vertical displacement at crown, shoulder and springline. Two WPS-500-MK30-P10 CDSs from GEOKON were installed to measure the change in diameter of pipe along crown-invert and springline sections. An AC-DC battery was used to provide excitation voltage for both the sensors and GL-820 data acquisition system from Graphtec was used to record the data. The configuration of the LVDTs and CDSs sensors inside the CMP with the data acquisition system is shown in Figure 3-32. For all the test same configurations were followed.

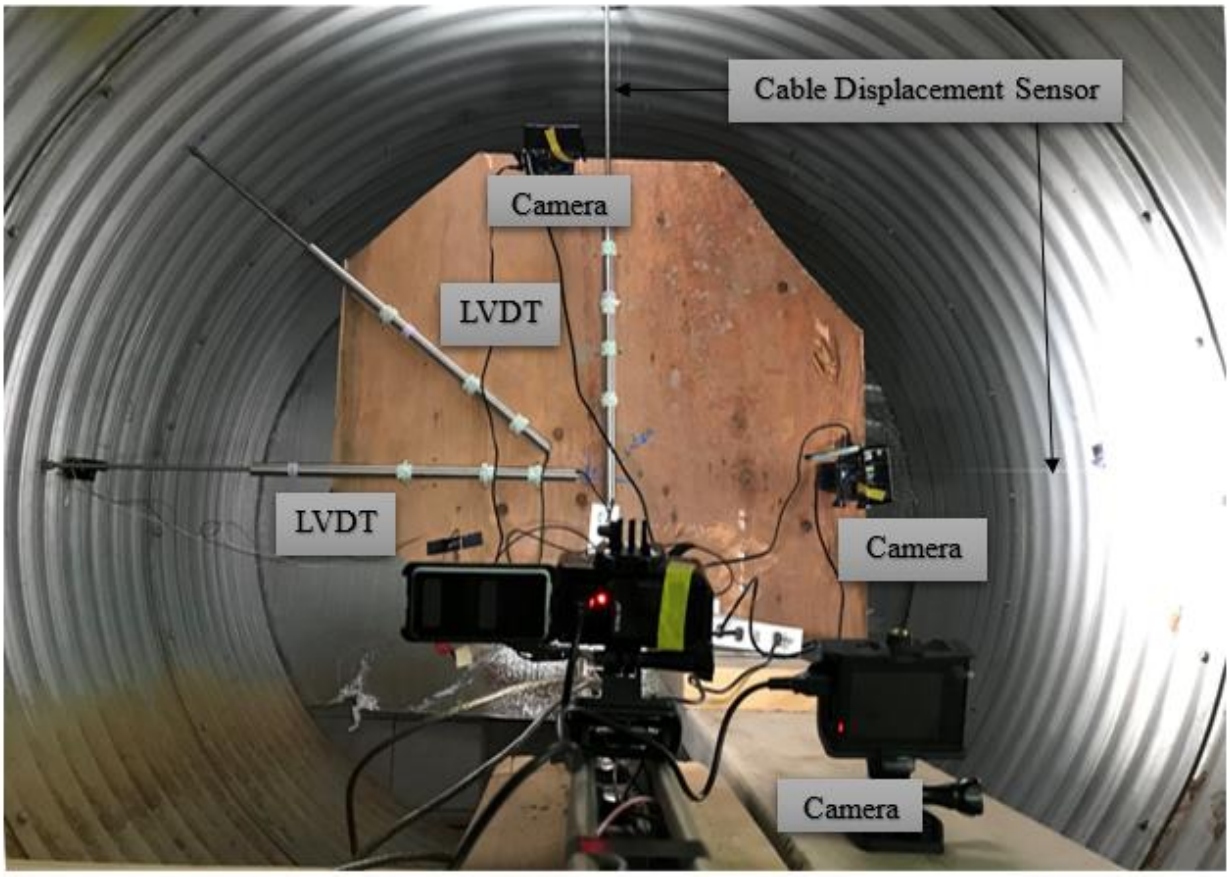

Figure 3-32 LVDTs and CDS sensor arrangement ((Chimauriya, 2019), Source: CUIRE Laboratory)

Four earth pressure cells were used to measure the increase in pressure during the application of the load. The earth pressure cells were placed at invert, on either side of spring-lines and at crown. All the earth pressure cells were placed 4 in. away from the CMP in order to eliminate the point load effect on the sensors provided due to corrugated shape of the CMPs. The earth pressure cells were from GEOKON, model 4815-350 kPa. LC-2X16 Series (Model 8002) vibrating wire data logger from GEOKON was used to collect the data using the LabView software. The arrangement of the earth pressure cells is shown in Figure 3-33.

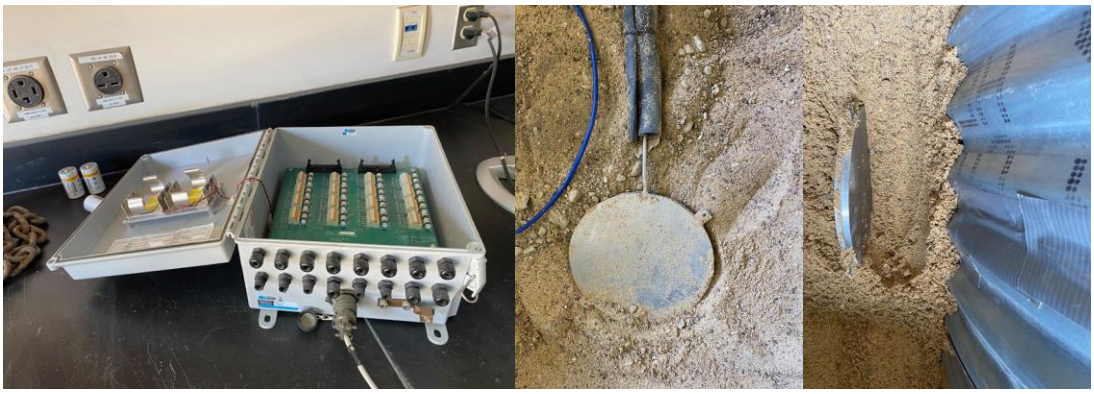

Figure 3-33 Data acquisition system for earth pressure reading, earth pressure cell placement (4 in. away from CMP) (Source: CUIRE Laboratory)

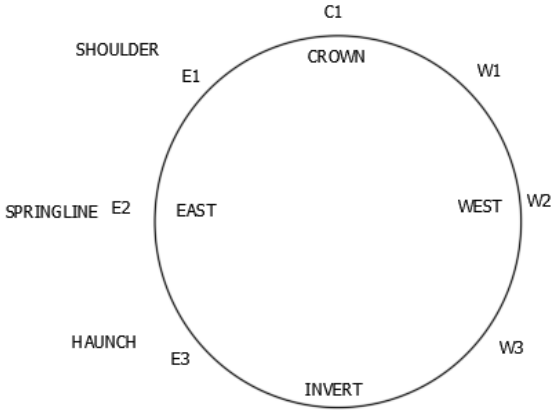

Figure 3-34 Location of the placement of strain gage along the circumference

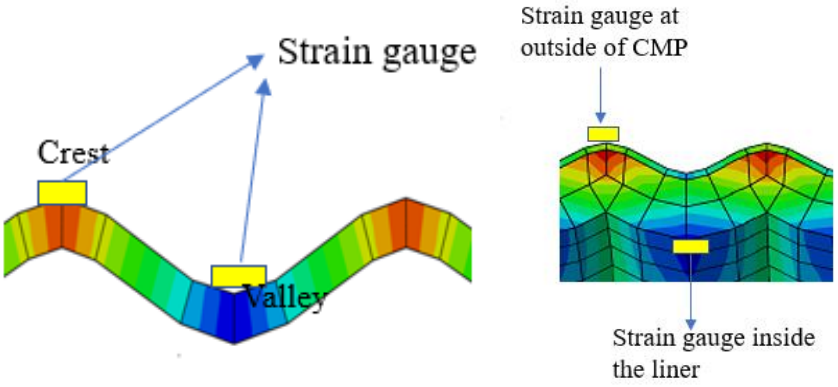

Figure 3-35 (a) Strains variation in the crest and valley of the CMP for control test (b) Strain gage placement in the CMP and the liner

(Source: CUIRE Laboratory)

To calculate the bending moment and the thrust, the change in the strains in the CMPs are required. For that reason, 16 uniaxial strain gauges, model C2A-06-250LW-120 from Micro-Measurements were used around the CMPs in the direction of the hoop stress at the center of the pipe. For control tests, strain gauges were placed in valley and crest on the outer face of the CMPs while after the application of the liner one layer of the strain gauges was placed in the outer crest while another layer of strain gages was placed in the inner valley of the CMP. The configuration of the strain gage for the control test and the application of the liner is shown in the Figure 3-34,Figure 3-35. The data were collected from the strain gages using System 7000 data acquisition system from Micro-Measurements. The nomenclature of the strain gages is presented in the Table 3-1 and same names are followed for all the data analysis after this.

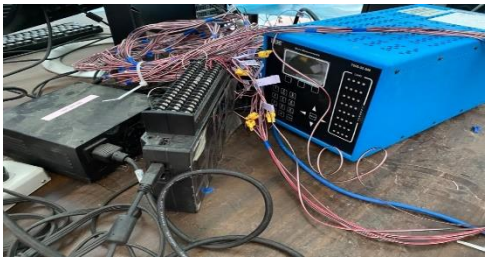

Figure 3-36 Data acquisition system for the strain gage (Source: CUIRE Laboratory)

Location	Layer	Designation
East haunch	Crest	E3-C
	Valley	E3-V
East springline	Crest	E2-C
	Valley	E2-V
East shoulder	Crest	E1-C
	Valley	E1-V
Crown	Crest	C1-C
	Valley	C1-V
Crown offset	Crest	C2-C
	Valley	C2-V
West shoulder	Crest	W1-C
	Valley	W1-V
West springline	Crest	W2-C
	Valley	W2-V
West haunch	Crest	W3-C
	Valley	W3-V

Table 3-1 Nomenclature for the strain gage (Chimauriya, 2019)

The strain gauges placed in valley were moved to inner face of the CMP in the liner tests. The nomenclature of the strain gauges were kept same as the control test (Figure 3-38).

Figure 3-33 Placement of strain gage in control test (Both outside) (Source: CUIRE Laboratory)

Figure 3-38 Strain gage in the inside of the CMP after the application of the liner

(Source: CUIRE Laboratory)

3.2.3 Removal of the Invert

Study conducted by Stratton et al. (1990) across the State of Kansas, found that 36% of the CMPs had rusted invert while 24% of the CMPs had heavily corroded invert. In the previous experimental studies, the invert deterioration was represented by reduction in wall thickness of the invert, (Mai et al., (2013), Regier et al., (2018)), which only represents partial deterioration of the pipe but not the perforated pipes. So, in order to represent the complete deterioration of the CMP's invert, it was decided to remove the 18" of the

invert of the intact pipe once the pipe was buried inside the soil. The arrangements for the invert removal process is shown in the Figure 3-35.

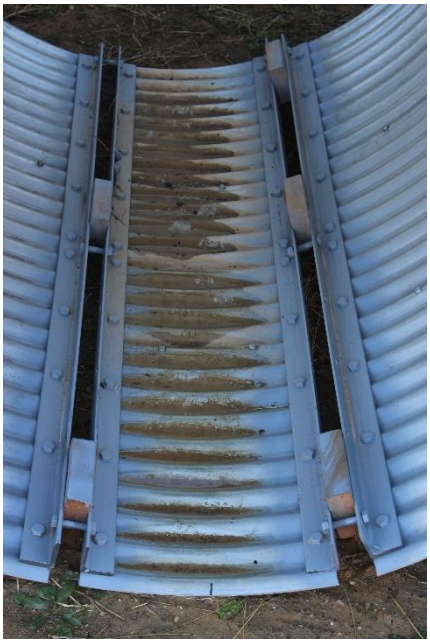

Figure 3-35 CMP with invert removal arrangement (Source: CUIRE LAB)

For the control test whole invert was removed completely from the CMP at once. A huge movement of the soil and the pipe was observed during the instantaneous removal of the invert. This instantaneous removal of the invert caused the damage on the installed instruments and made difficult to control the amount of movement and achieve consistency for all CMPs. Hence, instantaneous removal of complete invert was aborted. For lined CMPs, 1 in. strip of the invert was left off at the end of the CMPs and only the middle portion of the invert was removed (Figure 3-38). Once the pipe was lined, the remaining 1 in. strip of the invert was cutoff. Using these processes, it was observed that soil and CMP movement was minimal.

3.2.4 Application of the liner

After the control tests established base line data for structural capacity of intact circular CMP and invert removed CMP, the next sets of tests were done on the circular invert removed CMPs lined with the Spray Applied Polymeric Liners (SAPL). Three circular pipes were lined with SAPL for three thickness: 0.25 in., 0.5 in. and 1 in. The liners were applied by spraying in the layers with the layer thickness of 0.25 in. The complete curing time of the liner was 72 hours.

Figure 3-36 (Left) CMP just after removal of the invert (b) CMP ready for lining (Source: CUIRE LAB)

Figure 3-37 (Left) Spraying Process (Right) CMP after the application of the liner (Source: CUIRE LAB)

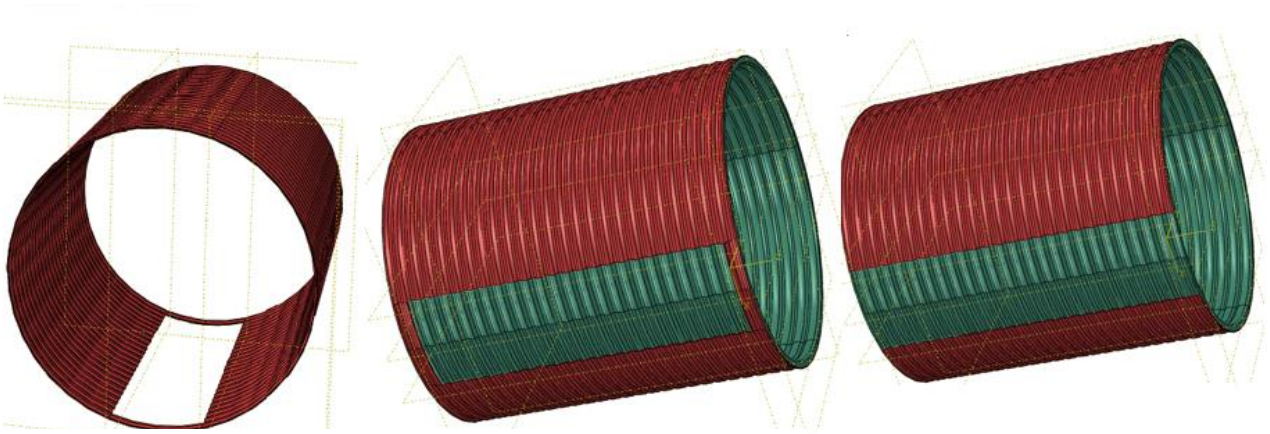

c. Removal of mid portion b. Application of liner a. Complete Removal of invert

Figure 3-38 Process of end strip removal

Figure 3-39 End Strip removed (Source: CUIRE LAB)

3.3 Loading Mechanism

According to AASHTO LRFD Bridge Design Specifications, the load through a vehicle on the pavement will be transferred as uniform stress over a rectangular area equal to the contact area of the wheels. Thus, the test is carried for tH20 truck with a service load of 16 kips from each wheel load Since, for an H20 truck, the contact area will be 10”x20” thus it was decided to choose the load pad size of 20”x10”. Figure 3-40 shows the pattern of load distribution through the top of the pavement to the top of the pipe. But during the first control test it was observed that load pad punched through the soil and failure of the soil was observed before the failure of the pipe which was not desirable condition for our test. Hence to prevent the failure of the soil before the failure of the CMP and the liner the smaller load of size 10”x20” was replaced by the load pad of the size of 40”x20” for the invert cut bare CMPs onwards.

For a test, to provide the suitable loading rate is an important aspect to get proper and accurate results. So, a detail study was carried out to select a suitable loading rate. A loading rate could either be force controlled

or displacement controlled. The force-controlled loading rate is used when we know the limit of the load to be applied in the structure. While the displacement-controlled loading rate is applied when we want to know the post failure behavior of the certain structure and determine the ultimate load for that structures. In displacement-controlled mechanism, it reads the displacement when the load is being applied and since the displacement of the structure always keeps on increasing even when the load drops which thus provides the post failure condition for the given structure.

For flexible pipes, ASTM suggests the displacement control mechanism. ASTM D2412, which provides the guidelines for parallel testing of plastic pipes, suggest the loading rate of 0.5 in./min. While for the soil, ASTM D1633 suggest the 0.05 in./min of the loading rate to determine the compressive strength from unconsolidated undrained triaxial compression test. But since the parallel load test is for the standalone pipe so its loading rate could not be adopted directly for the soil-pipe interaction system.

Referring to the previous studies made on the buried pipe such as Lougheed (2008) used the 0.039 in./min to perform the test on deeply buried large span corrugated metal pipe. Also, similar study carried out by Sargand and Hazen for plastic pipes chose a load rate ranging from 0.01 to 0.06 in./min.

Hence referring the previous studies and ASTM standards the load rate of 0.03 in./min was chosen.

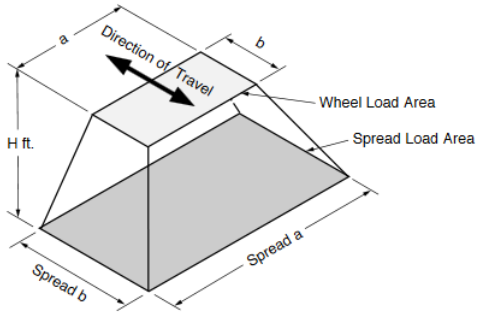

Figure 3-40: Load distribution below the wheel area (American Concrete Pipe Association, 2009)

3.4 Results

The results obtain form the test are discussed in the following section

3.4.1 Intact CMP

The intact CMP was tested under the load pad size of 10x20 in^2 (Figure 3-41) with the cover backfilled with Poorly Graded Gravel (GP). The loading rate as mentioned earlier was 0.03 in./min. The results are discussed below.

Figure 3-41 Loading of the intact CMP (Source: CUIRE LAB)

i. Load displacement plot

The load-displacement plot for both pipe and soil were plotted independently with the applied load. It was observed that, since the load pad was small, the load pad punched through the soil at around 21 kips of load and 5 in. displacement i.e., failure of soil occurred before the failure of pipe. The failure mode of the pipe was local buckling at crown just below the load pad. Before the failure of soil, the soil was displaced by about 5 inches while the displacement just below the crown was observed to be 1 inch. The ultimate load of the system was 25 kips.

Displacement was recorded at the spring line of the CMP using LVDT. It was observed that the displacement at the springline was only 0.294 in. at 21 kips of load and it remained constant at the ultimate load condition of 25 kips. The movement of the shoulder was found to be 0.76 in. at 21 kips of load while at 25 kips the shoulder displacement was observed to be 0.757 in. Figure 3-43,Figure 3-44 shows the plot of the load displacement for the soil and CMP.

Figure 3-42 Deformation of the CMP after loading (Source: CUIRE LAB)

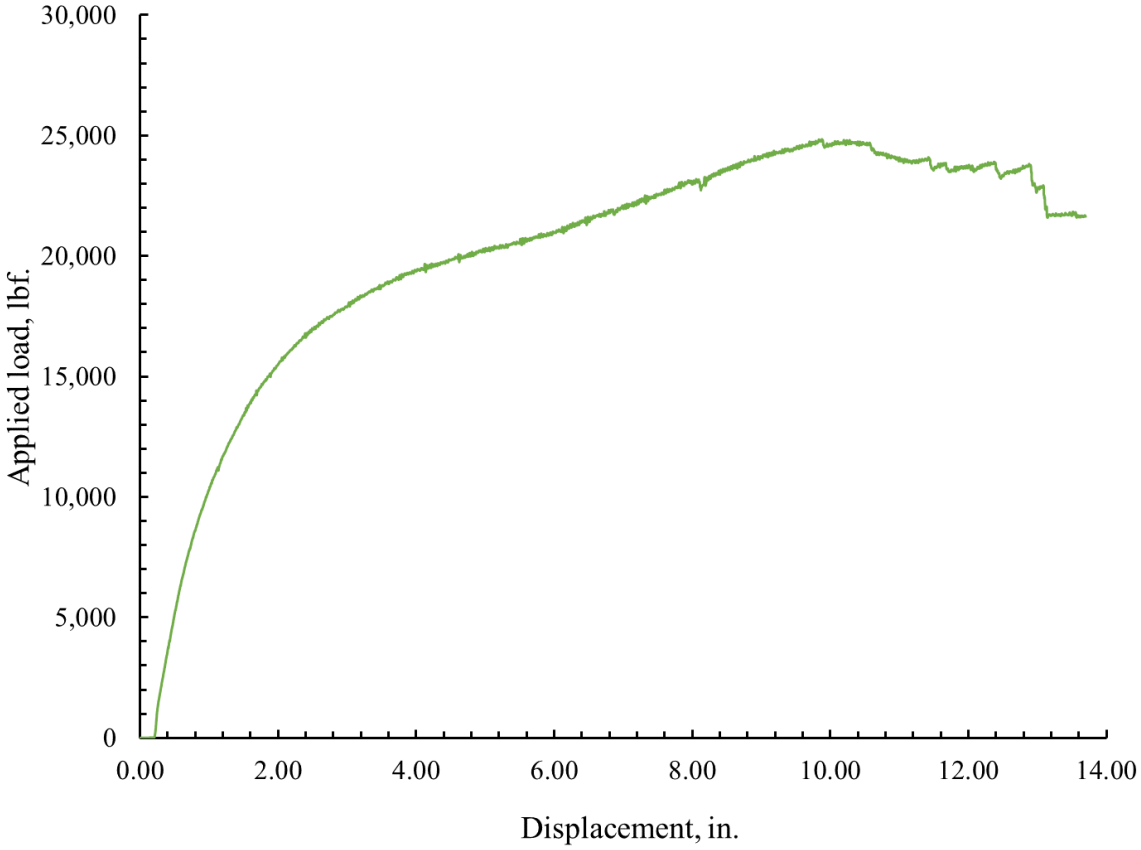

Figure 3-43 Load-displacement curve for soil for intact CMP (Chimauriya, 2019)

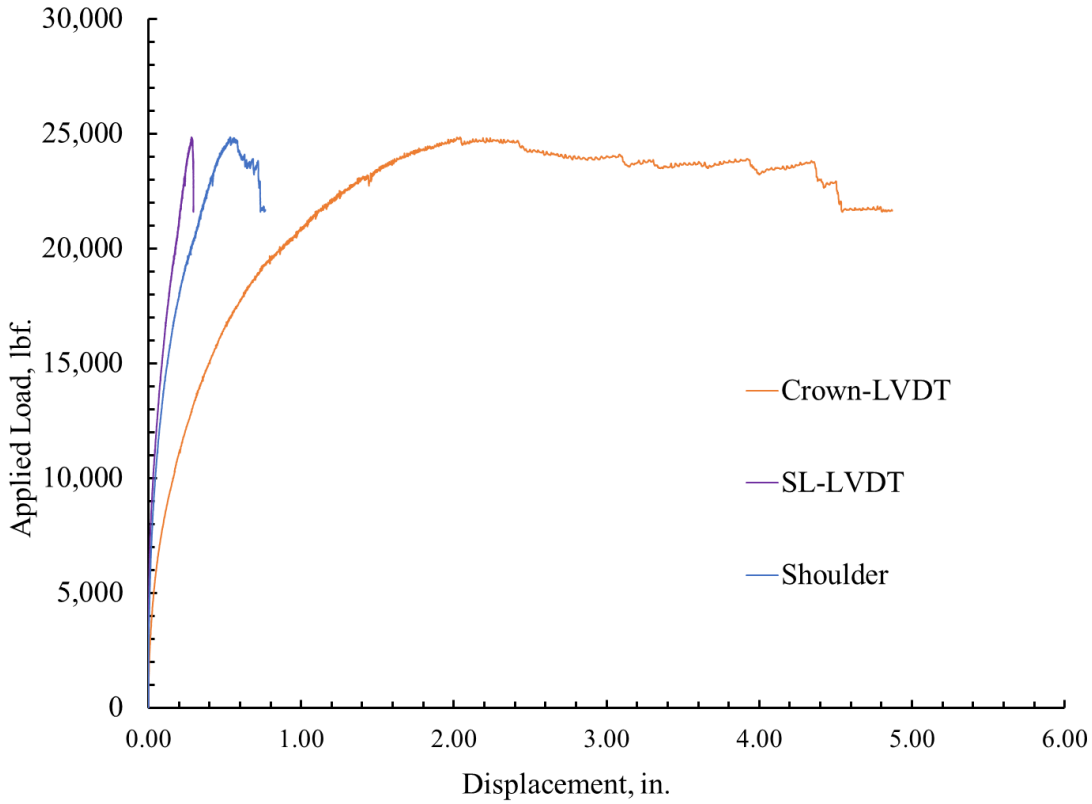

Figure 3-44 Load-displacement curve for the displacement in the crown, springline and shoulder for intact CMP (Chimuriya, 2019)

ii. Earth Pressure

Earth pressures were monitored at four different locations using the earth pressure cells. It was found that maximum earth pressure occurred just above the crown, below the load pad. On the other hand, other load cells at sides and invert did not show significant amount of change in pressure. This may be because with small load pad size, the load transfer area following the 1:2 rule lied within the pipe and did not go outside of the pipe. The maximum pressure during the punching of the soil was 42 psi and at the ultimate load it reached to 81 psi. The plots of the pressure vs. soil displacement is shown in Figure 3-45.

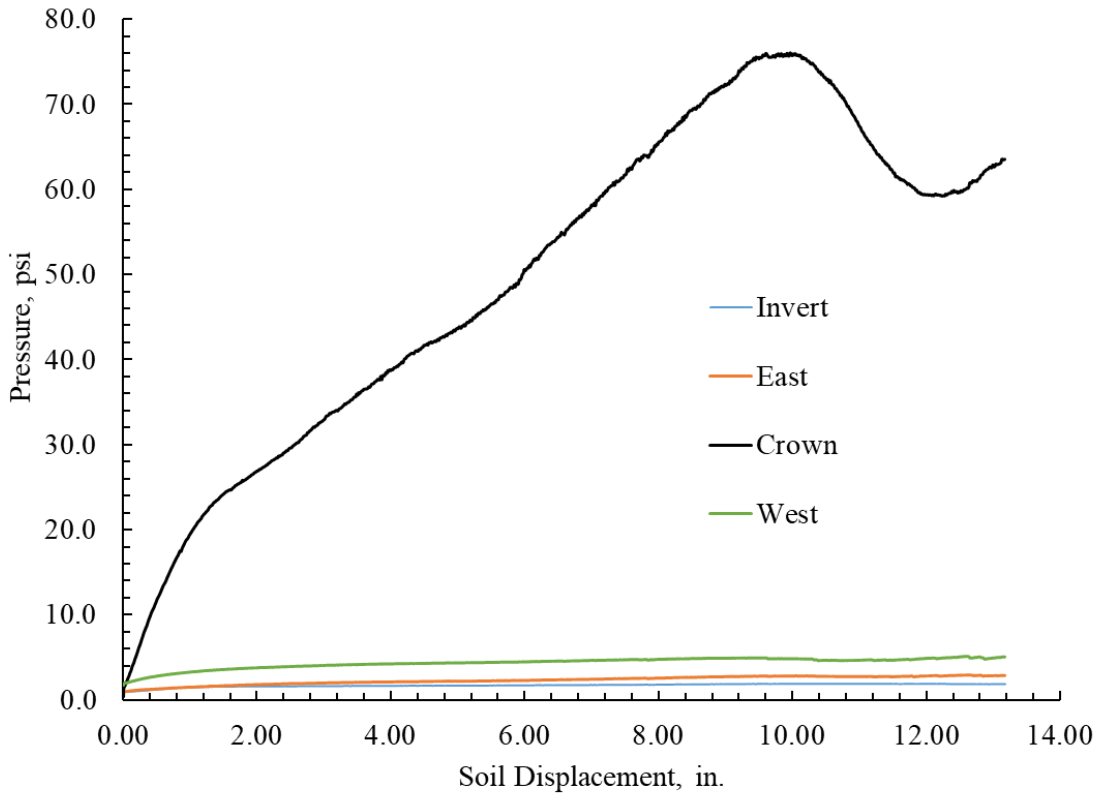

Figure 3-45 Earth Pressure Distribution for the intact CMP (Chimauriya, 2019)

iii. Strains:

The strain gages placed around the circumference of the CMP as shown in Figure 3-34. The strains were later plotted against the displacement of the soil.

These strains recorded were used to calculate the bending moments and the thrust in the CMP later in the Finite Element Analysis. The plot between the strains and the soil displacement shows that after the failure of the soil at 5 in. of soil displacement the strains increased sharply at the crest and the valley located at the top of the CMP. This sharp increase may be attributed to the fact that after the failure of the soil the pipe started to take mode load thus giving high change in strain. Figure below shows the plot of the soil displacement vs strain at different location.

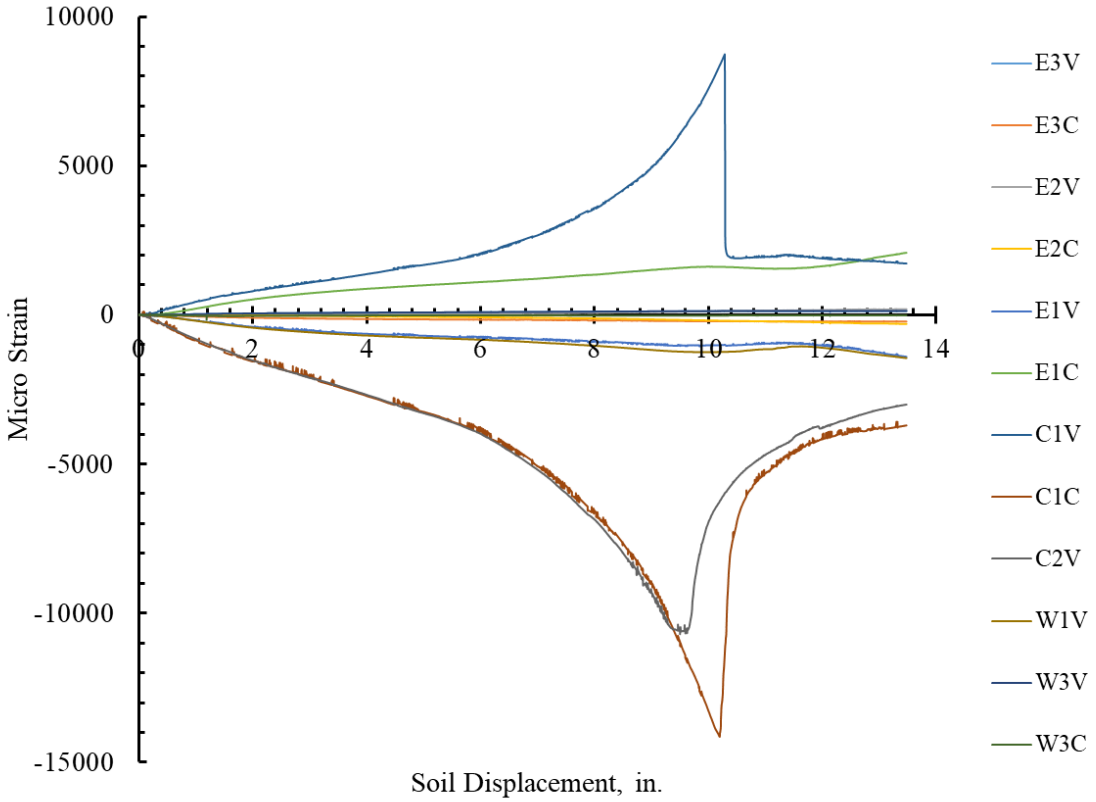

Figure 3-46 Strains around the CMP for intact pipe (Chimauriya, 2019)

Assuming linear distribution of strain, the circumferential bending moment and thrusts at different locations in the CMP were calculated by using the strain from crest and the corresponding valley as follow (Elshimi 2011):

$$M_\theta = \frac{EI_\theta(\varepsilon_{crest} - \varepsilon_{valley})}{d}$$

where:

M_θ= Circumferential bending moment (lbf-in./in.),

I_θ= Moment of inertia per unit length in the circumferential direction (in.4/in.),

ε_{crest}= circumferential strain measured at crest of the corrugation,

ε_{valley}= circumferential strain measured at valley of the corrugation,

d= depth of corrugation (in.), and,

$$N_\theta = \frac{EA_\theta(\varepsilon_{crest} + \varepsilon_{valley})}{2}$$

where:

N_θ= circumferential thrust (lbf/in.),

A_θ= cross-section area per unit length in the circumferential direction.

3.4.2 Invert Cut CMP

Since for the intact test it was observed that failure of the soil occurred prior to the local buckling of the pipe and from the pressure cells it was observed that effect of the load on the spring line was very minimal. So, to prevent the premature failure of the soil the small load pad (10x20 in^2) was replaced by the bigger load pad (20x40 in^2).

Figure 3-47 Load pad arrangement for invert cut CMP test (Source: CUIRE LAB)

The invert was removed after the CMP was buried in the soil. During the detachment of the invert, due to the complete loss in the ring stiffness and active pressure from the soil, the movement in the CMP and the soil was observed. It was observed that the soil settled by more than 6 inches just above the CMP while for the CMP itself, the measurement showed the pipe sample moved 3.1 in. vertically and 3 in. (7.62 cm) horizontally (Darabnoush Tehrani, et al., 2020). Also, it was observed that the pipe got rotated slightly. The pipe movement was monitored during the invert removal through Digital Image Processing (Figure 3-48) (Darabnoush Tehrani, et al., 2020).

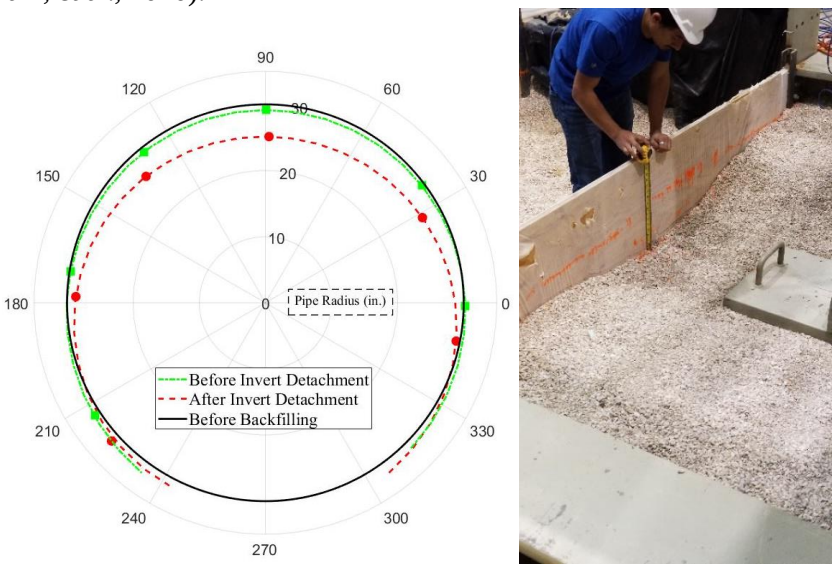

Figure 3-48(Left) Movement of the CMP monitored during the invert removal through Digital Image Processing (Darabnoush Tehrani, et al., 2020), (Right) Settlement of soil after invert removal

After the invert detachment the CMP was loaded with the loading rate of 0.03 in./min. and the results obtained are discussed below:

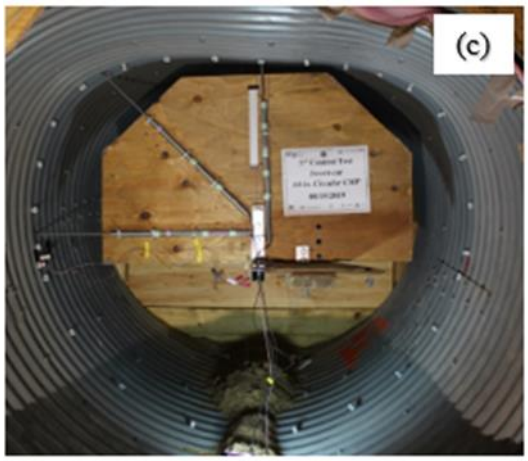

Figure 3-49 Deformation of the invert cut CMP after complete loading (Source: CUIRE Laboratory)

i. Load Displacement plots:
Initially, it was observed that the pipe-soil system showed the stiff behavior up to the 4 kips of load in which almost insignificant displacement of the pipe soil system was observed. This steep rise in the load initially may be attributed to the friction resistance developed due to the movement of the CMP during the removal of the invert. After the static frictional resistance was overcome, the CMP started to move continuously inside without much increase in the load until the two-cut part ends met and CMP's ring stiffness was re-established. Until the two-cut end meet it was observed that CMP had squeezed by 5 inches along the spring line while the vertical diameter reduced by 3 inches (Figure 3-51). But the load taken until that point was less than 10 kips of load. After the re-establishment of the ring stiffness of the pipe it behaved like the new pipe and took the ultimate load of 37 kips. Ultimately the CMP failed due to local bending at the top instead of the local buckling.
This unusual phenomenon may not be seen in the field even after the complete loss of the invert. As it is known that the invert corrosion process is slow process and would take years of time to cause the corrosion of the complete invert. By the time of the complete corrosion of the invert, the CMP's wall also corrodes simultaneously increasing the friction between the CMP and the soil thus restricting the huge movement in the above pavement and the CMPs.

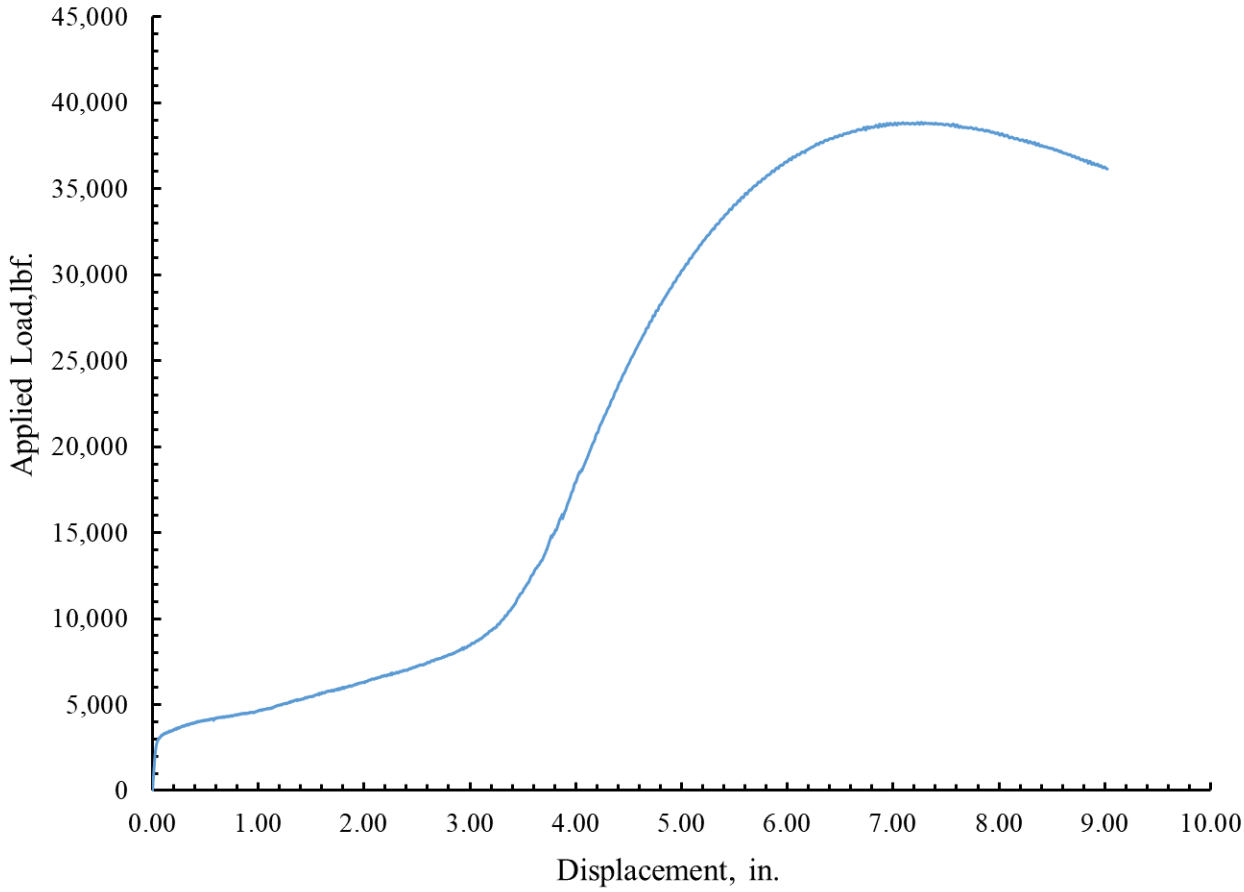

Figure 3-50 Load-displacement curve for soil in invert removed CMP

(Source: CUIRE Laboratory)

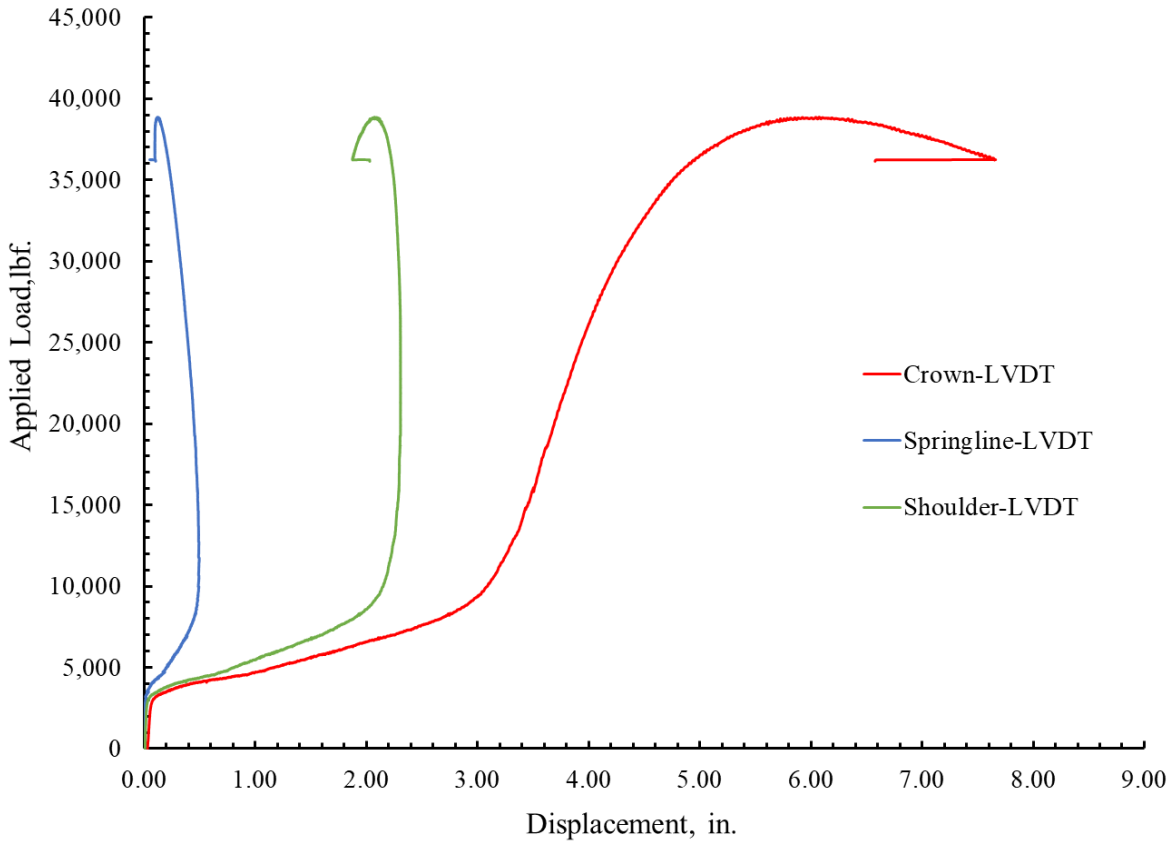

Figure 3-51 Load-displacement curve for the displacement in the crown, springline and shoulder for invert cut CMP (Source: CUIRE Laboratory)

ii. Earth Pressure Distribution

The earth pressure cells located at the invert, spring lines and the crown recorded the pressure in around the pipe. Like the intact pipe the maximum earth pressure was shown by the earth pressure cells located just above the crown. The crown also recorded low pressure of about only 5 psi until the re-establishment of the ring stiffness. After the establishment the pressure rose to the about 30 psi till the failure of the CMP and the soil system.

The earth pressure located at the other places showed little change in the pressure. But due to use of the larger load pad the pressure in the springline was significant at around 10 psi of load. The invert showed no increase in the pressure.

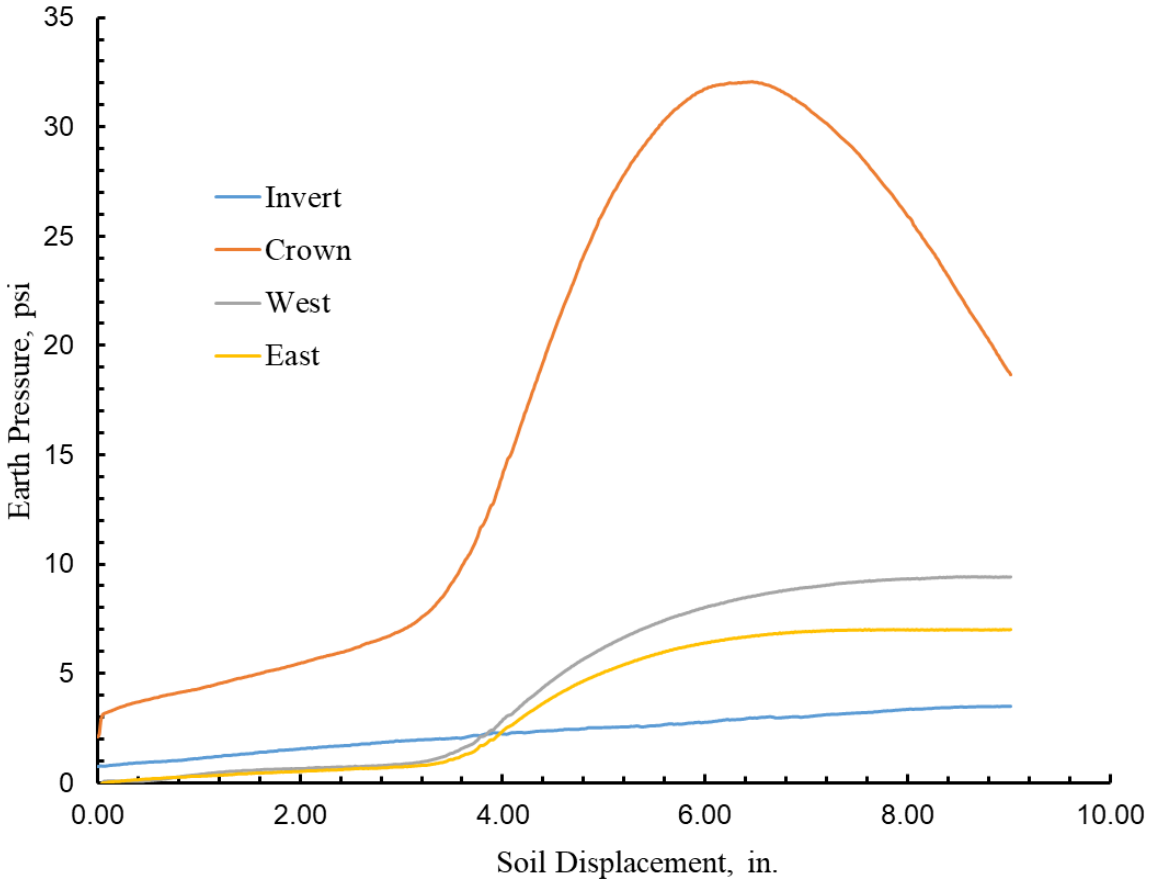

Figure 3-52 Earth Pressure Distribution in the invert cut CMP

(Source: CUIRE Laboratory)

iii. Strain Measurements:

Some of the strain gages were damaged during the invert removal process. The strain gages located in at the east spring line and at the crown got damaged. These strains were plotted against the soil displacement as shown in the Figure 3-53.

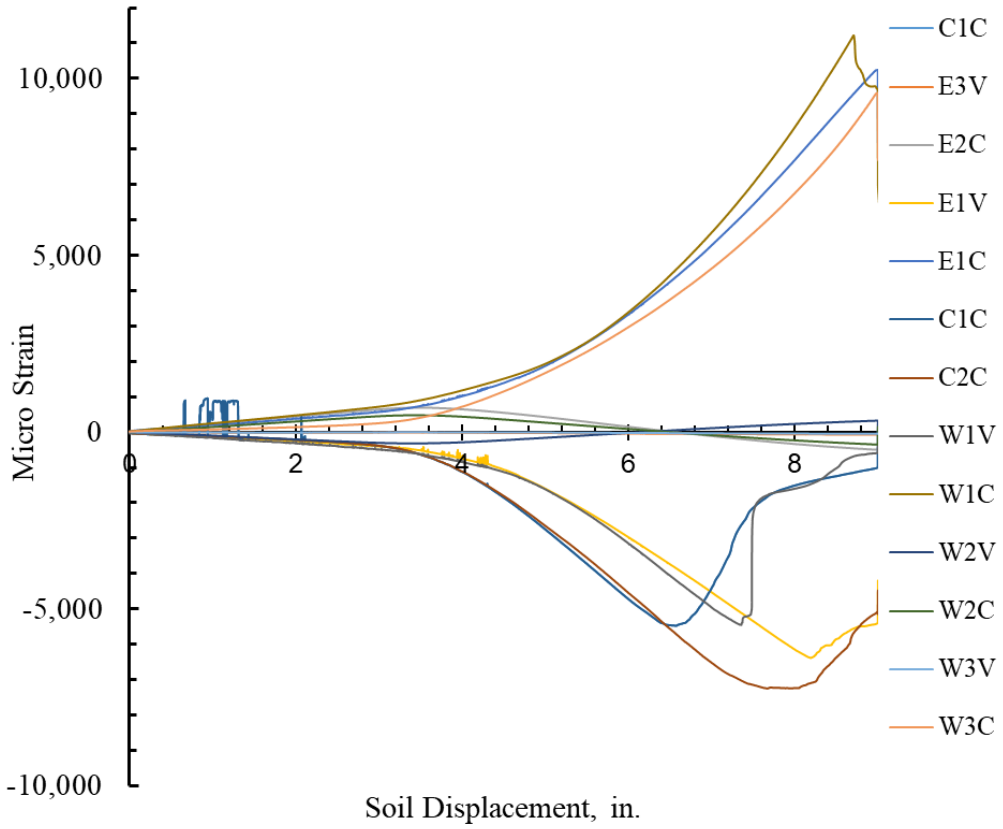

Figure 3-53 Strains around the invert cut CMP

(Source: CUIRE Laboratory)

3.4.3 Lined CMP

After the control test, next set of tests were performed in invert removed circular CMPs rehabilitated by the spray applied polymeric liner. The tests were performed on the three different thickness of the polymeric liner i.e. 0.25 in., 0.5 in. and 1 in. to find the suitable thickness required to increase the structural performance of the invert loss CMP greater than the intact CMPs. Since the material properties suggests the brittle nature, the failure mode of the CMP was excessive cracking rather than the deflection of the CMP.

Figure 3-54 Invert detached CMP before and after the application of the liner (Source: CUIRE LAB)

1. 0.25 in. thick liner

(a) (b)

Figure 3-55 (a) Load plate arrangement (b) Inside instrumentation for the 0.25 in. liner (Source: CUIRE Laboratory)

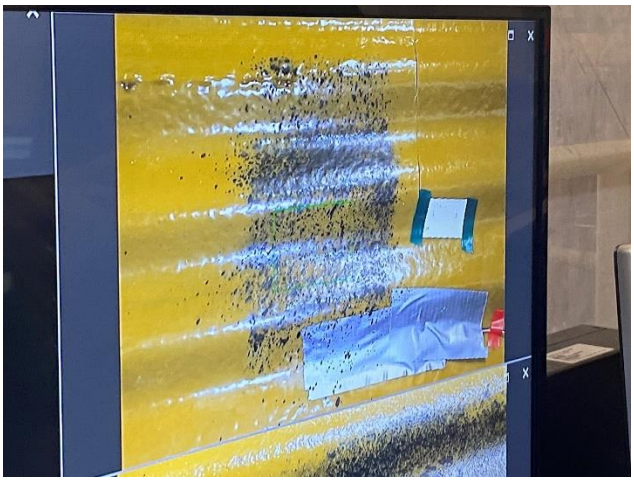

Figure 3-56 Appearance of the 1st crack in the lined CMP for 0.25 in. thick liner (Source: CUIRE Laboratory)

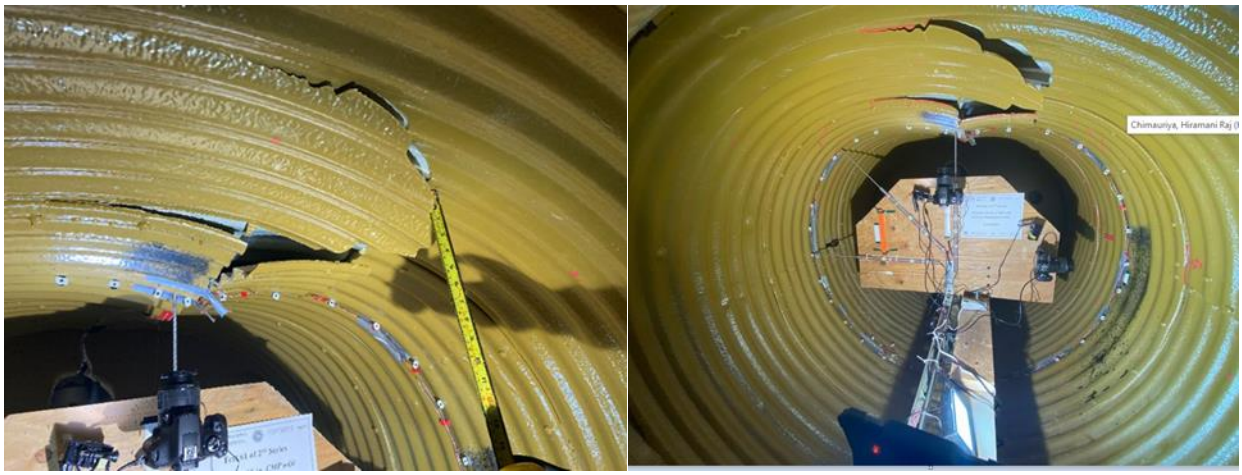

Figure 3-57 Cracks in lined CMP after the completion of test for 0.25 in. thick liner (Source: CUIRE Laboratory)

The first test pipe was lined with the 0.25 in. thick liner. The load was applied at the rate of 0.03 in./min. The results from the 1st liner test is summarized below:

i. Load displacement plots

The load displacement plots of the soil displacement vs. applied force which was recorded by actuator and liner displacement at the crown and the spring line recorded by the LVDTs are shown in the Figure 3-58. The load displacement plot shows the drop in the load at various instances during the application of the load. The initial drops in the load was caused by the detachment of the liner from the wooden wall which was caused due to over spraying of the liner during the liner application process. The first crack was observed at 40 kips of the load which appeared exactly along the center of the pipe just below the load pad Figure 3-56. Also, a slight drop in the load was seen at that instance. At that moment, the displacement of the liner recorded by LVDTs at crown was 2.576 in. while the spring line displacement was recorded to be 1.4 in. (outward) and no movement was recorded at the shoulder area. The crack propagated all through the crown longitudinally (Figure 3-57). After the first crack occurred, it was observed that the liner at around the crack area had gotten completely detached from the CMP (Figure 3-57) resulting in the independent movement of the CMP and the liner after that in the crown region. The CMP-liner system ultimately took the ultimate load of 46 kips. The ultimate load occurred after 4.2 in. displacement of the liner. At the ultimate load conditions the liner at the crown got completely detached from the CMP and the buckling of the CMP was observed. After the end of the test upon inspecting the CMP, some circumferential cracks were also seen in the CMP.

No cracks were observed in the invert region of the liner where the invert of the CMP was separated.

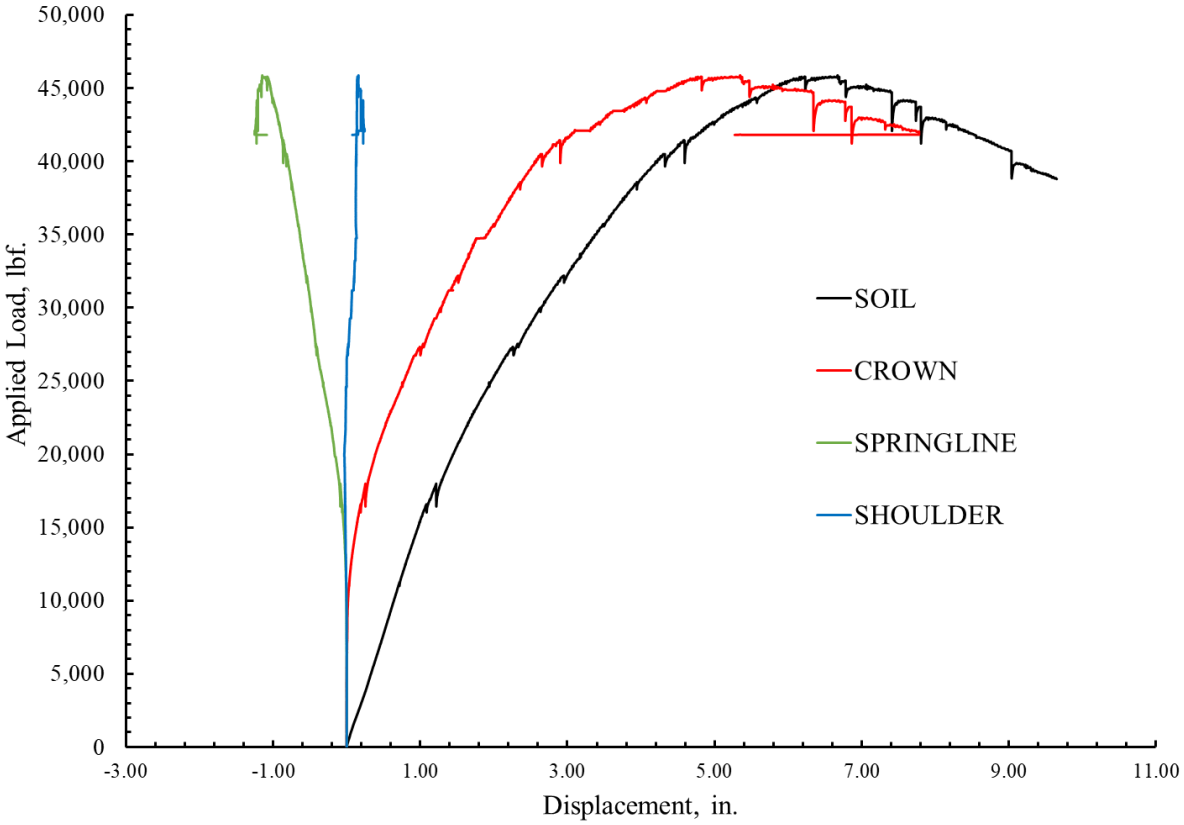

Figure 3-58 Load-displacement curve for the displacement in the crown, springline and shoulder for CMP lined with 0.25 in. thick liner

(Source: CUIRE Laboratory)

ii. Earth Pressure Distribution

The earth pressure distribution at around the CMP is show in the Figure 3-59. Evidently, the maximum pressure was recoded just above the crown below the load pad. Like in the bare intact CMP and the invert cut CMP, low pressures were recorded by the earth pressures located at the spring line and at the invert. The pressure during the first crack was found to be 38 psi while at the ultimate load the pressure was found to be 42.22 psi. The pressure at the spring lines at ultimate load conditions were 4.7 psi and 4.9 psi on east and west side of the CMP wall.

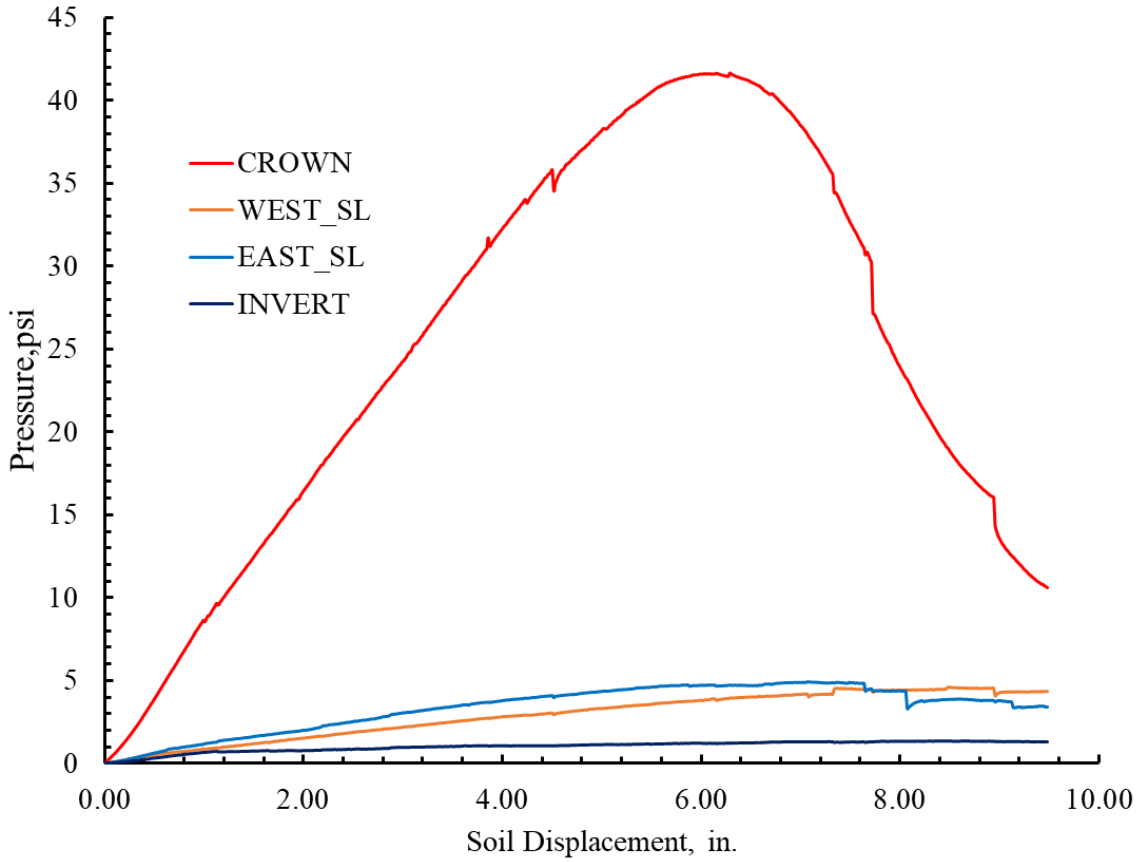

Figure 3-59 Earth Pressure distribution around the CMP lined with 0.25in. thick liner

(Source: CUIRE Laboratory)

iii. Strain Distribution:

Unlike the control test the strain gage were placed inside the crest of the liner instead of the outside valley of the CMP. The nomenclature was assumed to be same. For example, E1V previously meant the strain gage kept at the shoulder of the CMP on the east side in the valley region but now E1V refers to the strain gage kept at the shoulder inside of the liner on the east side in the crest. The arrangement was made to calculate the bending moment of the composite structure.

But due to some malfunction in the data acquisition system the strains for all the strain gage were not recorded. Only the half of the strain gage data could be recovered among which the data recorded by the strain gage kept in the inside of the liner were faulty.

The maximum strain was observed in the crown of the CMP followed by the strain gauge kept at the crest of the shoulder of the CMP (Figure 3-61).

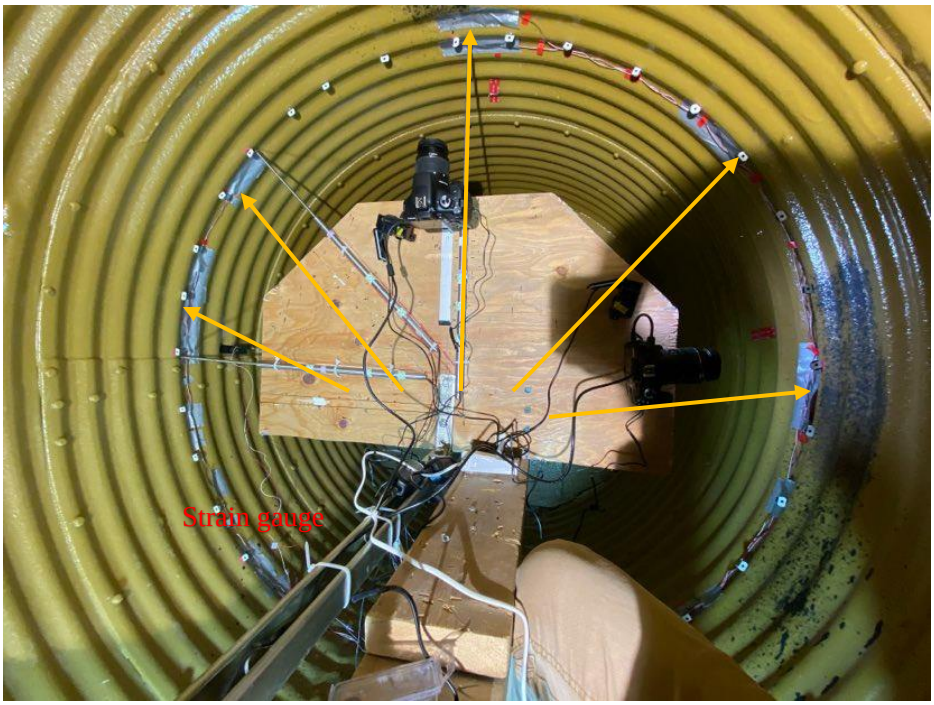

Figure 3-60 Inside arrangement of the strain gage (Source: CUIRE LAB)

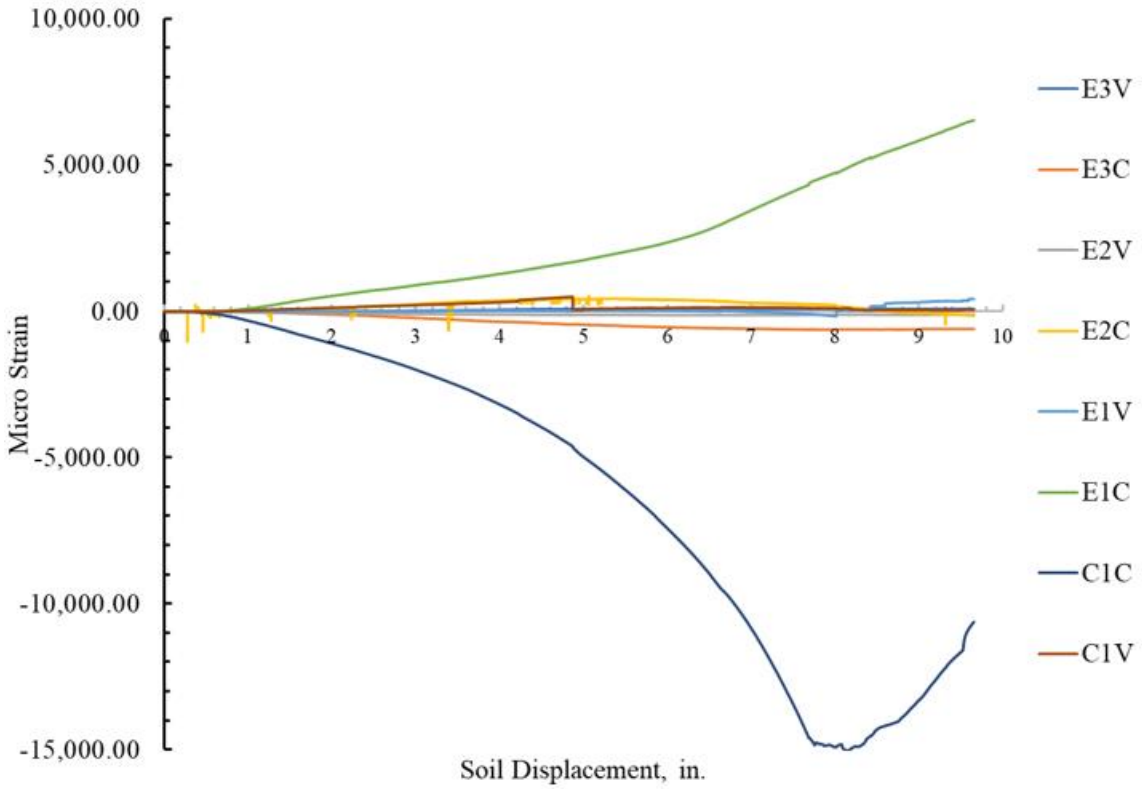

Figure 3-61 Strain distribution around the CMP for 0.25 in. thick liner (Source: CUIRE Laboratory)

2. 0.5 in. thick liner

The second test was conducted on the 0.5 in. thick liner. The results are summarized as:

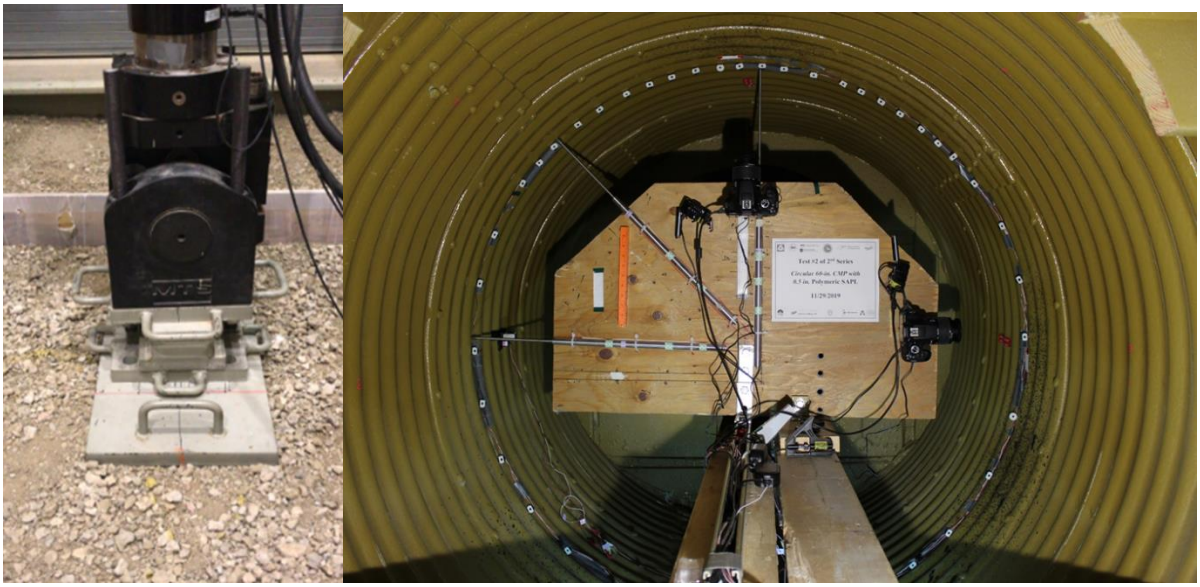

Figure 3-62(a) Load plate arrangements (b) Inside instrumentation for the 0.5 in. thick liner (Source: CUIRE Laboratory)

Figure 3-63 Crack in 0.5 in. thick liner after the completion of test for 0.5 in. thick liner (Source: CUIRE Laboratory)

i. Load Displacement Plots

The load displacement plots of the test plotted for the soil displacement vs applied load and the displacement of the CMP at the crown and the spring line recorded by the LVDTs are shown in the Figure 3-64. From the load displacement graph, we could see the load drop in the test and the change in the stiffness in the system at 27 kips of load and 1.5 in. of soil displacement. This was caused by the separation of the over sprayed liner from the wooden wall, which after separation reduce the stiffness of the system.

The first crack was observed at around 43 kips of the load which occurred at the crown just below the load pad. The displacement of the liner at that moment of the first crack was 1.8 in. at the crown (vertically down), 1.3 in (outward) at the spring line and 0.12 in. at the shoulder (outward). The major cracks were located along the crown region longitudinally with the complete separation for the CMP. The system ultimate load carrying capacity was 52.46 kips. At ultimate load conditions the displacement of the liner at the crown was 4.8 inches.

After the completion of the test the CMP was inspected carefully. On careful inspection it was observed a complete separation between the liner and the CMP was seen and at certain portion the liner had broken off and fell off (Figure 3-63). Also, the fine cracks were observed along the seam line and some circumferential cracks were observed along the centerline region of the CMP. There were also the fine hairline cracks along the shoulder longitudinally which indicated inside portion of the CMP in the shoulder region to be in tensile zone.

No cracks were observed in the invert region of the liner where the invert of the CMP was separated.

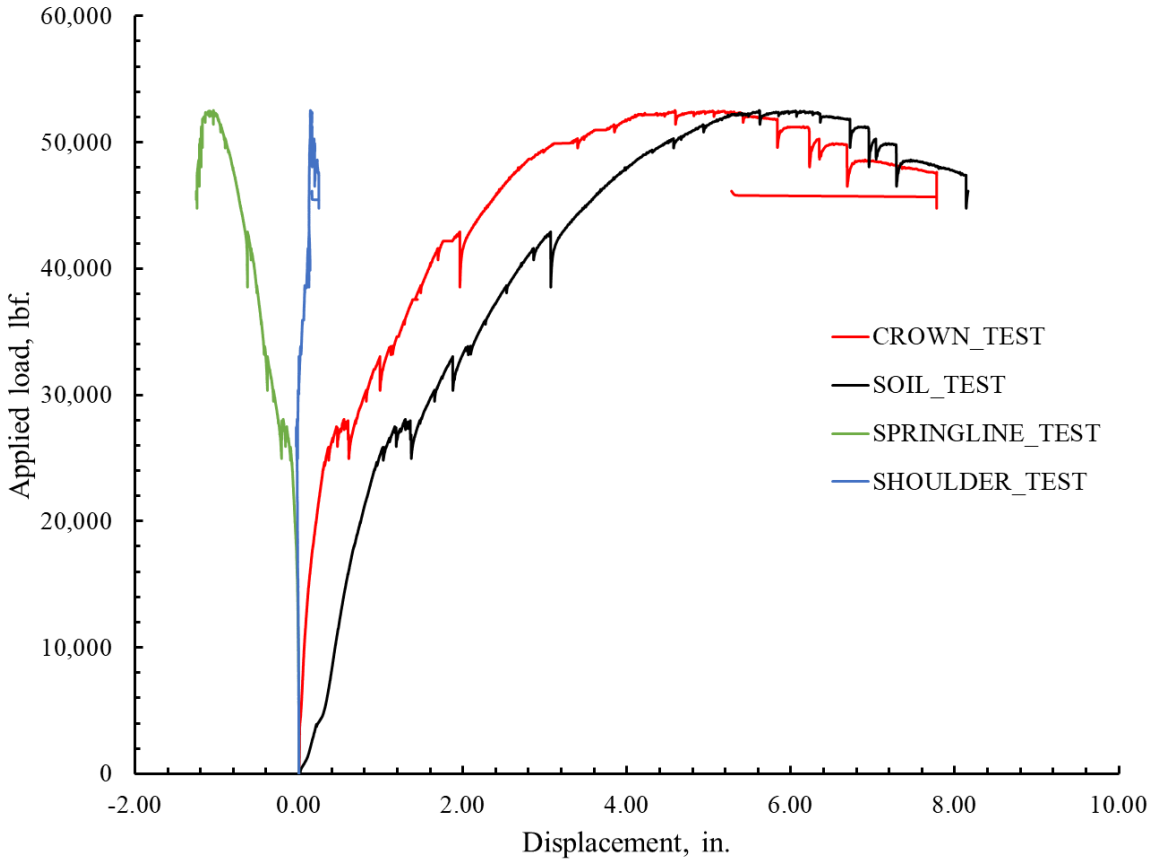

Figure 3-64 Load-displacement curve for the displacement in the soil, crown, springline and shoulder for CMP lined with 0.5 in. thick liner (Source: CUIRE Laboratory)

ii. Earth Pressure Distribution

The earth pressure distribution at around the CMP is show in the Figure 3-65. Like all the previous test the maximum pressure was recorded just above the crown below the load pad. The pressure during the first

crack was found to be at 27 psi while at the ultimate load the pressure was found to be 40.63 psi. A drop in the pressure was observed during the first crack of the liner and it rose steadily up to 40 psi of pressure and then it started to flatten out and ultimately drop off in around 44 psi. The pressure at the spring lines at ultimate load conditions were 8.6 psi and 6 psi on east and west side of the CMP wall.

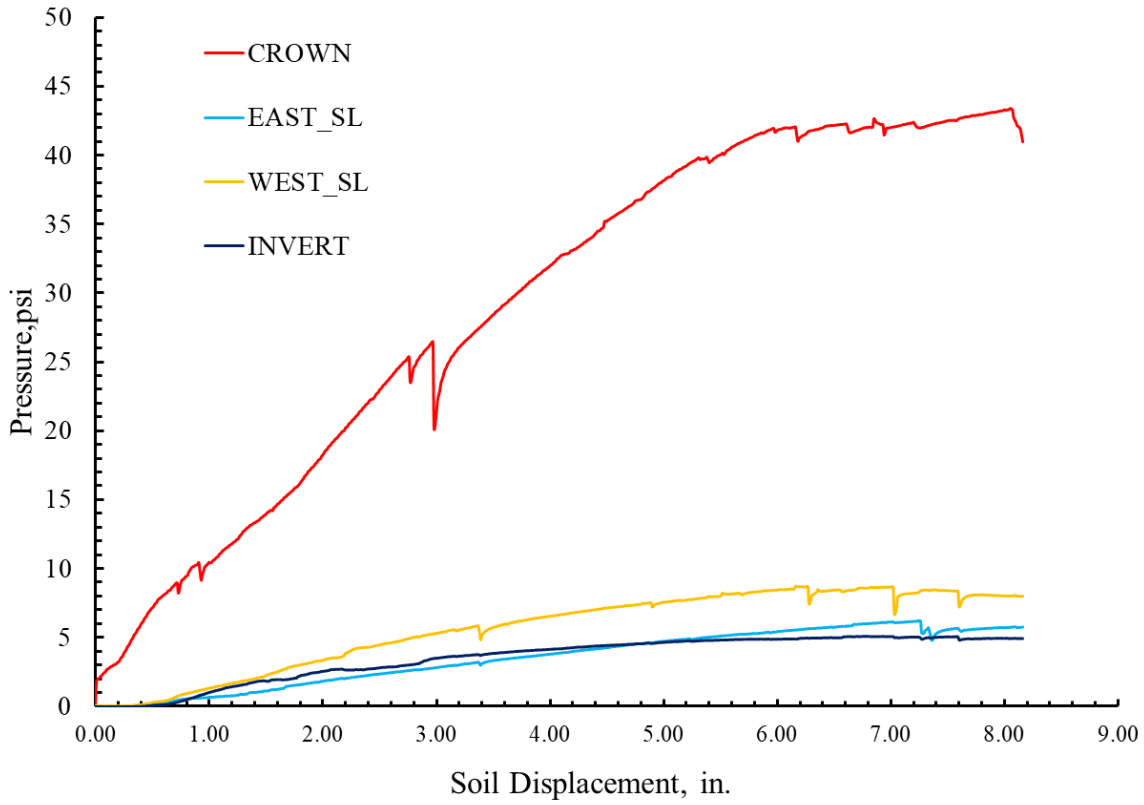

Figure 3-65 Earth Pressure distribution around the CMP lined with 0.5 in. thick liner (Source: CUIRE Laboratory)

iii. Strain Distribution

The strains recorded by the data acquisition is shown in the graph Figure 3-66.

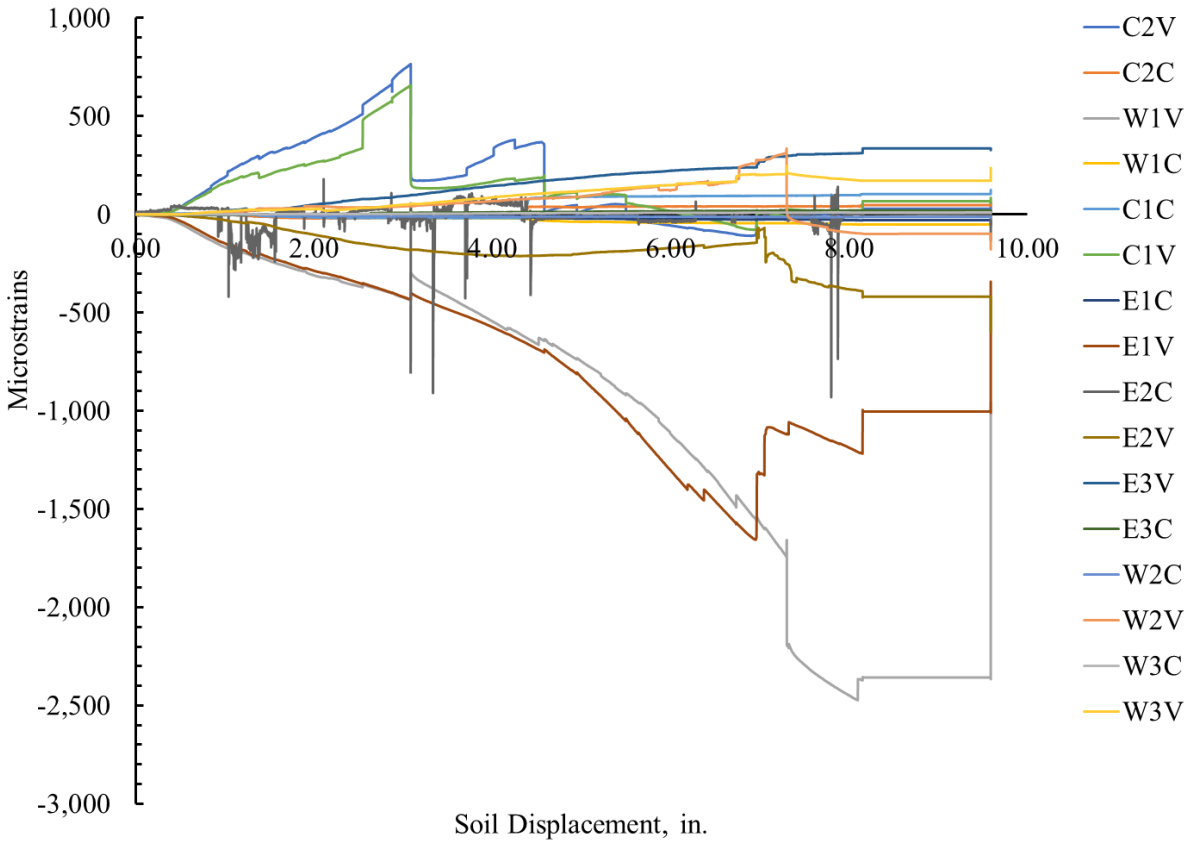

Figure 3-66 Strain distribution around the CMP for 0.5 in. thick liner (Source: CUIRE Laboratory)

3. 1 in. thick liner

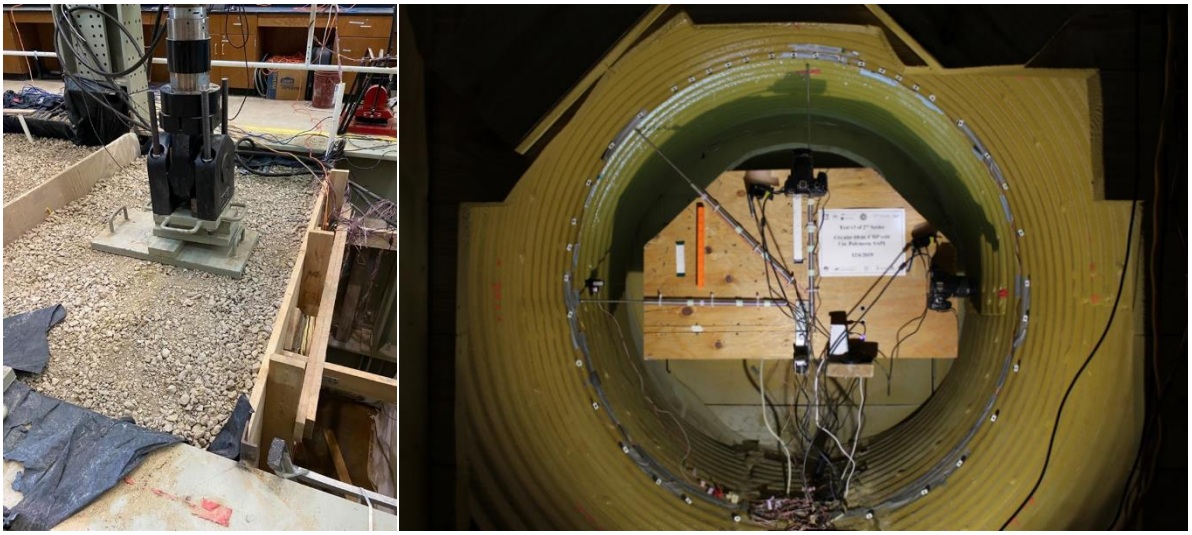

Figure 3-67 (a) Load plate arrangements (b) Inside instrumentation for the 1 in. thick liner (Source: CUIRE Laboratory)

Figure 3-68 Crack in 1 in. thick liner after the completion of test for 1 in. thick liner (Source: CUIRE Laboratory)

The results from 1 in. thick liner are described as:

i. Load Displacement plots

With the increase in the thickness, the system of CMP and the liner showed the stiffer response compared to the 0.5 in. thick and 0.25 in. thick liner. There was also a sudden change in the curve at around 40 kips of load because of the detachment of the over sprayed liner in the wooden wall. The first crack was observed at 66.37 kips of the load where the crown had displaced by 2.4 in. vertically downward. The liner was completely separated from the wall after this load. The horizontal movement of the lined CMP at the one end of the spring line was 1.4 in. in outward direction and the inclined movement of the lined CMP was 0.19 in. outwards (Figure 3-69). Like others lined CMP the 1st crack occurred right along the crown just beneath the load pad. A huge drop in the load was observed during the 1st crack. The ultimate load carrying capacity of the soil -lined CMP system was 72.22 kips with around 4 inches of the liner displaced vertically down at the crown. Like the other lined CMP, a complete separation of the liner from the CMP was seen after the ultimate load conditions.

Upon inspecting the pipe after the completion of the test, complete separation of the liner and the CMP wall was found in the upper region of the CMP (Figure 3-68).

No cracks were observed in the invert region of the liner where the invert of the CMP was separated.

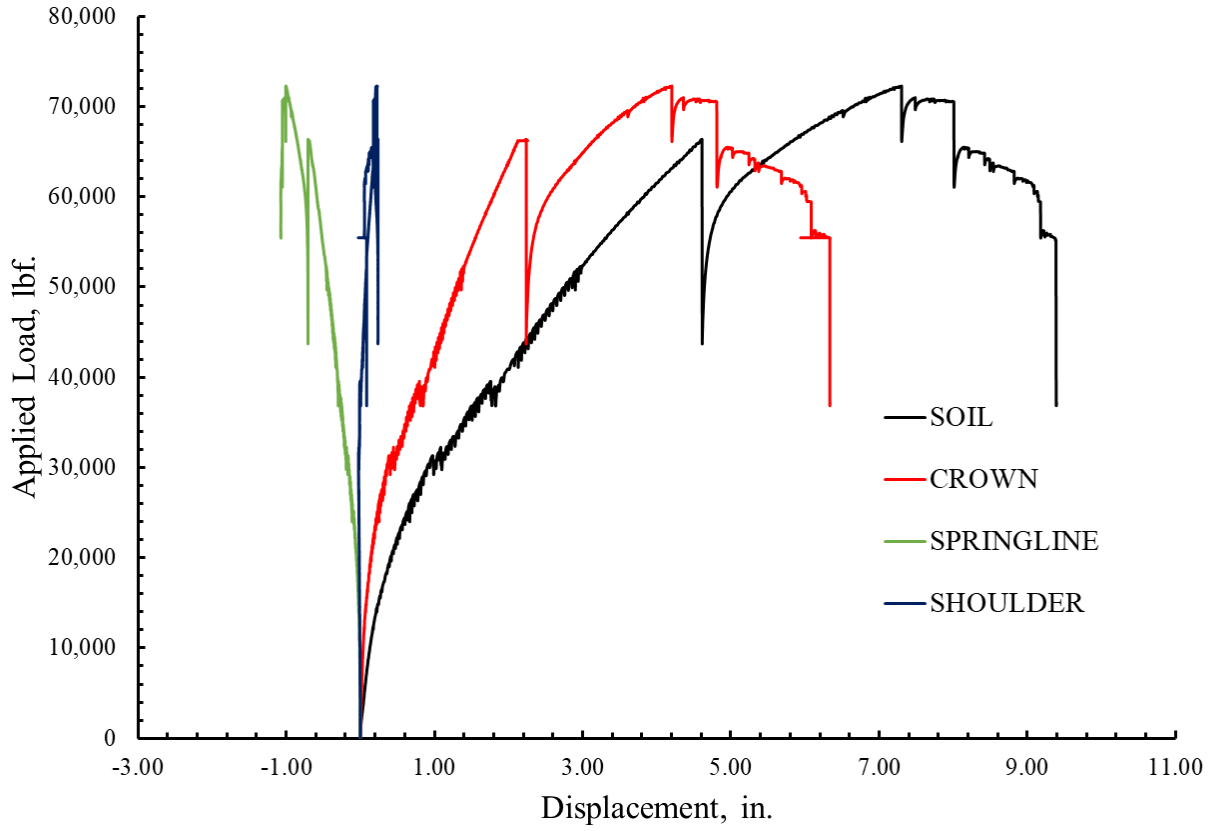

Figure 3-69 Load-displacement curve for the displacement in the soil, crown, springline and shoulder for CMP lined with 1 in. thick liner (Source: CUIRE Laboratory)

ii. Earth Pressure Distribution

The earth pressures around the CMP are plotted as shown in the Figure 3-70. The maximum earth pressure recorded just above the crown was 71.53 psi at the ultimate load. At the 1st crack the earth pressure read in the earth pressure cell was 63 kips. Just after the first crack, like the drop in the load, a huge drop of pressure of more than 30 psi was observed after that it rose steadily up to the ultimate pressure. Also, with the increase in load the pressure in the spring lines were also increased compared to the previous lined CMP. The pressure in the spring lines were 9 psi and 13 psi at the west and east side of the CMP.

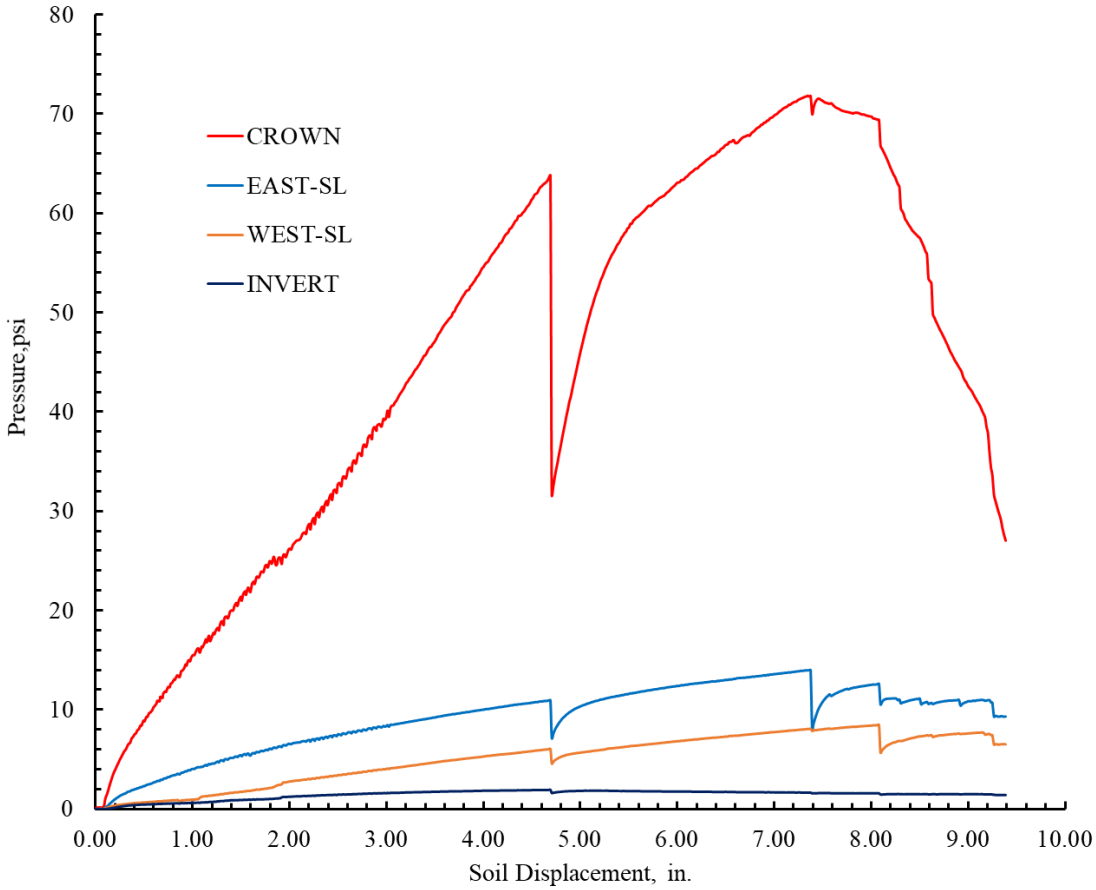

Figure 3-70 Earth Pressure distribution around the CMP lined with 0.5in. thick liner

(Source: CUIRE Laboratory)

iii. Strain Distribution

For this set of test, half of the data could be recovered i.e. east side of the CMP (Figure 3-34). The strain recorded was maximum at the crown (both inside the liner and outside the CMP) followed by the maximum strain at the shoulder region with the opposite sign to the respective location at the crown of the CMP (Figure 3-71). For other strain gage locations strains were too small (less than 500 microns). Compared to the strain in 0.25 in. liner, the strains recorded were low at the greater load conditions which shows the increase in the rigidity of the liner with the increase in the thickness of the liner.

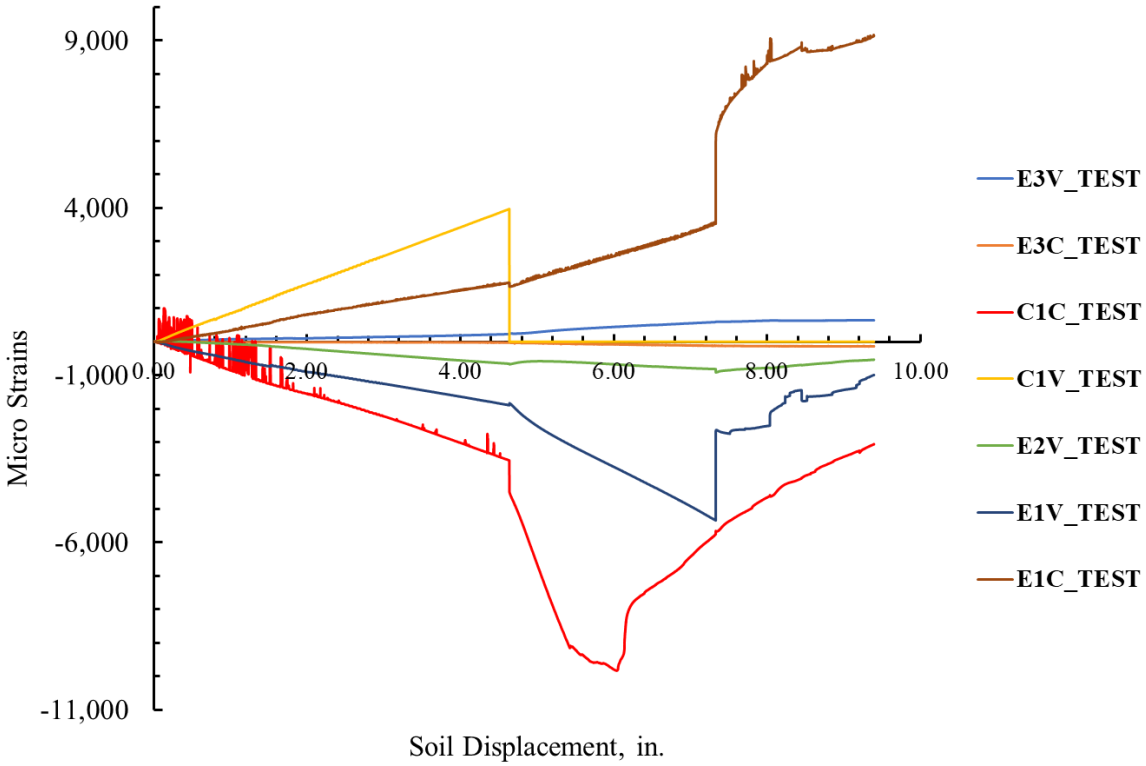

Figure 3-71 Strain distribution around the CMP for 1 in. thick liner

(Source: CUIRE Laboratory)

Chapter 4: 3D Finite Element Analysis

The Finite Element Analysis (FEA) is the simulation of any given physical phenomenon using the numerical technique called Finite Element Method (FEM) (SIMSCALE,2020). Finite Element Analysis (FEA) is being used extensively in today's world to generate and analyze any given physical phenomena. Finite element has been the most useful tool in today's generation as it saves time for performing the multiple large-scale tests and gives multiple amounts of data to study the given physical phenomena more easily.

For our test for studying the spray-applied pipe liners only three thicknesses are chosen. But only three lab test data won't be enough to fully understand the load-carrying capacity of the liner, the contribution of the host pipe, and soil-structure interaction of the rehabilitated pipe. So, finite element analysis will be employed to generate other data points for other thicknesses. Before generating other data points through the finite element analysis, the FEM needs to be calibrated with the test results. Hence, this chapter deals with the Finite element analysis performed for the calibration of the FE model with the test data performed in CUIRE laboratory.

4.1. Model setup

The 3D-model contained three parts: Soil, CMP, and the Liner. Since the test had three different liner thickness, three different models were constructed for every three different thicknesses. The geometry of the model was complex, so CAD software was employed to generate the model and was imported to the ABAQUS. A full model of the soil-box was model to see the development of the plastic strains around the CMPs.

4.2 Boundary Condition and Loading

To obtain accurate results from the FEM analysis, defining the proper boundary condition is an important task. The boundary conditions were defined similar to the experimental setup. The restriction of the movement of the soil outside the soil-box due to end walls in their respective direction was defined by defining the boundary conditions which restrict the movement of the soil outside the soil-box system. The boundary condition at the soil boundary was defined such that horizontal movement along the CMP was restricted in Z- direction while the horizontal movement perpendicular to the CMP was restricted along X-direction. The vertical movement of the soil was restricted at the bottom of the model. The boundary conditions are shown in Figure 4-1.

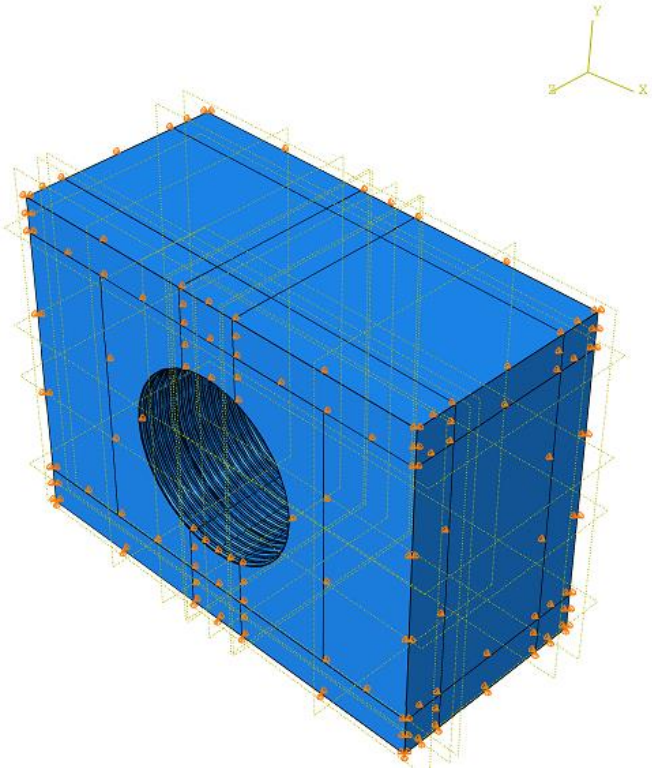

Figure 4-1 FE model of the soil-pipe-liner system

To avoid the complexity in the model the load pad was not modeled in the model for the application of the load. Instead of that, a master node was defined which constrained all the nodes within the load pad area by defining equation constraint. This equation definition ensured the simultaneous movement of all loaded nodes (simulating load transfer from rigid load pad), such that any movement in the central node was mirrored by all the nodes with the equation constraint. The load was applied by providing the displacement of the master soil node in the load pad. The maximum soil displacement applied was 8 in.

4.3 Material Model

4.3.1 Soil Properties

Three types of soil: Poorly Graded Sand (SP), Poorly Graded Gravel (GP), and TxDOT specified Grade D sub-base layer classified according to ASTM D -2487 were considered as the backfill and cover soils, respectively in the experiment. For the first control test the GP soil was used as the cover soil but it was replaced by TxDOT specified Grade D sub-base layer (RCA). These soils were modeled using the Drucker Prager Model available in the ABAQUS material model library. The material properties used in the FEM model are listed in Table 4-1.

Drucker Prager Model is a three-dimensional pressure-dependent model through which the strength properties of the soil increased with the application of the pressure (SIMULIA, 2014). The property of the poorly graded sand was taken from the laboratory experiment carried at the Geotech lab of UTA while the property of the poorly graded gravel (GP) was taken from CUIRE (2012) final report. The properties for the RCA soils were chosen from Arulrajah et al. (2012). All the soil properties are chosen as the representative soil properties that can be achieved with the selected soils in the soil box. The density used

for the model was reduced to match the 85% compaction of the maximum dry density of the soil. Also, the soil Young's moduli were chosen according to the ASTM D-3839-14 considering the depth dependency of Young's moduli. In the calibration process, the internal friction angle of the sand and gravel was adjusted slightly to better match the experiment results. The properties shown in Table 4-1are the finalized values after the calibration process.

Property	**Sand**	**Gravel**	**RCA**
Density (pcf) (Max. dry density)	115	130	130
Young's Modulus (psi)	510	1000	1000
Poisson Ratio	0.3	0.28	0.3
Angle of Friction	32.0	37.5	39
Dilation Angle	1	2	1

Table 4-1 Soil Properties

4.3.2 CMP Properties

The intact circular CMP is made of corrugated steel sheets conforming to ASTM 929 with yield strength 33 ksi and ultimate strength 45 ksi. The modulus of elasticity of the steel is 29,000 ksi. The elastic-plastic model available in Abaqus was used to model the behavior of CMP steel. The properties are listed below:

Property	Value
Density (lb./in3)	0.284
Elastic Modulus (psi)	29,000,000
Poisson's Ratio	0.3
Yield Stress (psi)	33,000
Ultimate Stress (psi)	45,000

Table 4-2 Properties of the steel

4.3.3 Liner Properties

The material property for this model was taken from the material test report provided by NTPEP. The test report of the NTPEP (Paredes, 2018) liner had a maximum of 1.5% elongation before the crack. The test report suggested the brittle behavior of the material with a small plastic zone with only 0.22% of strain difference between the yield and breaking strain. A simple elastic-plastic model was used to model the liner. In the FE model, the occurrence of the crack is identified by observing the plastic strain in the liner. Since the material had a small plastic region the occurrence of the 1st plastic strain was related to the occurrence of the 1st crack in the model. The properties of the material are given in the Table 4-3.

Property	Value
Density (lb./in3)	0.00014
Elastic Modulus (psi)	1,154,016
Poisson's Ratio	0.3
Tensile Yield Stress (psi)	7,482
Tensile Yield strain (%)	1.13
Tensile Break Strength (psi)	8,228
Tensile Break strain (%)	1.35

Table 4-3 Properties of the liner (Paredes,2018)

4.4 Soil-CMP and Liner-CMP interaction

One of the most essential parts of modeling the buried pipes in the soil is the interactions between the pipe and the soil. ABAQUS allows the user to define different interaction models for the interface between the pipe and soil for example tie interaction, surface to surface interaction, etc. In this model, the interaction between the pipe and soil interface is represented using the surface-to-surface contact model where the pipe is treated as the master surface and the soil is treated as the slave surface. Considering the corrugated surface of the pipe a rough friction coefficient of 0.5 is defined between the CMP and Soil, and the contact is defined as a hard contact i.e., the pipe does not "pierce" the soil but displaces it. This friction coefficient was optimized to calibrate the FE model for the intact CMP..

While the interaction between the CMP and liner was defined as the value of a rough friction coefficient of 1 which signifies the perfect contact but allows the independent movement of the pipe and liner. A hard contact was defined between the liner and the CMP to represent the normal contact between them. In the experiment it was observed that once the liner was broken, there was no contact with the pipe wall.

4.5 Element Type

A. Soil:

The soil was modeled as the solid elements in all the FE model. The soil was meshed using linear C3D8R element type, which is 8 noded linear brick, reduced integration with control in the hourglass.

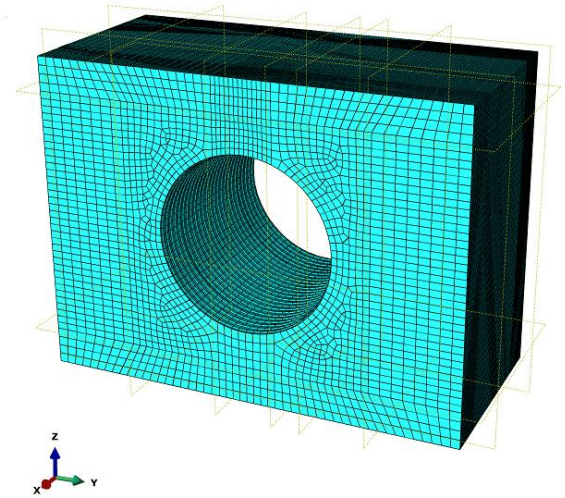

Figure 4-2 Soil Model in FE

B. CMP

The CMP is also modeled as the solid element using linear hexagonal C3D8R element type. The mesh size of the CMP used was 1.8 in.

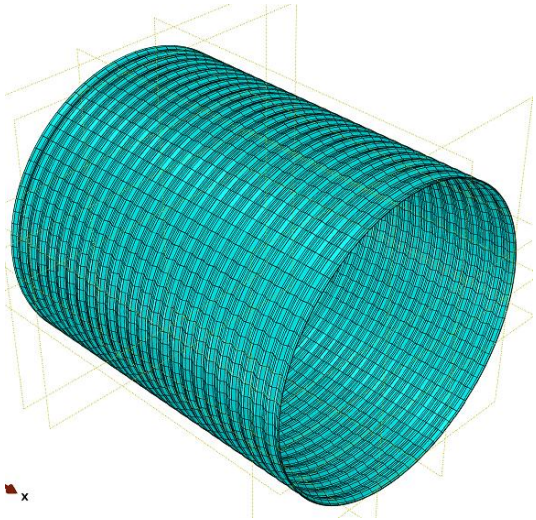

Figure 4-3 CMP Model in FE

C. Liner

All the three-thickness liner were modeled as the linear hexagonal C3D8R element type with the mesh size of 1.8.

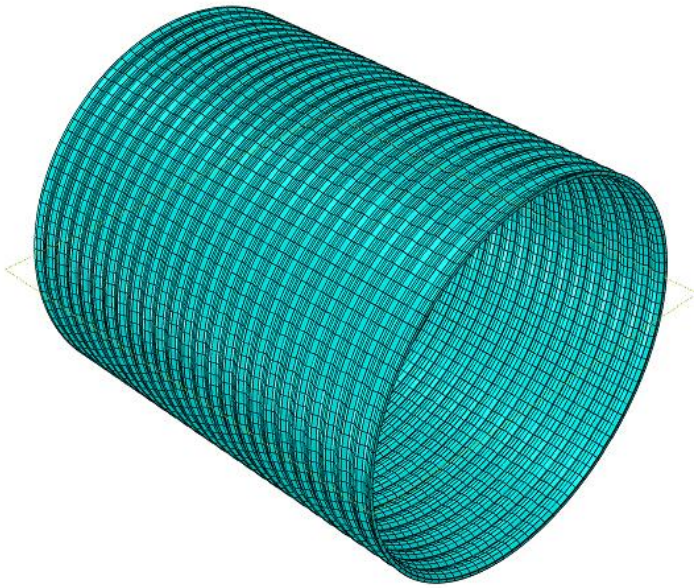

Figure 4-4 1 in. Liner model in FE

4.6 Mesh size study

The finite element method approximates the unknown function over the domain. The domain is divided into small elements represented by the element nodes. The number of elements, i.e. element size, for the modeling domain dramatically affects the results from the analysis. If the size of the element is coarser, the model could become stiffer and yield inaccurate results, while the finer elements lead to more accurate

results with the cost of computation time. Hence selecting the proper mesh size is one of the essential steps in the FEM analysis to make the model independent of the mesh size.

To determine the mesh sensitivity of the model, total energy, load-displacement for soil and pipe, and the Von Mises stress for the pipe were compared among the mesh sizes of 3.4, 3, 2.4 inches. For the soil, the differences in the values of plastic strain and load-displacement didn't vary by a significant amount for mesh sizes 3.4, 3, 2.4 (Figure 4-5) (Chimauriya, 2019).

Mesh Size (in.)		Run Time
Pipe	Soil	(hrs.)
3.4	3.4	0.5
3	3	1
2.4	2.4	4
1.75	2.4	6
1.5	2.4	20
1	2.4	25
0.75	2.4	96

Table 4-4 Mesh size and Run time

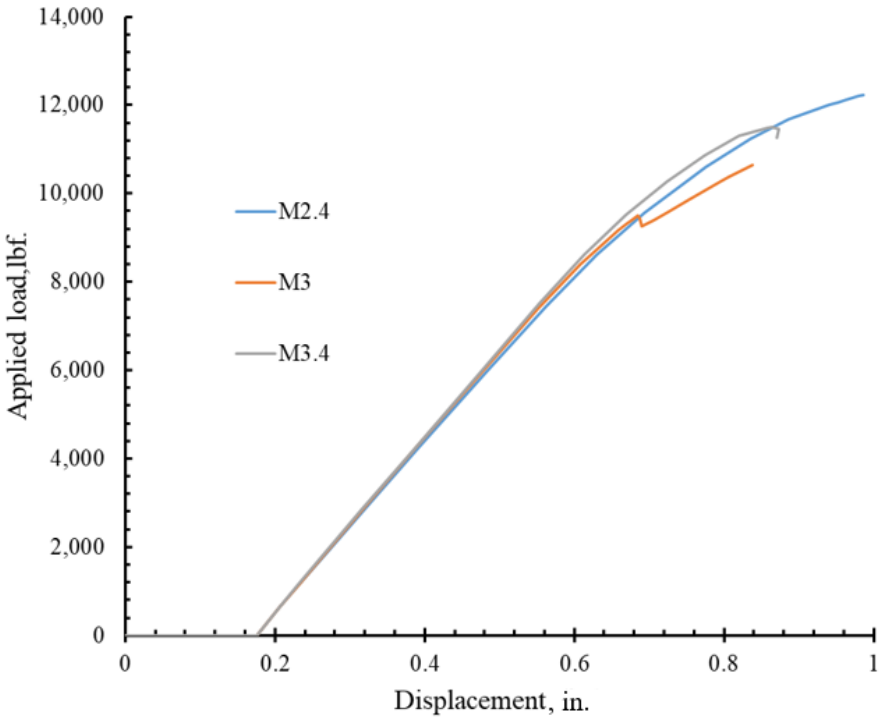

Figure 4-5 Load displacement plot for the soil (Chimauriya, 2019)

From Figure 4-5, Figure 4-7, Figure 4-8, the mesh size for the soil was taken as 2.4 in. around the vicinity of the pipe and at the edges the mesh size of 4.2 was chosen. For the mesh size study of the CMP, the mesh size differed from 3 to 0.75. In the study performed for the displacement of the crown and the von mises stress in the pipe it was seen that after 1.8 in. of the mesh size, the parameters did not change much. Thus, the mesh size of 1.8 was chosen for the CMP and the liner.

Also comparing the run time and mesh size of pipe and liner, the model with the mesh size smaller than 1.8 was taking a considerable amount of the computational time. Thus, the mesh size of 1.8 was chosen for the CMP and the liner.

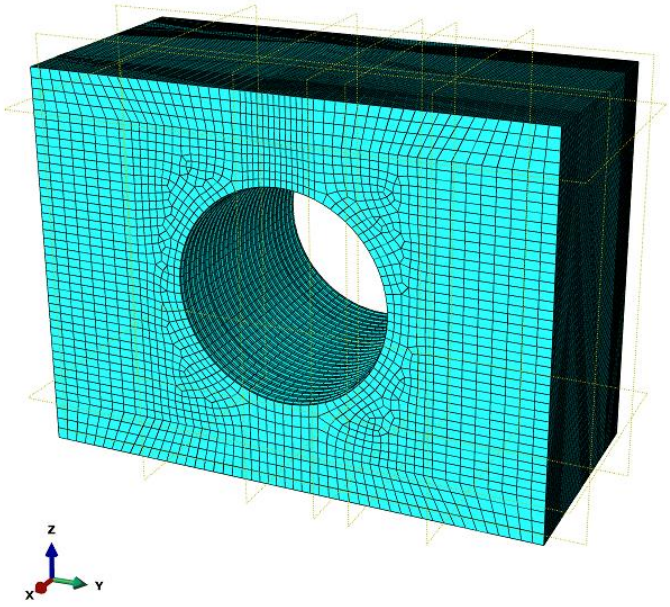

Figure 4-6 Mesh size distribution in the soil

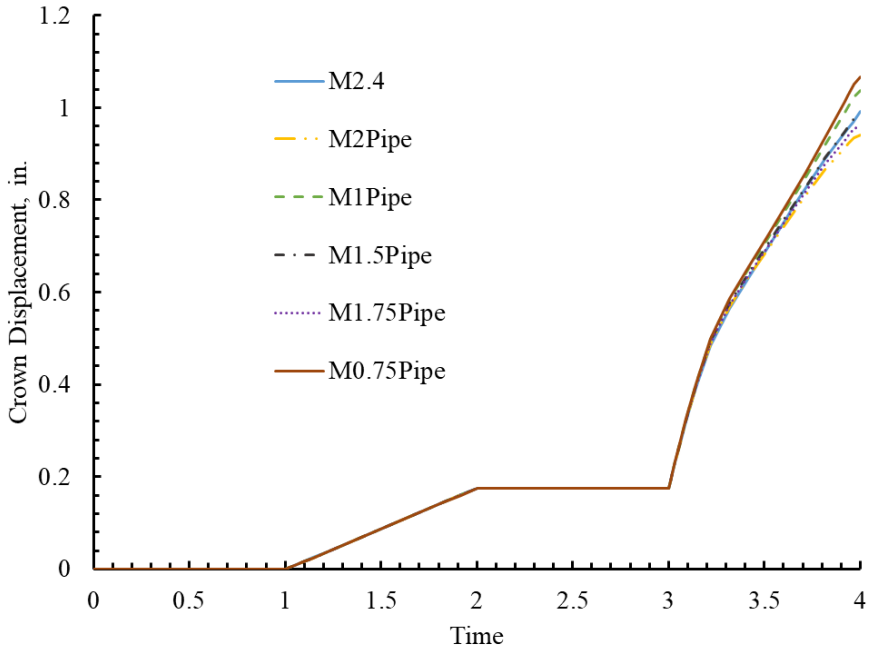

Figure 4-7 Load displacement plot for the pipe at the crown (Chimauriya, 2019)

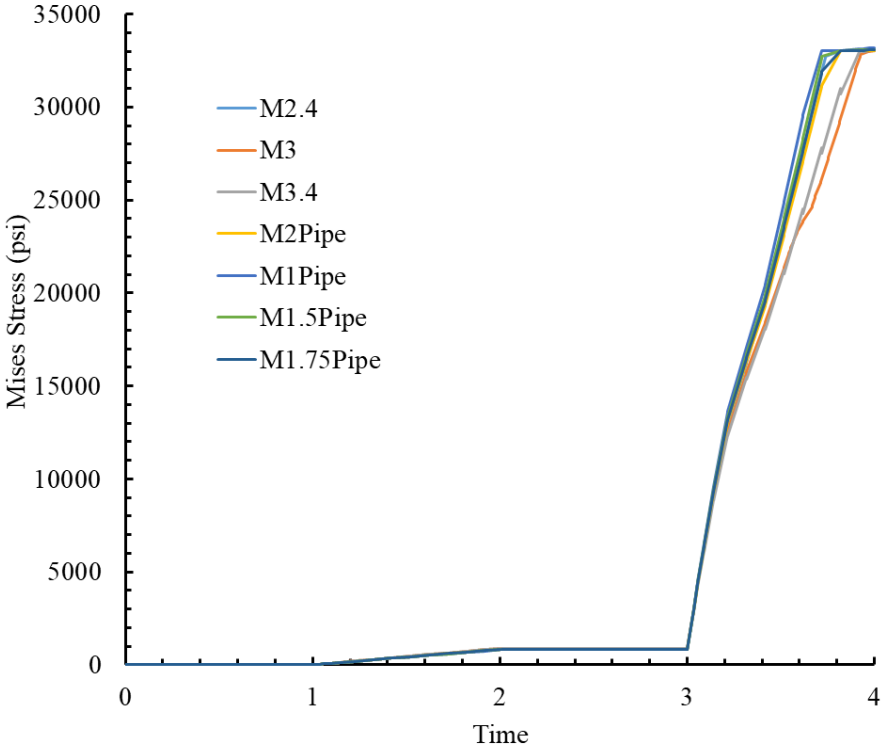

Figure 4-8 Von Mises Stress in the pipe (Chimauriya, 2019)

4.7 Modeling steps

The step followed to obtain results from the FE model are described below:

STEP-1: Geostatic step: In this step, geostatic (in-situ) stress including vertical and horizontal stress is established for the soil domain without considering the CMP pipe. The vertical stresses were calculated using equation 4.1 below while the lateral stresses were calculated as in equation 4.2.

$$\sigma = \gamma H \tag{4.1}$$

$$\sigma_h = (1 - sin\varphi)\gamma H \tag{4.2}$$

STEP-2: Activation of the CMP load. In this step, the gravity load of the pipe is activated, and pipe soil interaction is established.

STEP-3: Removal of the invert. (Not applicable for the intact CMP)

STEP-4: Activating the liner and establishing the liner-CMP interaction. (Not applicable for the intact and invert cut CMP)

STEP 5: Application of the load on top of the 1ft. cover.

4.8 Results for Control Test

All the results obtained from the Finite Element were directly compared to their respective experimental test.

The test results obtained from the FE analysis for the intact CMP are discussed as below:

4.8.1 Intact CMP (10x20 in^2 load pad)

With the use of the smaller load pad, in the experiment, the soil was punched by the load pad before any major deformation in the CMP. Like the experimental results, our FE model also predicted the failure of the soil before any significant deformation in the CMP. The soil could not be displaced more than 5 in. in the FE model as the analysis was implicit and could not predict the post-failure condition of the model. The development of the significant plastic strain in the loaded area could be seen in the model before the significant deflection in the pipe. (Figure 4-9)

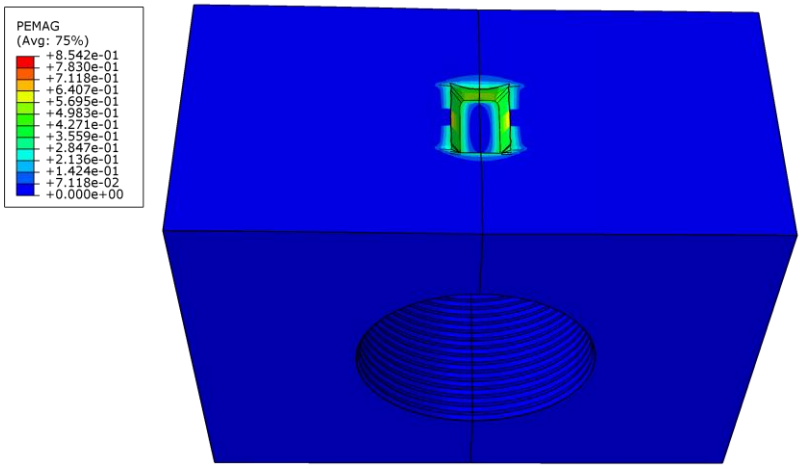

Figure 4-9 Plastic strain due to the soil failure in the loaded area

The prediction of the failure of the CMP from the experiment and FEM was similar. In the experiment, the CMP's major deformation was concentrated in the crown region of the CMP just below the load pad. The FE results also showed a similar deformation pattern just below the load pad when the deformation was scaled up..

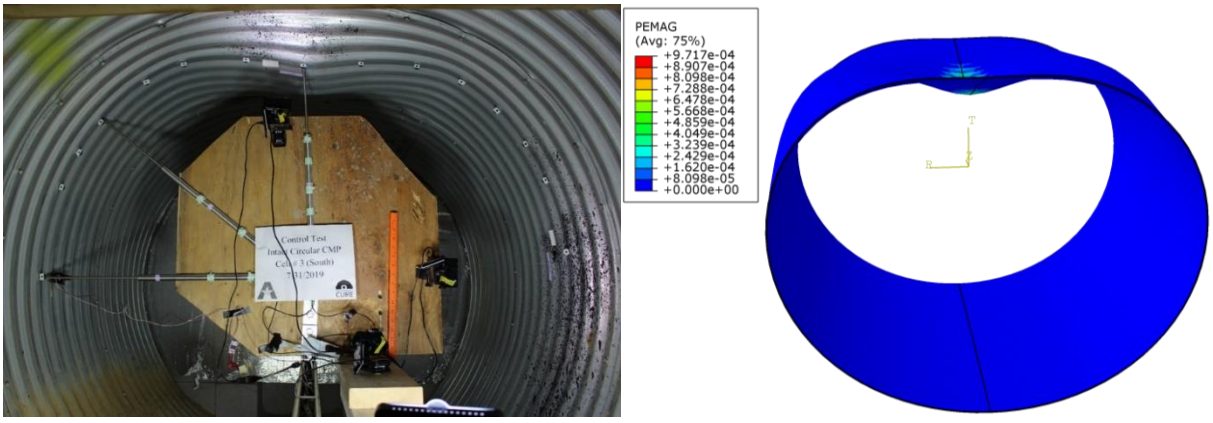

(a) (b)

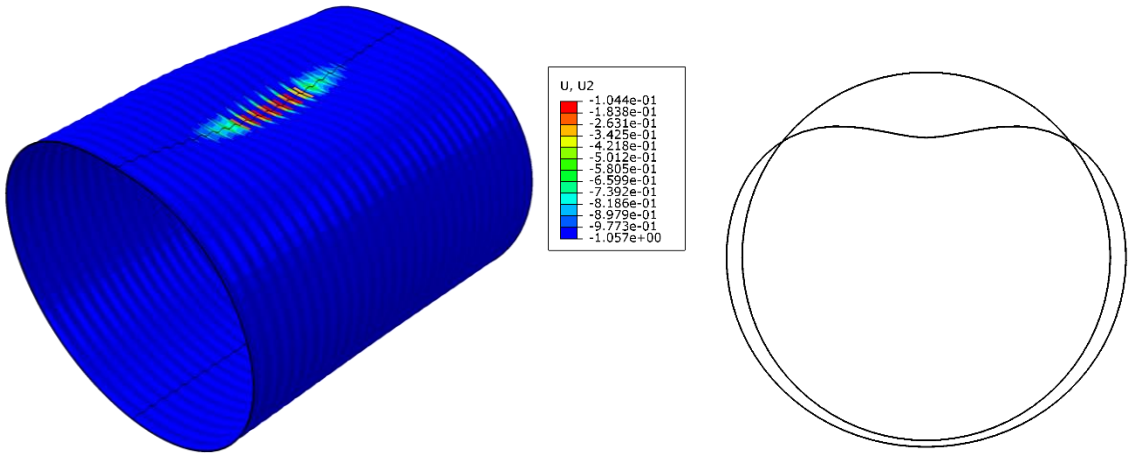

(c) (d)

Figure 4-10 Plastic strain and deflection pattern in CMP (a) Experimental Result (Source: CUIRE Laboratory) (b) (c), (d) FEM Result (scaled up by 5 times)

1. Load displacement plot

To study the behavior of the pipe under the applied load, the load-displacement curve was plotted. The load-displacement plot starts from the time when the external load is applied to the system and excludes the displacement due to the geostatic load or dead load due to backfill cover. For intact CMP two load-displacement curves were compared. The first load-displacement curve is obtained for the displacement of the crown at the center of the CMP which represents the result from the LVDTs placed to read the displacement of the crown in the experiment. While another load-displacement curve was obtained for the soil settlement during the application of the load from the actuator. (Figure 4-13, Figure 4-14). The FE plot was obtained for the 5 in. displacement of the soil.

The experiment was continued (Figure 4-11, Figure 4-12) even after the failure of the cover soil by punching, and as the CMP took the load, the load-displacement curve rose again and dropped after the local buckling of the CMP. However, this second rise could not be modeled in FEM as once the cover soil fails, any further increase in load causes large displacements of soil which was not captured by the material model of the soil that was used to define the soil model and the numerical model failed to converge. Thus, the comparison of the FE model and test was made for up to the 5 in. displacement of the soil.

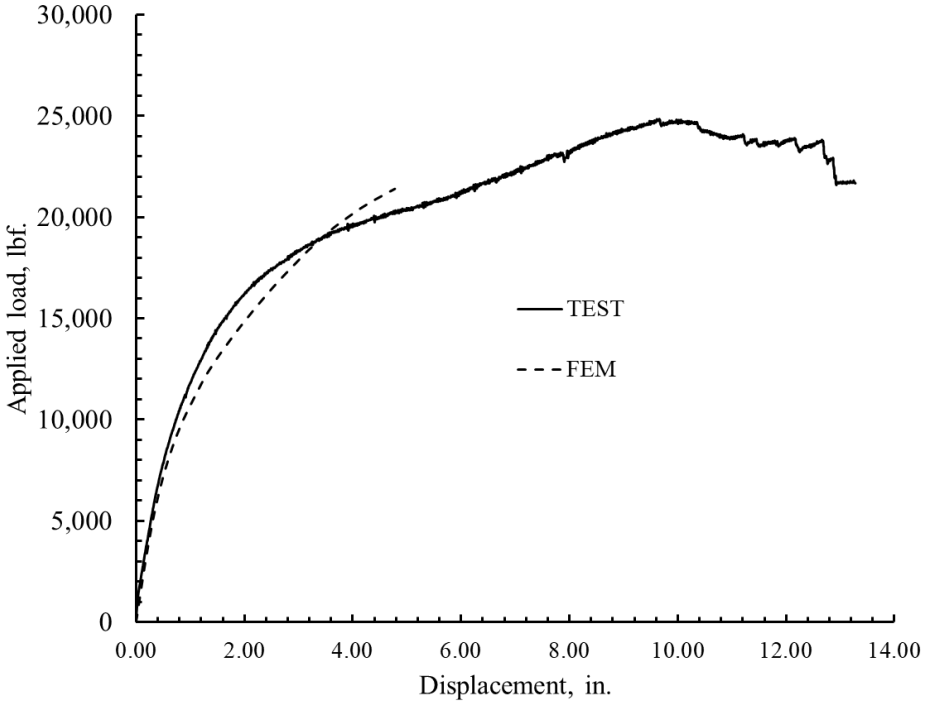

Figure 4-11 Load Displacement curve for soil of intact CMP

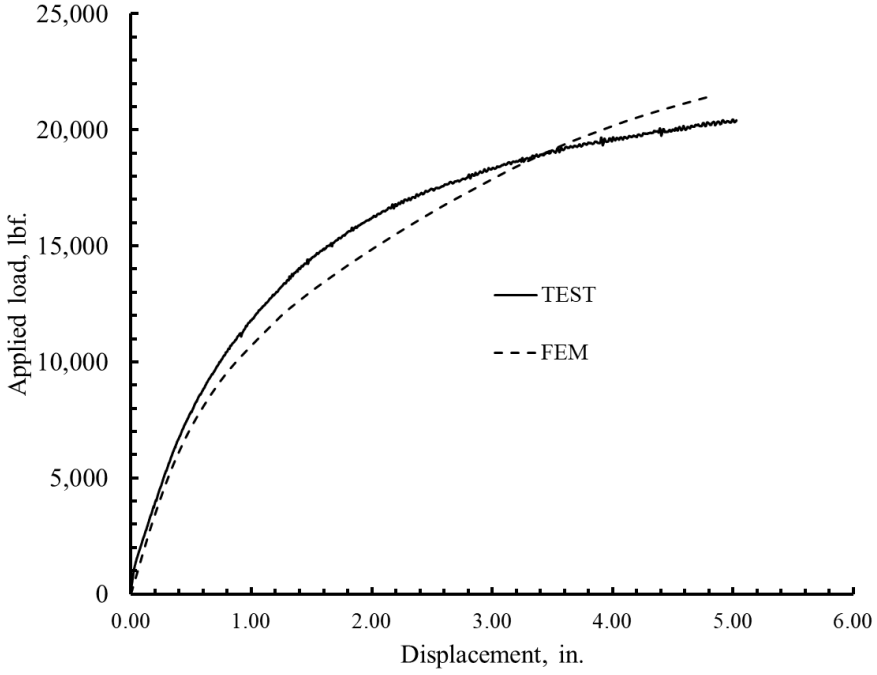

Figure 4-12 Load Displacement curve for soil at 5 in. displacement of soil of intact CMP

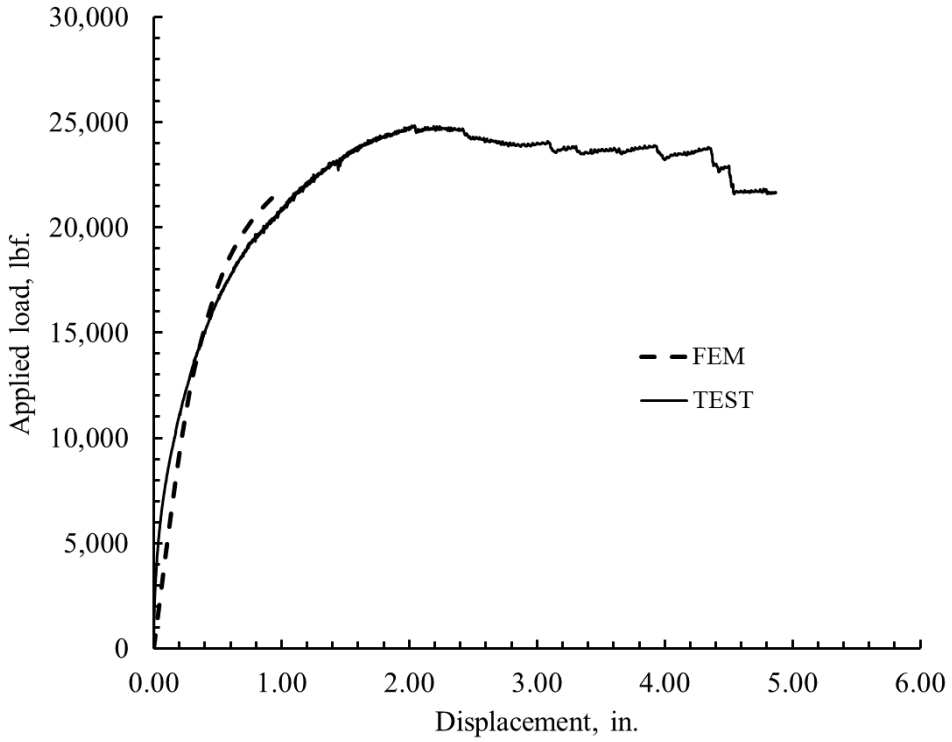

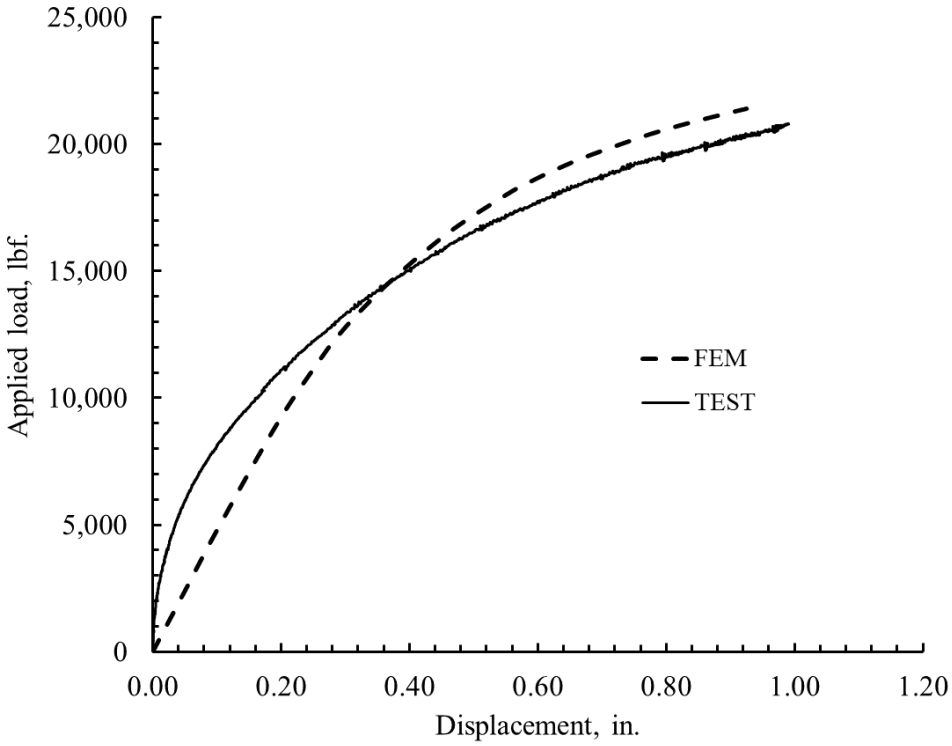

Figure 4-13 Load Displacement curve for the crown of intact CMP

Figure 4-14 Load Displacement curve for the crown at 5 in. displacement of the soil of intact CMP

The load vs displacement plot showed a good match between the experimental and FEM results. The discrepancy between the load at the 5 in. displacement of soil for the experiment and FEM is about 5 % while the discrepancy between the pipe crown displacement in experiment and FEM is about only 1.5 % (Table 4-5).

Table 4-5 Comparison of the results from FEM and Experiment

Model	Applied Displacement of soil (in.)	Maximum Applied Load (kips)	Max. vertical displacement of pipe at crown	Discrepancy in displacement (%)	Discrepancy in load (%)
Experimental	5	20.43	0.93		
FEM	5	21.4	0.92	1.08	4.75

2. Earth Pressure Distribution

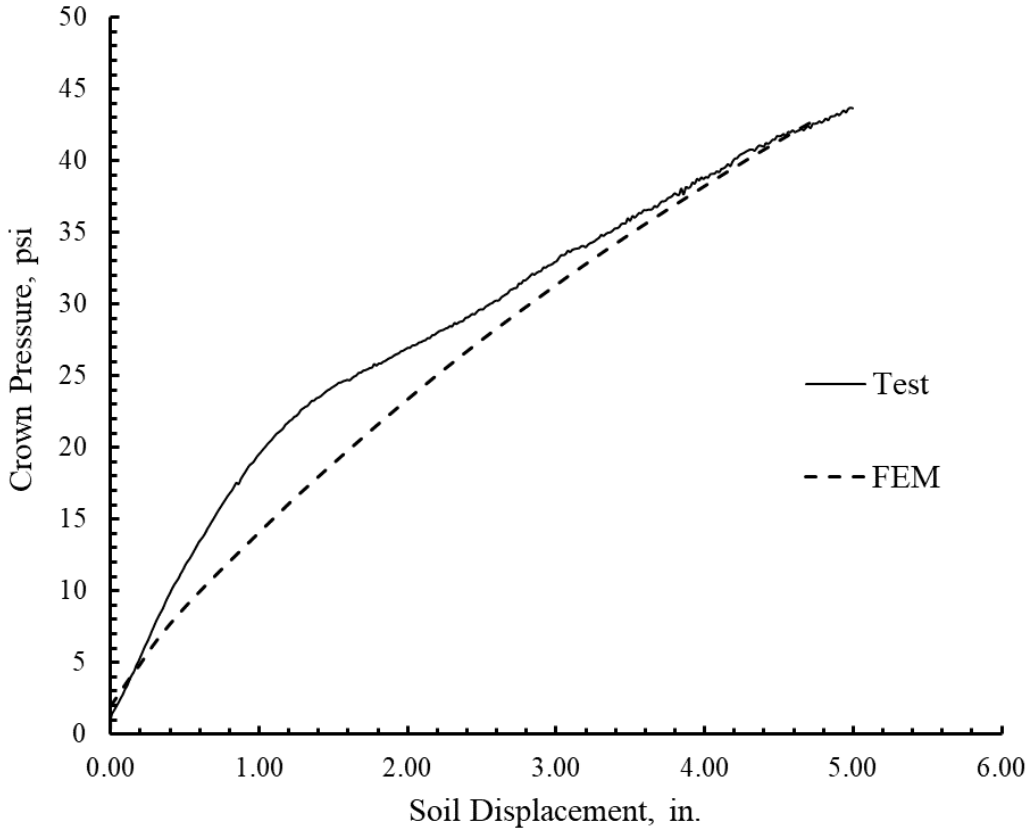

Figure 4-15 Earth pressure distribution just above the crown of the pipe of the intact pipe

Since the experiment results showed the maximum earth pressure around the CMP is located just below the load pad and a very small amount of the pressure was observed in the spring line and the invert, the FEM comparison was made only for the earth pressure at the crown. The earth pressure variation at the crown of CMP obtained from experimental results and the FE model at a similar location followed a similar curve (Figure 4-15). It is observed that (Figure 4-15) the FE model seems to predict the vertical stress at a crown level well.

3. Strain Bending moment and thrust

The results for the strains that were recorded were plotted against the movement of the soil and the comparison is shown in Figure 4-16. For the FEM comparison, since the maximum change in strain was seen in the crown and the shoulder, the comparison is made in that region. The strain vs displacement graph shows that the strains for the crown and the shoulder region followed a similar pattern. But the values of the strains showed the variation, especially at the crown region. Initially, the strains on the crown region were small but after the soil was displaced by about 2.5 in. as a sudden increase in the strain was seen.in the FEM model. This behavior was not observed for the experimental results. The strains read at the shoulder region matched well for the experiment and FE results.

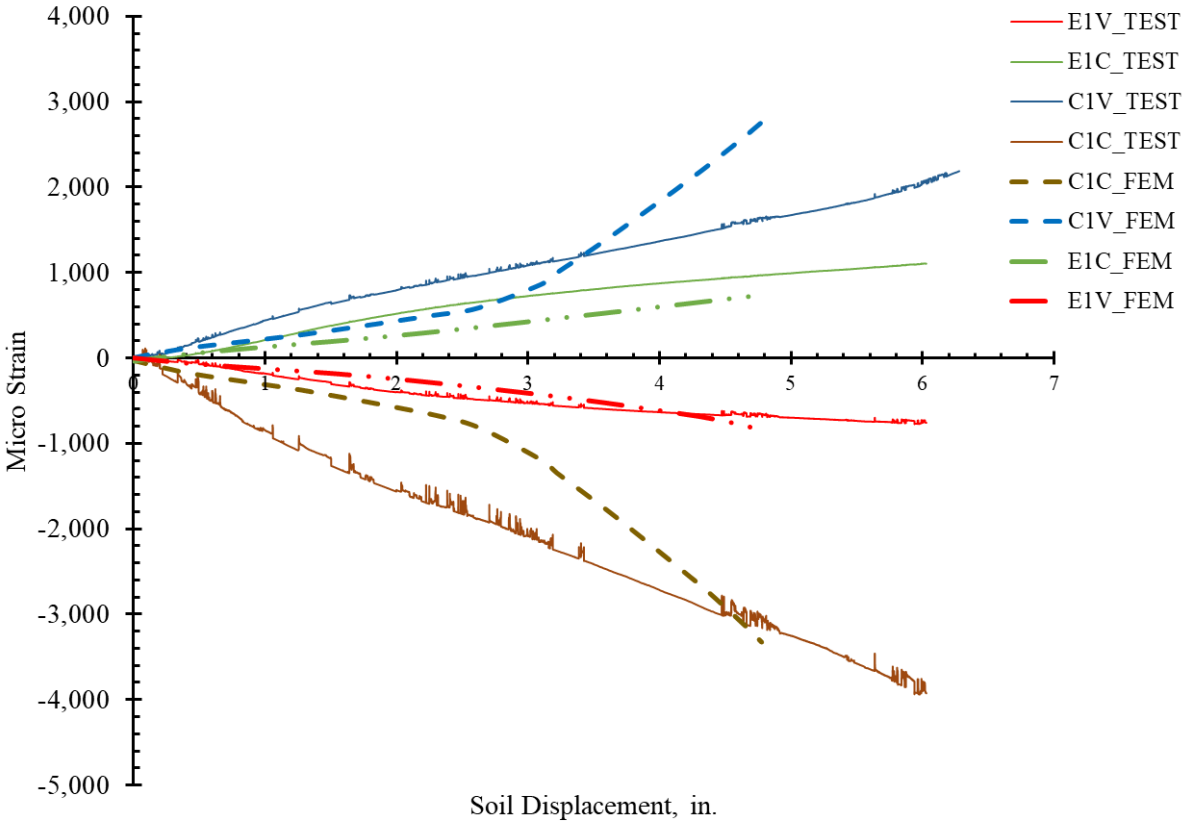

Figure 4-16 Comparison of strain at the crown and the shoulder region of an intact pipe

The aim of measuring the strains in the CMP is to calculate the bending moment and thrust in the CMP. Assuming the linear distribution of strain, the circumferential bending moment and thrusts at different locations in the CMP can be calculated by using the strain from the crest and the corresponding valley as follow (Elshimi 2011):

$$M_\theta = \frac{EI_\theta(\varepsilon_{\text{crest}} - \varepsilon_{\text{valley}})}{d}$$

where:

M_θ= Circumferential bending moment (lbf-in./in.),

I_θ= Moment of inertia per unit length in the circumferential direction (in.4/in.),

ε_{crest}= circumferential strain measured at crest of the corrugation,

ε_{valley}= circumferential strain measured at valley of the corrugation,

d= depth of corrugation (in.), and,

$$N_\theta = \frac{EA_\theta(\varepsilon_{\text{crest}} + \varepsilon_{\text{valley}})}{2}$$

where:

N_θ= circumferential thrust (lbf/in.),

A_θ= cross-section area per unit length in the circumferential direction.

As the strains compare well, the bending moment and the thrust are also well predicted. The bending moment obtained from the finite element model at the end of analysis was compared with the bending moment obtained from the laboratory test at a similar state. Both bending moments and thrusts at the different locations showed a good match with the experimental results.

The bending moments were compared when there was 5 in. displacement of soil at both FEM and Experimental results as shown in Figure 4-17. Except at the crown, the bending moment at the other position showed fair comparison. The maximum bending moment at the crown was 7.1 kip.in/in for experiment while from FEM it was calculated to be at 6.0 kip.in/in. Since the plastic deformation was seen in the crown at the 5 in. displacement of soil, so the bending moment theory may not be applied after the material has been yielded. For that reason, the bending moment at different load levels, before any plastic deformation was seen, was calculated and the comparison was made. It was found (Figure 4-18) that at the crown at the load levels of 5 and 10 kips the bending moment for experimental and FEM was matching well (Table 4-6).

Also, the thrust around the CMP was calculated and the results were compared at the 5 in. displacement of the soil (Figure 4-19). The results showed a fair comparison for the thrust except at the crown. The thrust was also plotted at the different levels of the loads and fair match was found between the FEM and experimental results (Figure 4-20, Table 4-7).

A calculation of the bending moment and thrust is calculated for the intact CMP model as the value of the ring stiffness is known. Later for the other test model, the comparison of the bending moment and the thrust is not made as with the introduction of the liner the combined ring stiffness of the CMP and the liner becomes complex in the calculation and needs more research. Also, the bending moment and the thrust would give the close match if the strain recorded matches closely. Thus, for further analysis, the comparison of the strains is made.

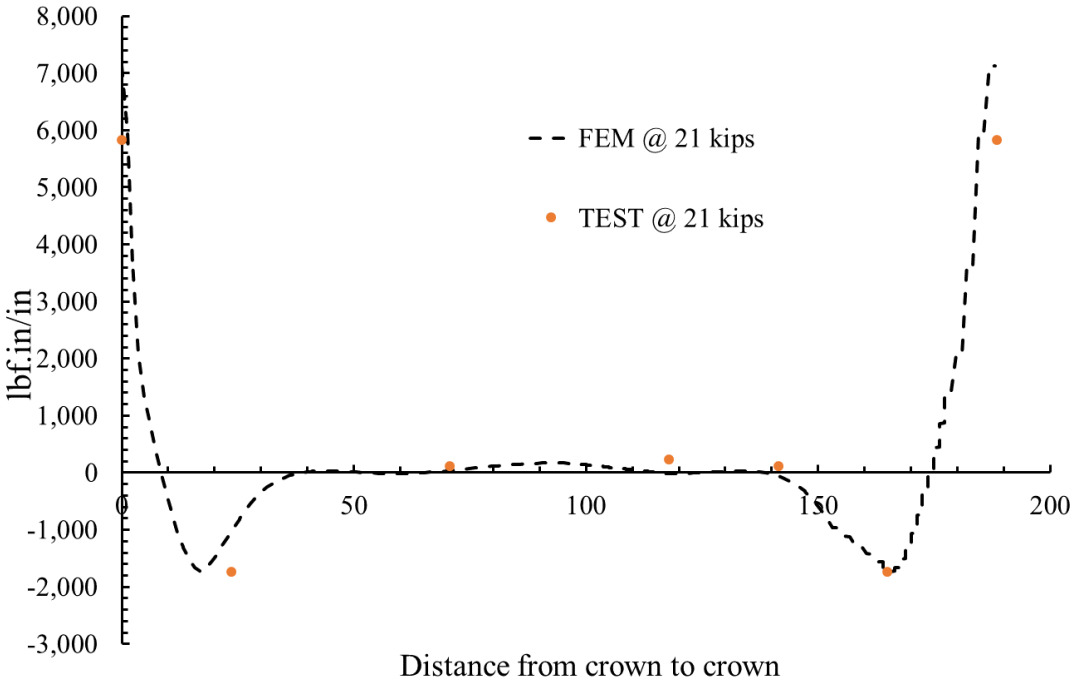

Figure 4-17 Bending Moment comparison at the 21 kips of load (@5 in. displacement of soil)

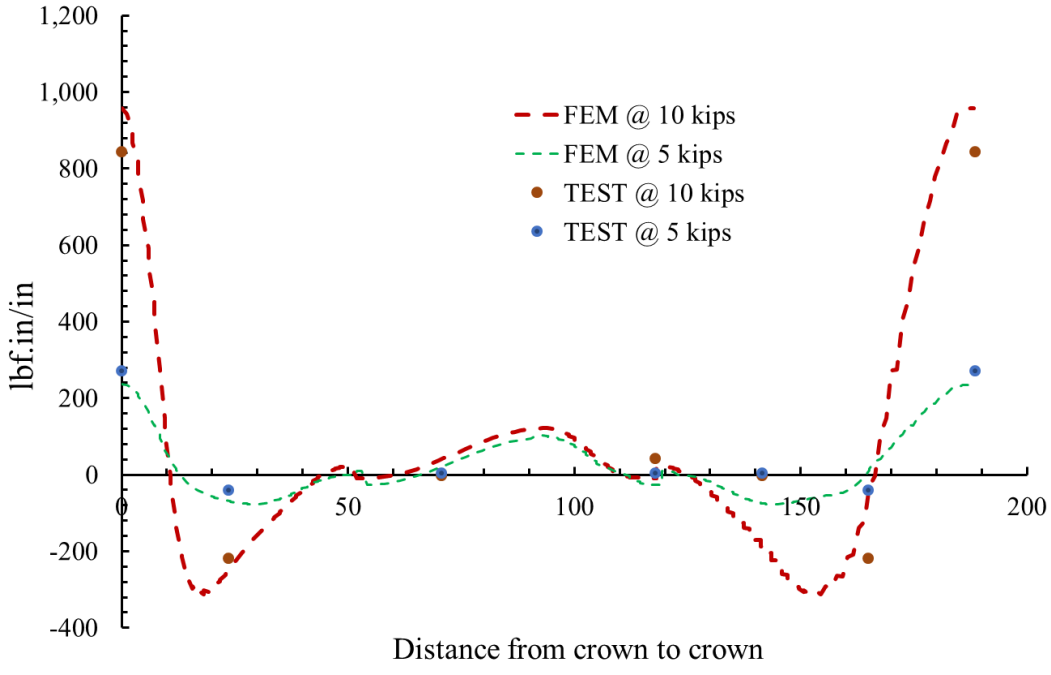

Figure 4-18 Bending moment comparison at 5 and 10 kips of load

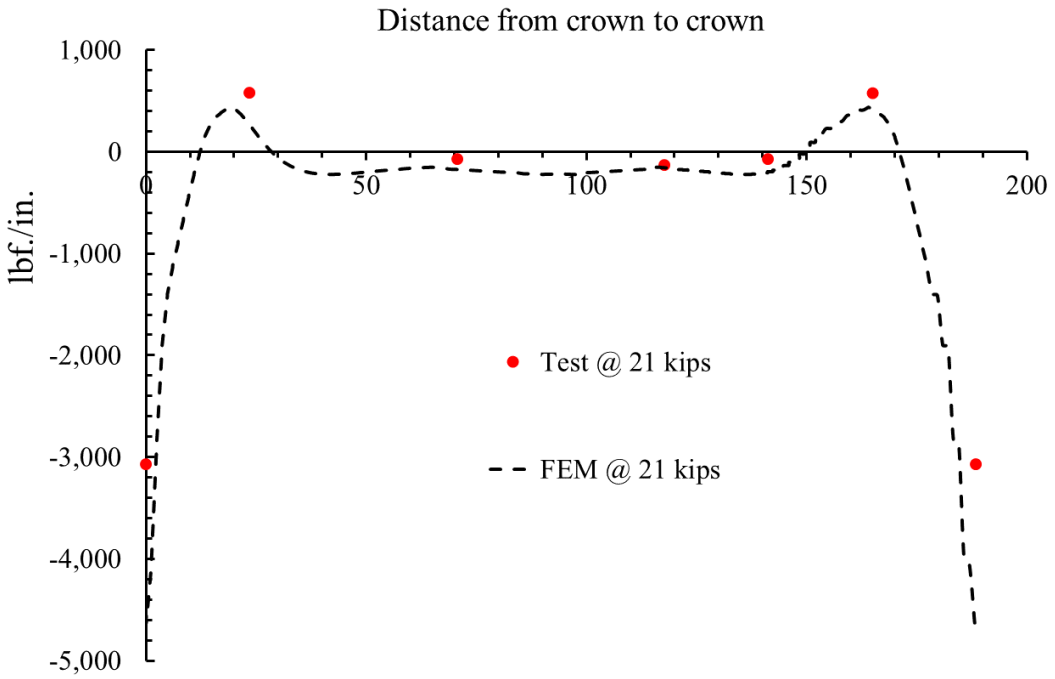

Figure 4-19 Thrust comparison at the 21 kips of load (@5 in. displacement of soil)

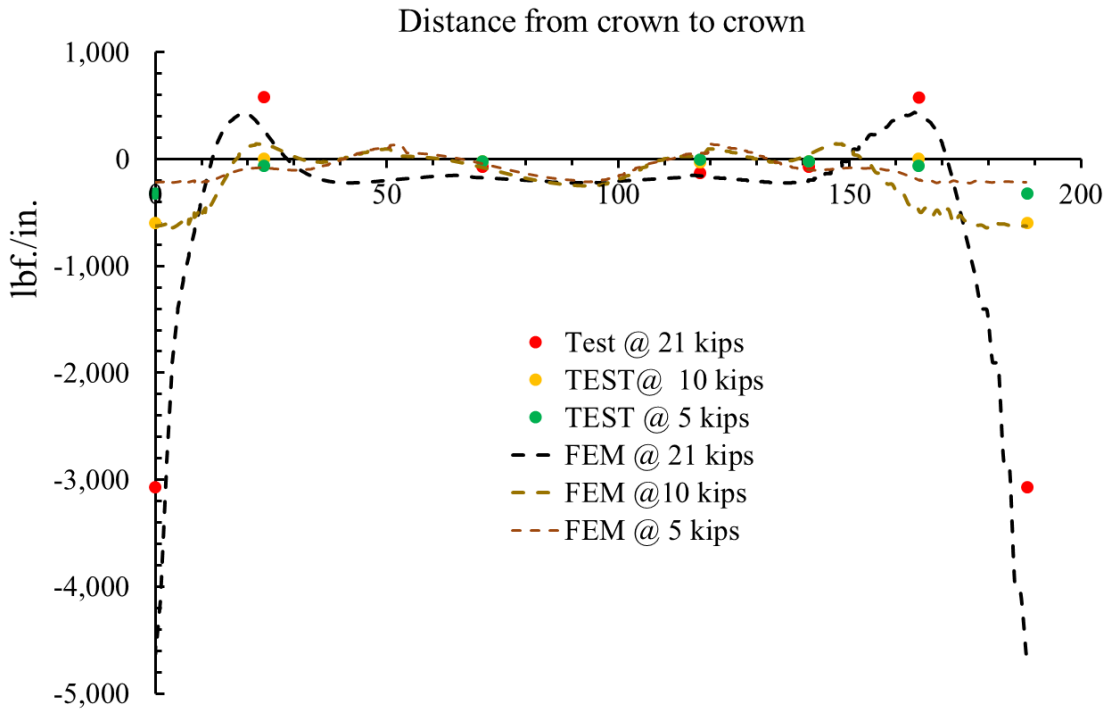

Figure 4-20 Thrust comparison at 5 and 10 kips of load

Table 4-6 Bending moment distribution at a different position

Bending Moment @5 in. displacement of soil		
Position	**Experiment (lbs.in/in.)**	**FEM (lbs.in/in.)**
Crown	**5937.968**	**7127.2**
Shoulder	**-1552.75**	**1680.38**
Springline	**88.4**	**80.08**
Haunch	**213.4**	**180.34**
Bending Moment @ 10 kips of load		
Position	**Experiment (lbs.in/in.)**	**FEM (lbs.in/in.)**
Crown	**843.8**	**956.99**
Shoulder	**-218.7**	**243.56**
Spring line	**-1.9**	**-2.82**
Haunch	**42.8**	**36.58**
Bending moment @ 5 kips of load		
Position	**Experiment (lbs.in/in.)**	**FEM (lbs.in/in.)**
Crown	**271.5**	**326.74**
Shoulder	**-40.1**	**-69.04**
Springline	**4.6**	**9.98**
Haunch	**5.6**	**4.5**

Table 4-7 Thrust distribution at different positions

Thrust @ 5 in. displacement of soil		
Position	**Experiment (lbs/in.)**	**FEM (lbs/in.)**
Crown	**-30 74.03**	**-4559.08**
Shoulder	**663.40**	**407.34**
Spring line	**-82.93**	**-177.23**
Haunch	**-142.7**	**-174.62**

Thrust @ 10 kips of load		
Position	**Experiment (lbs/in.)**	**FEM (lbs/in.)**
Crown	**-597.835**	**-760.58**
Shoulder	**0**	**112.45**
Spring line	**-26.999**	**-59.42**
Haunch	**-34.713**	**27.13**

Thrust @ 5 kips of load		
Position	**Experiment (lbs/in.)**	**FEM (lbs/in.)**
Crown	**-327.5**	**-289.558**
Shoulder	**-65.5**	**-91.80**
Spring line	**-25.26**	**-37.23**
Haunch	**-11.51**	**94.91**

4.8.2 Intact CMP (20x40 in^2 load pad)

Since after the 1st control test of the bare CMP, it was observed that, failure of the soil was observed before the significant deflection was seen in the pipe. Thus, it was decided to load the next set up of the experiments with the bigger load pad of size (20x40 in^2). Hence, to get the results and compare the results of other tests with the bare intact CMP, FEM was used to generate the results for the intact pipe loaded under the 20x40 in^2 load pad. As the FEM model was calibrated for the small load pad test, the same model was used to generate the results.

From the FEM test, it was found that due to the bigger size of the load pad the failure mechanism of the pipe soil system was changed. It was seen that unlike the local buckling just around the center of the crown (Figure 4-10 (a)), the pipe failed through the significant bending of the crown along the length of the pipe (Figure 4-21(b)).

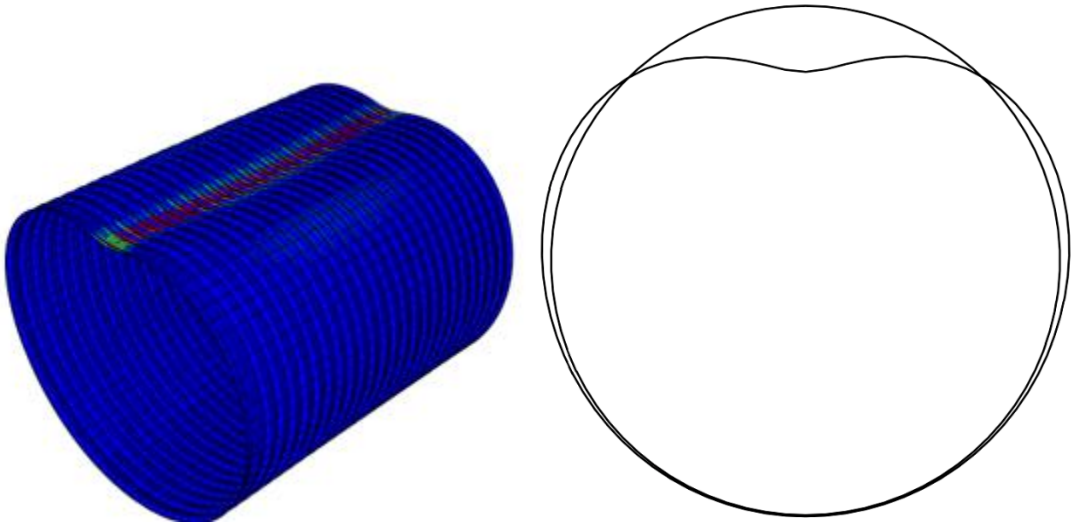

Figure 4-21 Plastic strain and the deformation of the pipe loaded under the 20x40 in^2 load pad

1. Load Displacement Plots

The load-displacement graphs were plotted from the FEM results against the applied load for movement of soil just below the load pad and displacement of the crown at the center of the CMP.

From the load-displacement graph, it was found that the crown of the CMP was displaced by more than 4.2 in. i.e. 6.67 % of the diameter of the CMP at the peak load condition while the displacement of the soil at peak load t was 5.9 in. Since flexible pipes have the 5% deflection criteria as its failure criteria, thus the CMP failed before the failure of the soil (Figure 4-22, Figure 4-23). The result suggests that the use of the bigger load pad avoids the failure of the soil through punching which was observed in the control test for the intact CMP. With the use of the bigger load pad configuration, the CMP carried nearly the double load as compared with the load-carrying capacity of the smaller load pad configuration. The results and the comparison are summarized in Table 4-8.

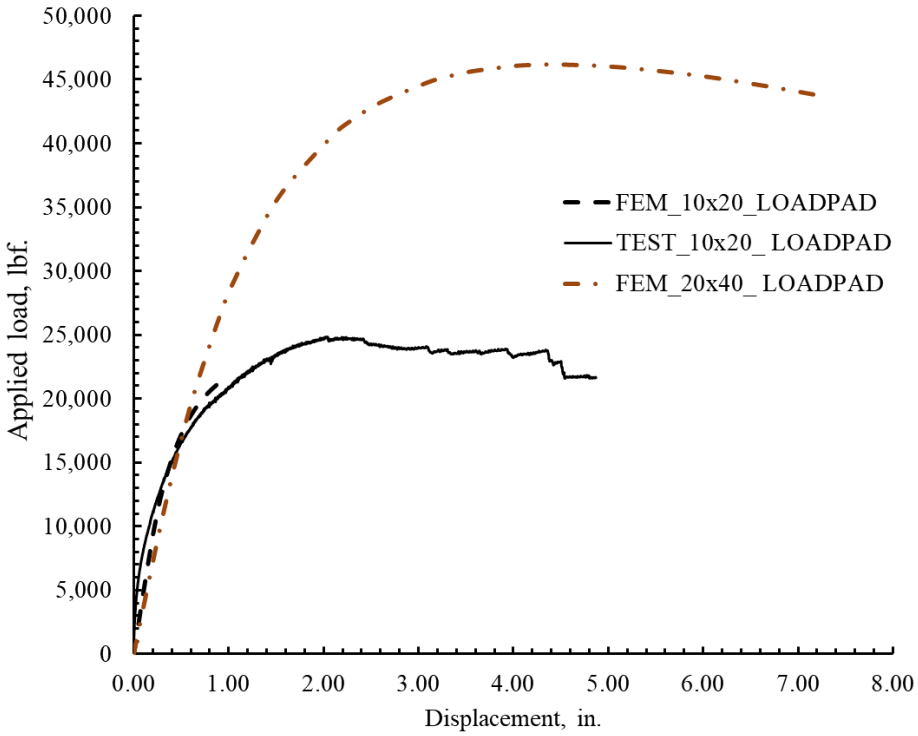

Figure 4-22 Load displacement at crown for the bigger load pad compared with the test result with smaller load pad (10x20 in^2)

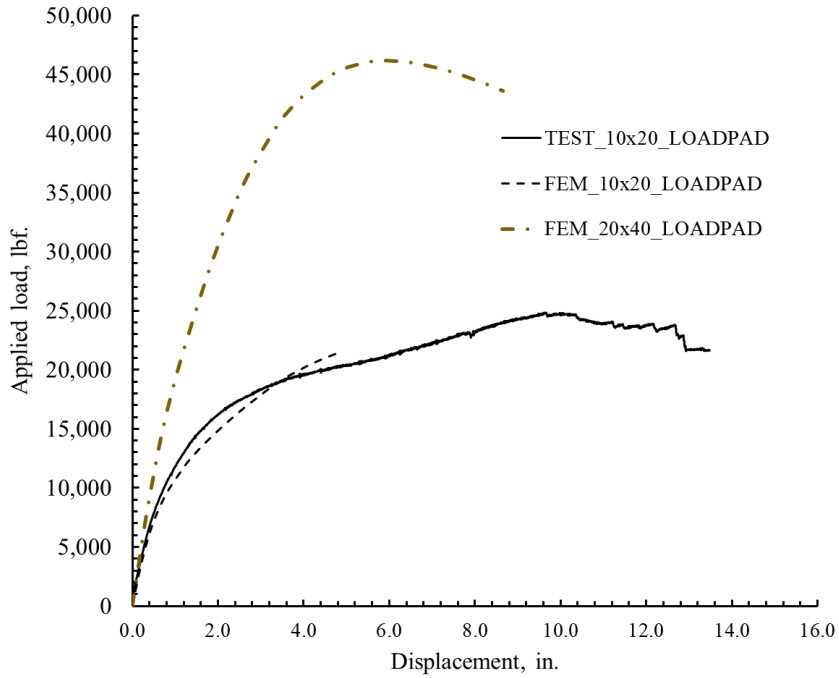

Figure 4-23 Load displacement from soil for the bigger load pad compared with the test result with smaller load pad (10x20 in^2)

Description (At failure of soil)	10x20 in^2 Load Pad	20x40 in^2 Load Pad
Ultimate load (kips)	21.01	46.05
Crown Displacement (in.)	1.3	4.26
Soil Displacement (in.)	5.0	5.99

Table 4-8 Comparison of the results for the intact CMP for smaller and bigger load condition

2. Earth pressure:

The earth pressure 4 in. above the crown for the bigger load pad region was plotted against the soil displacement and was compared with the earth pressure at a similar location for the smaller load pad. From the FEM it was noted that the earth pressure at the failure of the soil i.e., at 5 in. displacement of soil was nearly equal (about 38 psi). But the ultimate pressure at the crown for the bigger load pad (38 psi) compared with the smaller load pad (78 psi) was nearly half.

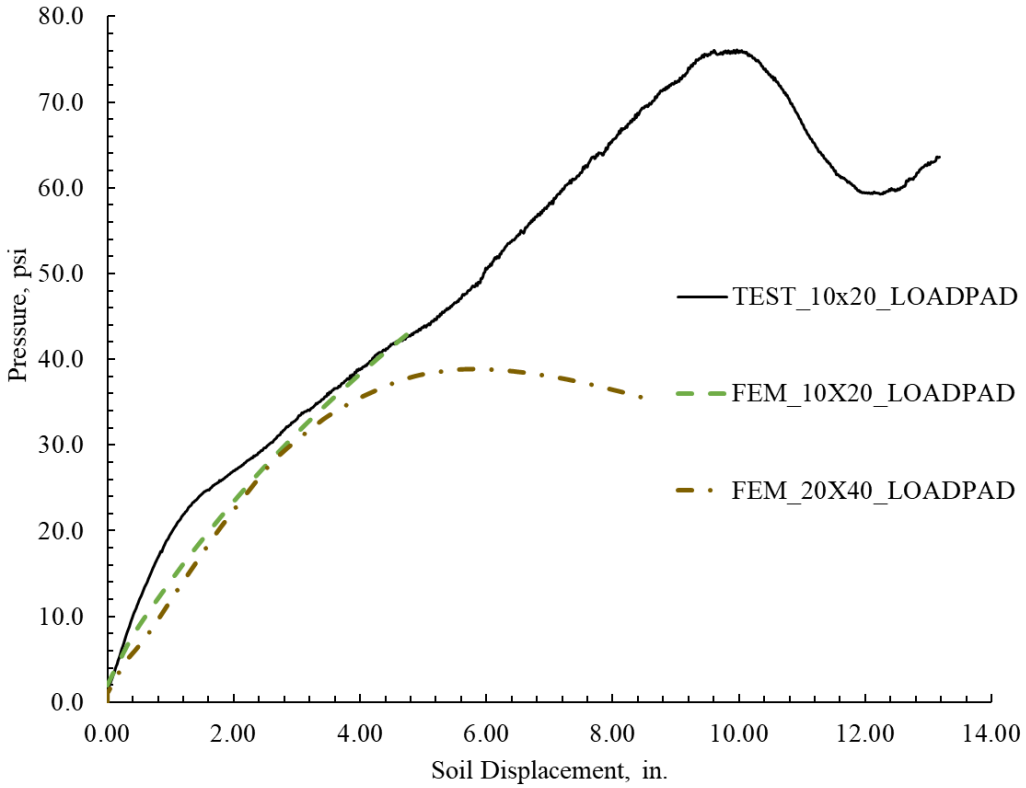

Figure 4-24 Earth pressure comparison for the bigger and smaller load pad conditions

4.8.3 Invert Cut CMP

After calibrating the results for the intact CMP, the same model was modified for modeling the experiment for the invert removed CMP. During the removal of the invert, the significant movement in the soil and the pipe was observed in the experiment, and the gap was created between the soil and the pipe. The FE model also tried to imitate similar behavior during the invert removal process. But the FE model was not able to predict the collapse behavior of the soil as in the experiment soil settled more than 6 in. while in the FE model the settlement of the soil was only about 1 in. Comparing the horizontal movement of the invert cut edges, it was seen in the experiment (Figure 4-25(b)) that after removal of the invert, the pipe had closed in by 3 in. each on either side causing the gap of 18 in. to be reduced by more than 6 in. From the FE results it was obtained that after the invert removal, the CMP invert edges moved by 2.4 in. form both sides resulting in the reduction of 4.8 inches of the gap (Figure 4-25(a), (c)). The test result for the invert removal case was reported by (Darabnoush Tehrani, et al., 2020). The results after the invert removal are summarized in Table 4-9 Comparison of the change in dimension of the pipe after removal of the invert. (Table 4-9)

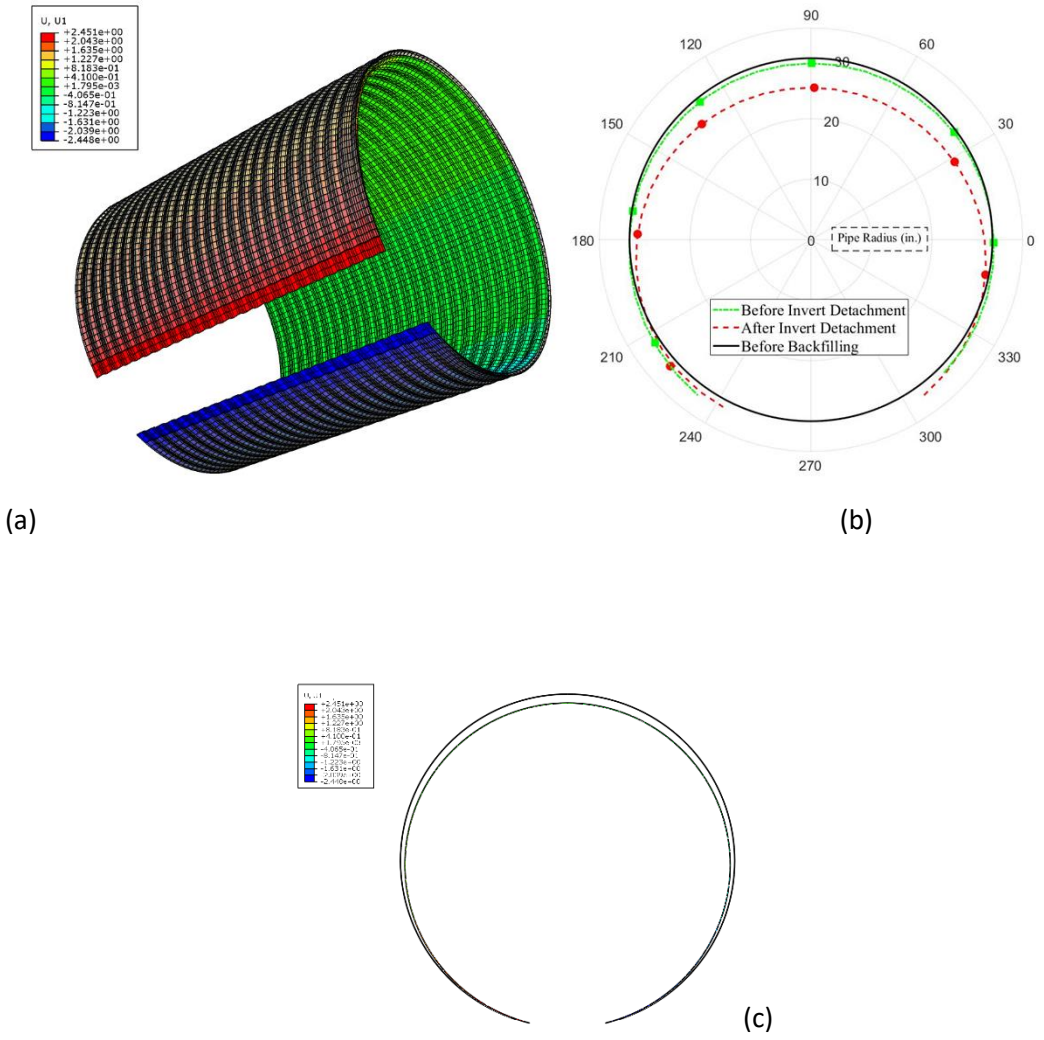

Figure 4-25(a) Reduction in the invert gap from FEM (b) Experimental recording of the reduction in invert gap by Digital Image Processing (Darabnoush Tehrani, et al., 2020) (c) Vertical diameter change from FEM after invert removal

Description	FEM	TEST
Reduction in the 18 in. invert gap (in.)	2.4	3
Reduction in vertical diameter (in.)	2.25	3.1
Soil movement (in.)	1.0	6.5

Table 4-9 Comparison of the change in dimension of the pipe after removal of the invert

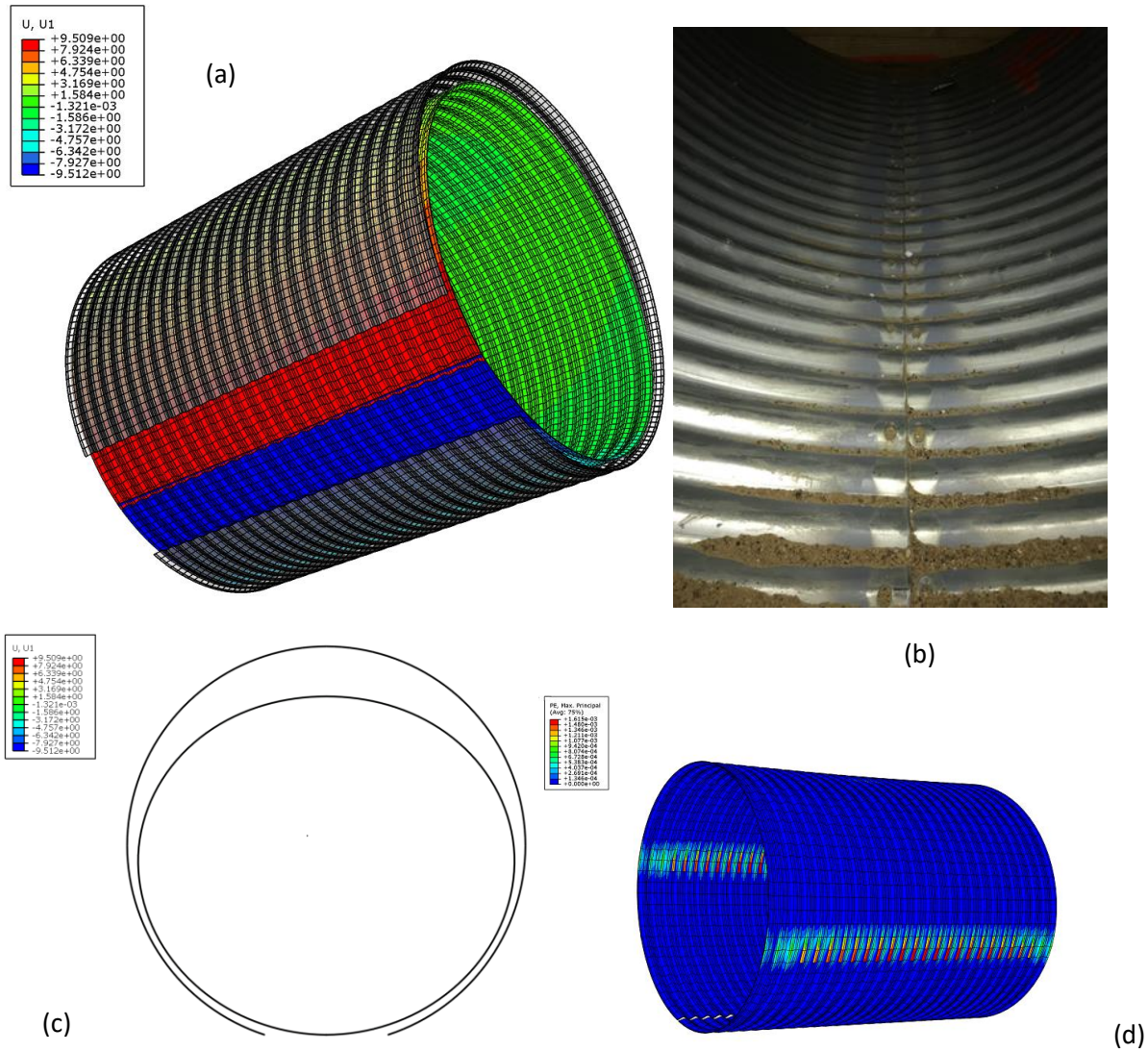

Figure 4-26 Complete closure of the invert after loading (a), (c) from FEM (b) closure of invert seen in the Experiment (Source: CUIRE Laboratory) (d) plastic strain at the spring line area

1. Load Displacement Plots

The load-displacement results exclude all the displacement before the loading of the system for both test and FEM results.

The comparison of the load-displacement plot showed a significant difference (Figure 4-26, Figure 4-27). In the test, it was observed that the CMP started to close in rapidly without much of the resistance and the invert edges met each other's ends after only 3 in. vertical downward movement of the crown taking only about 8 kips of the load. But in the FEM the invert edges met only after 6 in. vertical downward movement of the crown of the CMP taking 22 kips of a load. In the FEM model, 8 in. soil displacement was required for the inverts to meet but in the test, I invert edges meet after 3 in. displacement of soil. The reason for the significant difference in the soil movement can be given to the fact that in the test, the soil settled and got compacted by more than 6 in. after the invert removal process but in FEM it was observed that soil had only 1 in. settlement. The movement of the soil was less in FEM because the soil model used could not predict the flow behavior of the soil. Also, after the invert met, further displacement could not be applied to the FE model as the model stopped running due to the convergence error. Thus, the FE model could not predict the load-displacement curve after the establishment of the ring stiffness.

A significant amount of the plastic strain was developed in the spring line when the gap between the pipe and the soil was closed by more than 14 in. (Figure 4-26). No plastic strain was seen on the crown until the invert completely gets closed.

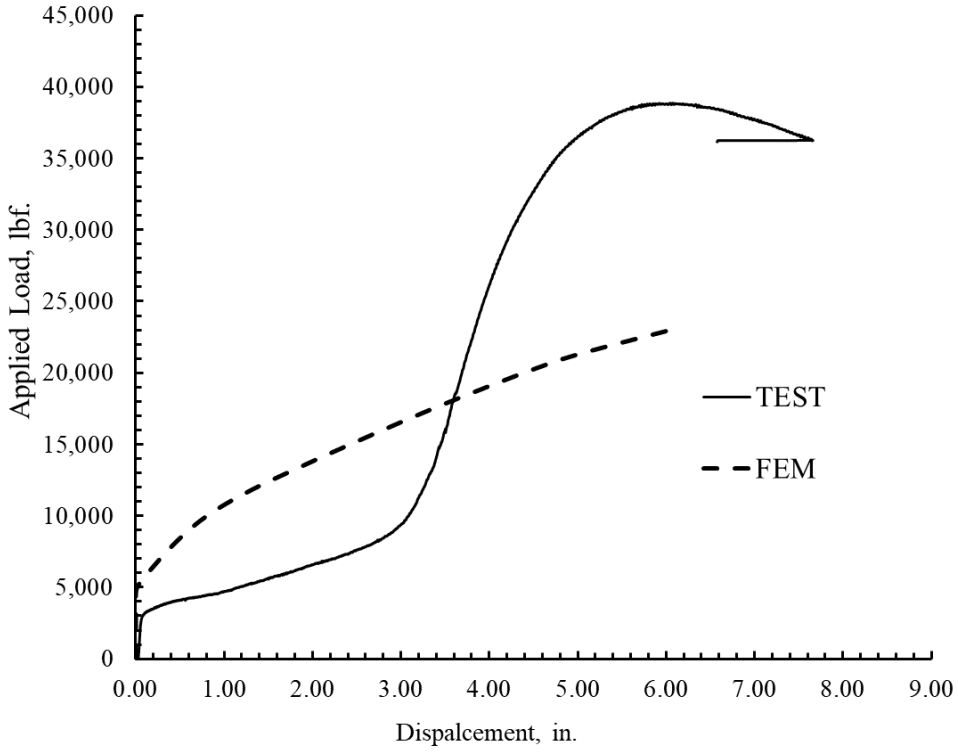

(a)

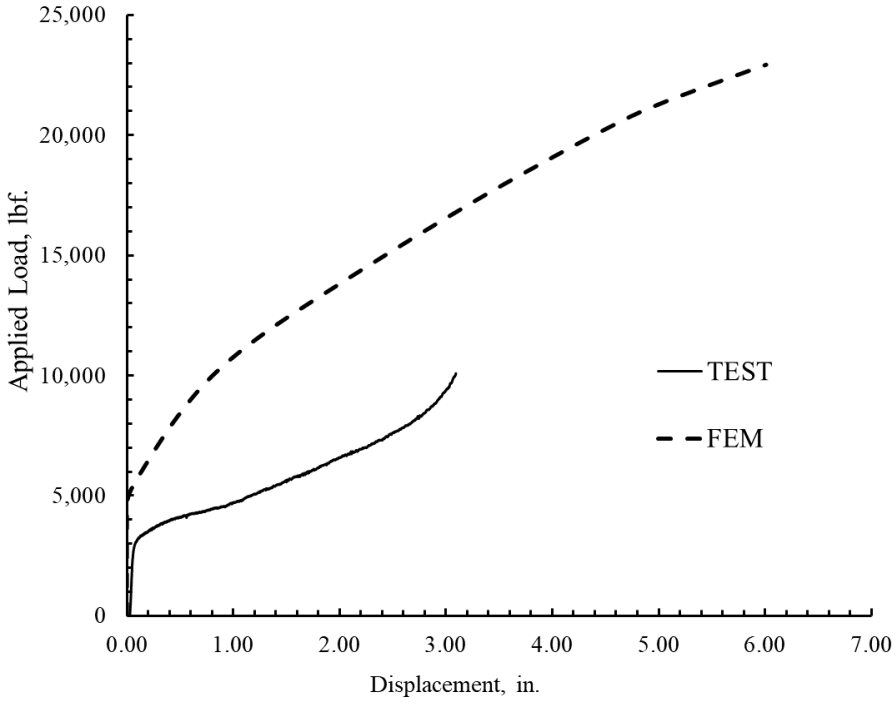

(b)

Figure 4-27 Load displacement plot for the movement of CMP's crown (a) Comparison at the ultimate conditions (b) Comparison when the inverts just meet

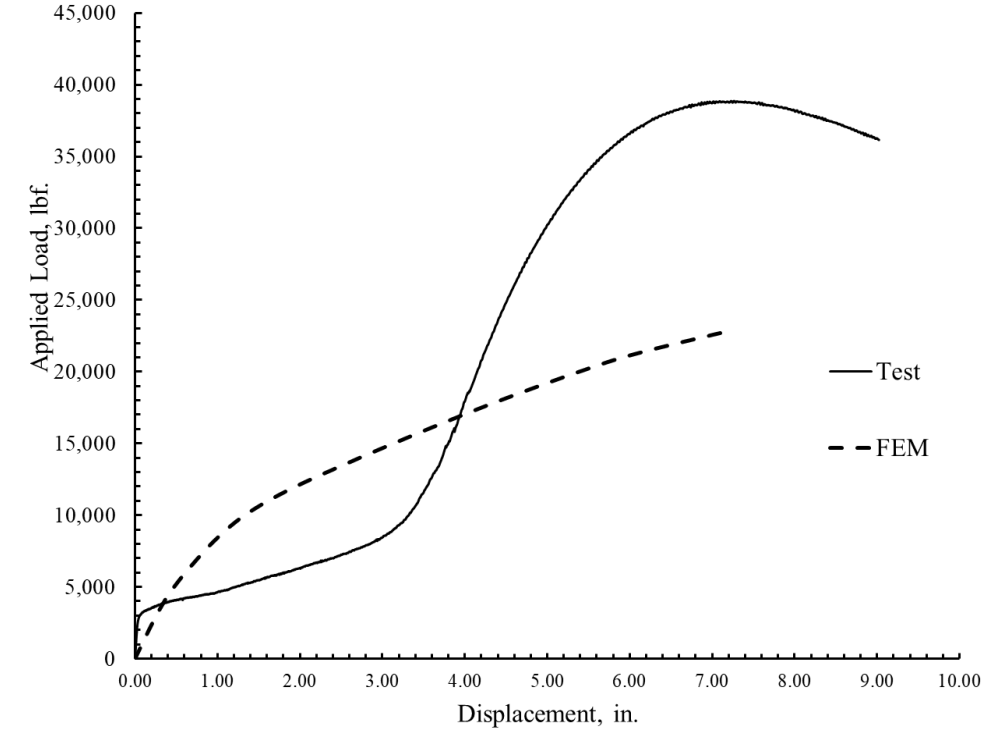

(a)

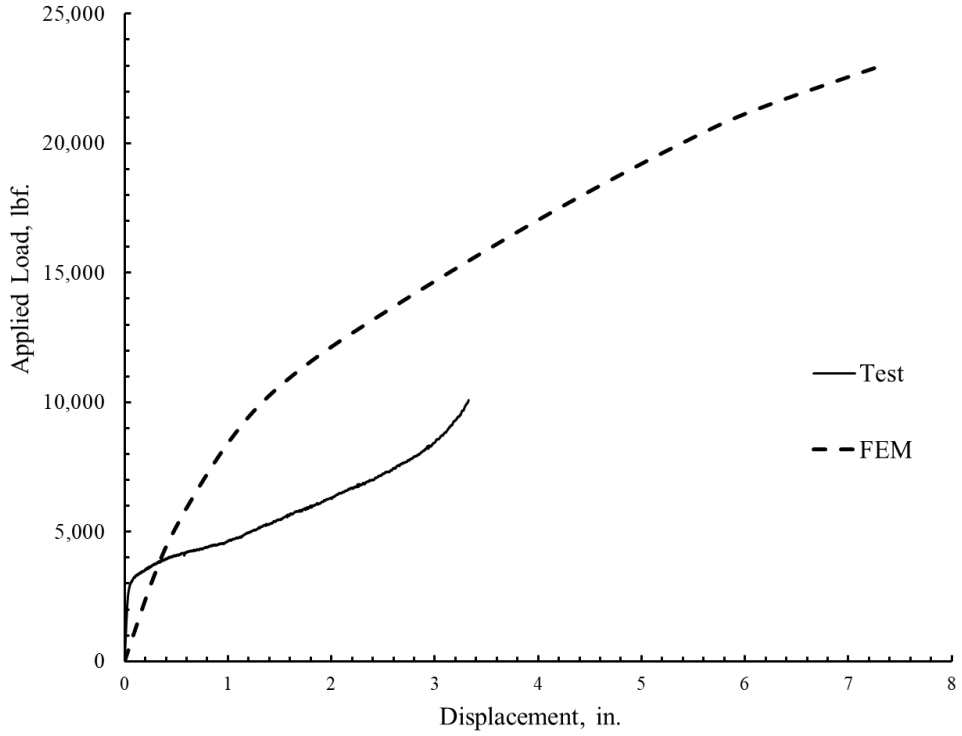

(b)

Figure 4-28 Load Displacement for the soil movement just beneath the load pad (a) Comparison at the ultimate conditions (b) Comparison when the inverts just meet

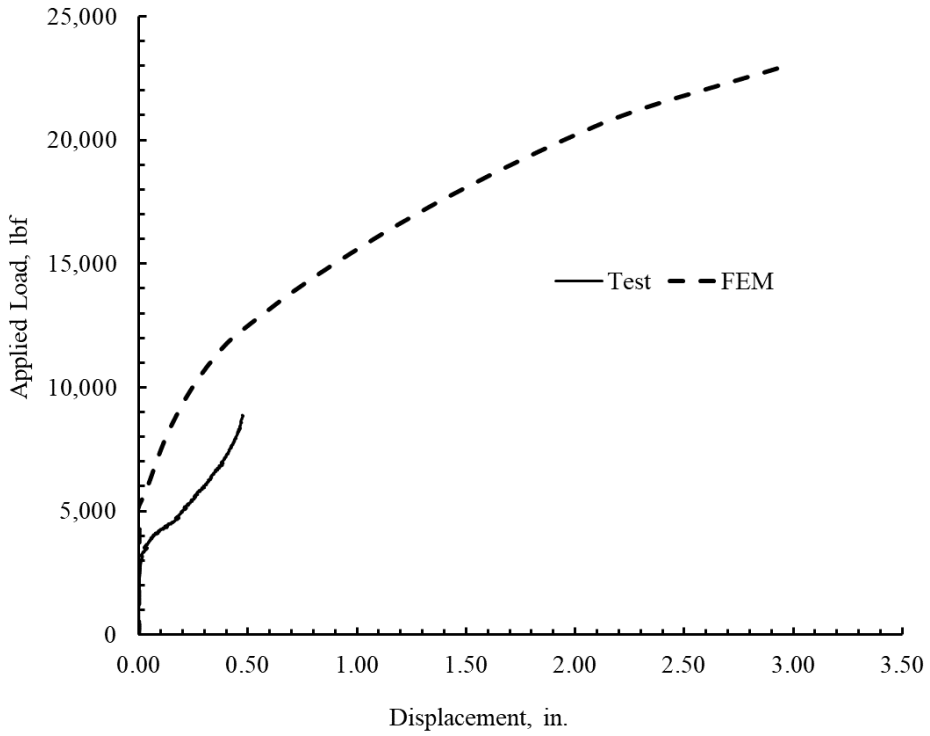

Figure 4-29 Movement of the spring line for FEM and TEST just before the meeting of the invert edges

2. Earth Pressure Distribution

Following the comparison of the load-displacement, the comparison of the earth pressure, 4 in. above the crown was made. The comparison of the FEM results showed the FEM over-predicts the earth pressure by about 125% to the test at the time when both the invert edges meet. (Figure 4-30)

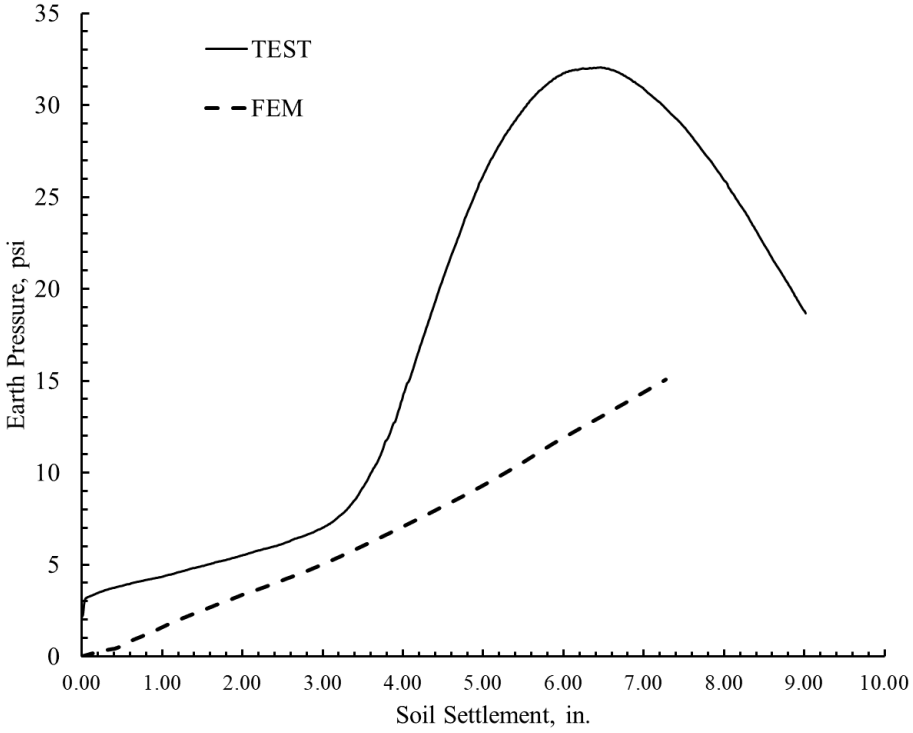

(a)

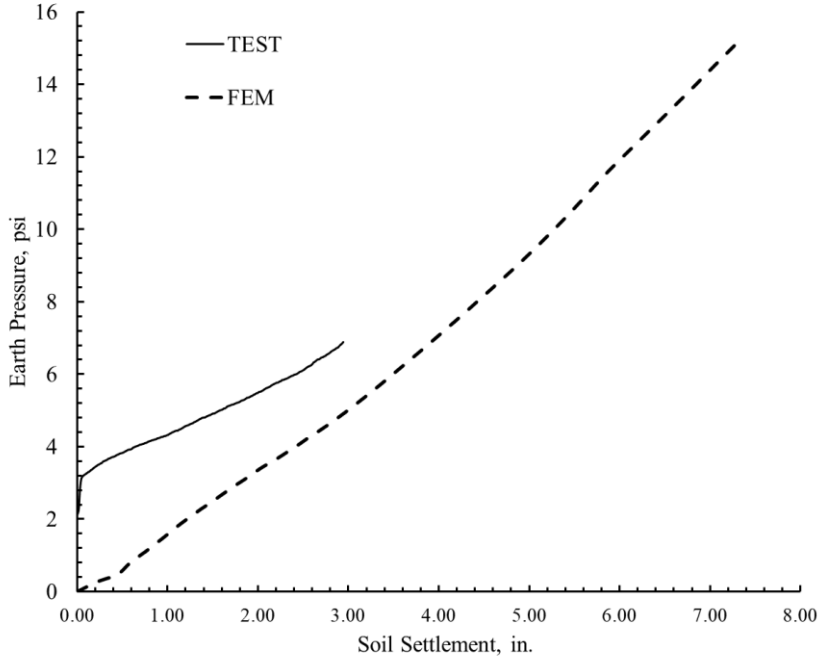

(b)

Figure 4-30 Earth Pressure Comparison (a) Comparison at the ultimate conditions (b) Comparison when the inverts just meet

4. Strains

Since due to the significant movement of the CMP, some of the installed strain gages were damaged during the invert removal process. The results for the strains that were recorded were plotted against the movement of the soil and the comparison is shown in Table 4-10. For the FEM comparison, as the maximum change in strain was seen in the crown and the shoulder of the CMP, the comparison is made in that region (Figure 4-31). The strain vs displacement graph shows that the strains were nearly equal up to the 3 in. of soil displacement. In the test after 3 in. displacement, the invert edge meet and the CMP started to behave as the intact pipe as the ring stiffness was reestablished, and hence, we could see the strains going up rapidly after that point. But in the FE model, the invert edges did not meet till 8 in. vertical displacement of the crown as of result no sudden change in the strains was seen after 3 in. of soil displacement.

Comparison of the strain at the 3 in. displacement of soil		
Location	FEM (Micro strains)	Test (Micro strains)
C1C	450	388
C1V	337	- (damaged)
E1V	567	400
E1C	561	573

Table 4-10 Comparison of strains

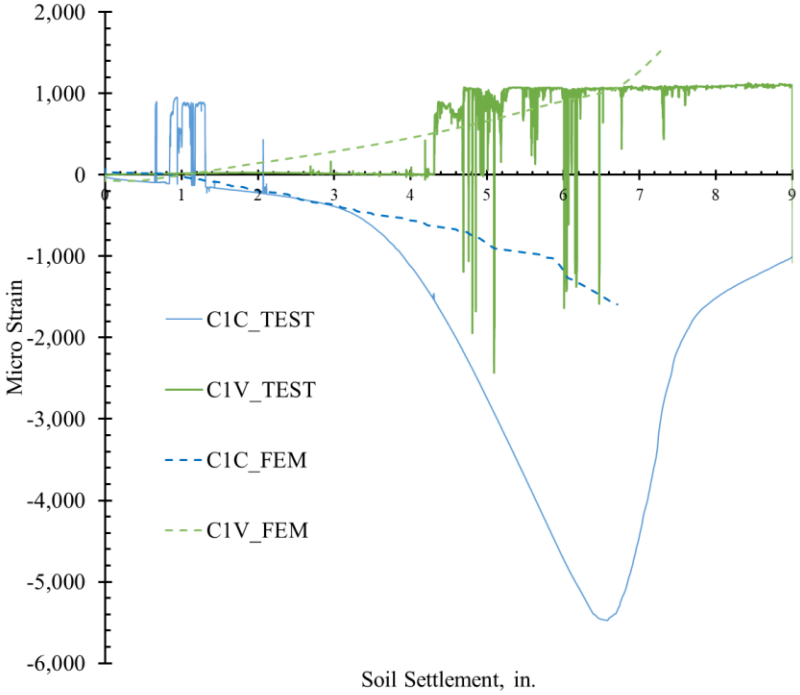

(a)

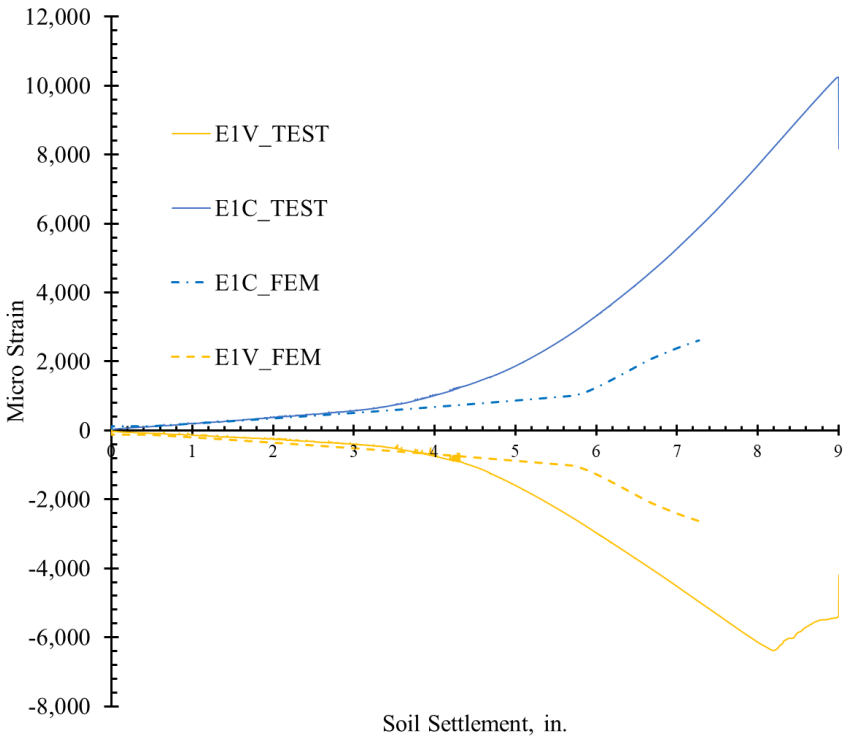

(b)

Figure 4-31 Comparison of strains for the test and FEM results (a) at Crown (b) at Shoulder (invert-cut CMP)

5. Summary of the invert cut FE model

Comparing the FE results and the experimental results for the test on invert cut CMP, the model over-predicts the load at time when the two invert edges meet. Also, the FE model could not predict the collapse of the soil as it was in the experiment condition. Thus, for the FE analysis of the invert removed model, a constitutive model that could model the large deformation of the soil is recommended to use.

4.8.4 Comparison of the Results for Control Test

After the FE model was calibrated for the intact CMP and the invert cut CMP, a comparison for the loss in the load capacity of the pipe before and after the removal of the invert is made. The results for the intact CMP are for the bigger load pad only as the invert cut CMP was tested with the bigger load pad only.

1. Load Carrying capacity comparison

Since only little resistance was provided by the invert cut CMP before the invert cut edges met, with a small amount of load, the invert removed CMP showed a significant loss in the structural capacity. The load carried by the CMP after the re-establishment of the ring stiffness is not considered in the comparison of the reduction of the load as with such large movement the system would be at the state of collapse.

The comparison result showed that there was a 50% reduction in the load-carrying capacity of the CMP before the invert edges meet from FEM while the load reduction was by 80% compared for the test results till the invert edges met. (Figure 4-32, Figure 4-33).

The comparison results are summarized in Table 4-11.

	FEM (@ Ultimate)		TEST (@ Ultimate)	
Description	Load Capacity (kips)	Pipe deflection (in.)	Load Capacity (kips)	Pipe deflection (in.)
Intact Pipe	46.17	4.17	-	-
Invert removed	22.73	6.86	9.5	6.1
Reduction (%)	50.76	-60.5	79.42	-46.4

* The pipe deflection for the invert cut CMP includes the displacement of the crown prior to loading

Table 4-11 Comparison results for the Intact and the Invert cut CMP from FEM and the Test before the invert edges meet

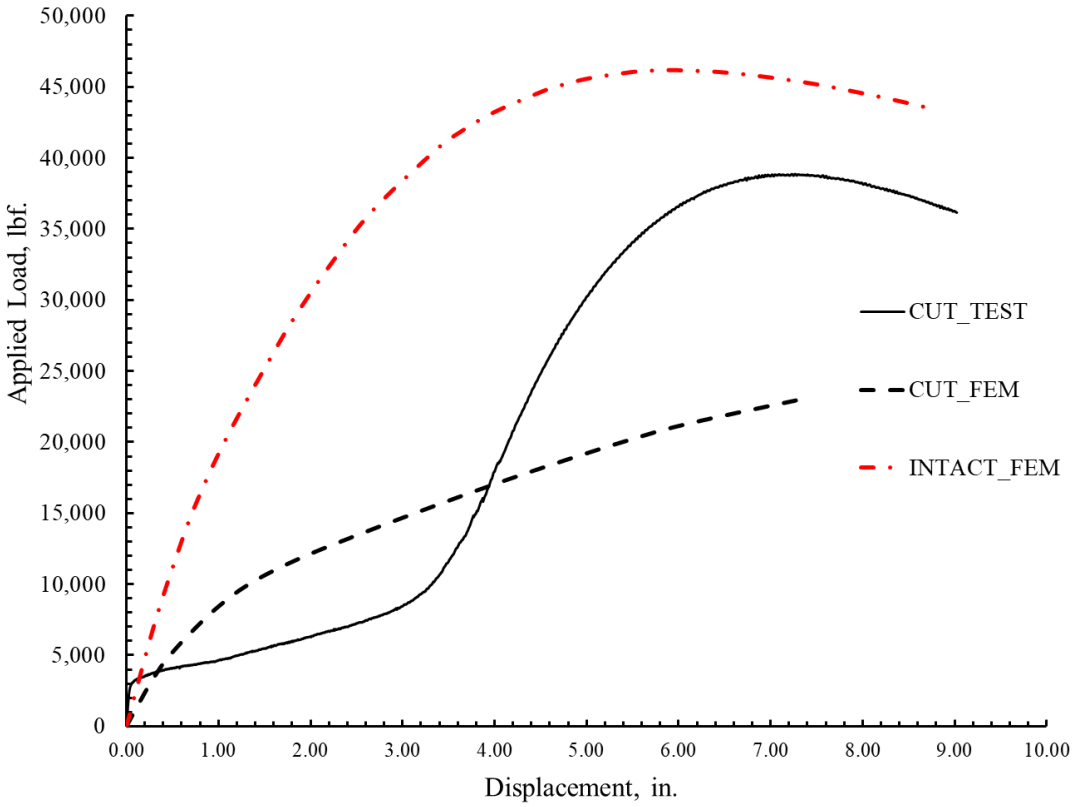

Figure 4-32Comparison of load displacement plots of soil for intact and invert cut CMP

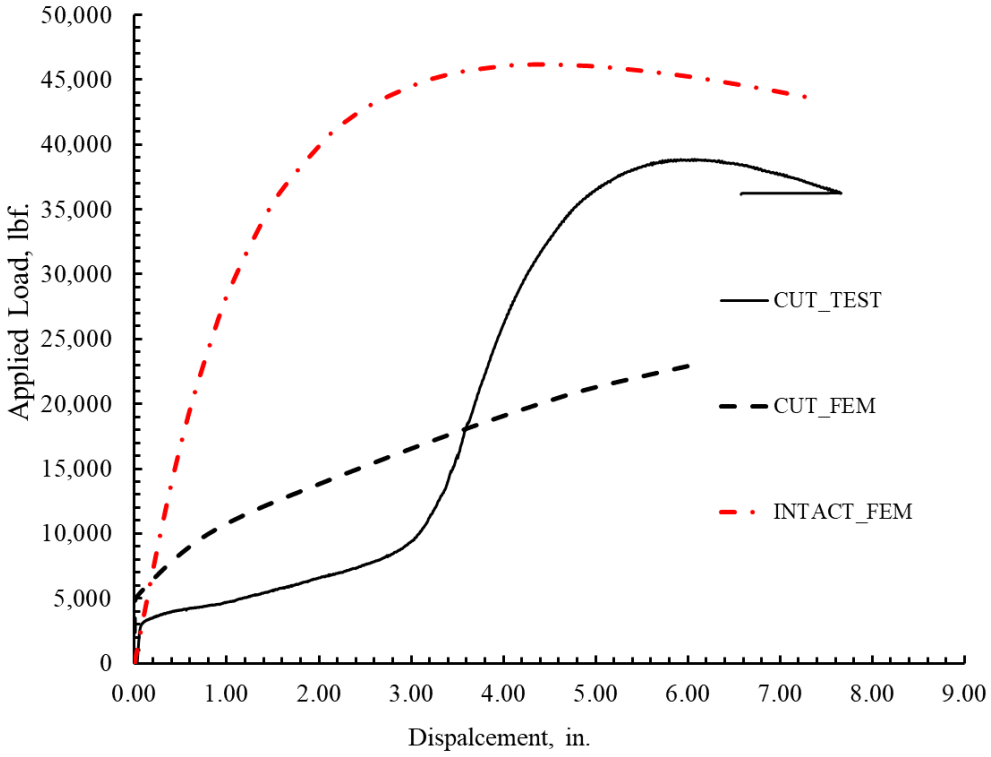

Figure 4-33 Comparison of load-displacement plots of CMP's crown for intact and invert cut CMP

2. Earth Pressure Comparison

When the earth pressure comparison was made it was seen that the pressure in the soil above the crown was significantly low (by about 80%) compared to the intact CMP loaded under the same loading configuration. The value of the pressure above the crown before the invert edges met was around 10 psi only (Figure 4-34) while the intact CMP at the peak load had near about 39 psi pressure. This also signifies that the load in the FEM and test before the invert edges met, it gets redistributed around the soil while the pipe was only taking a small amount of the load.

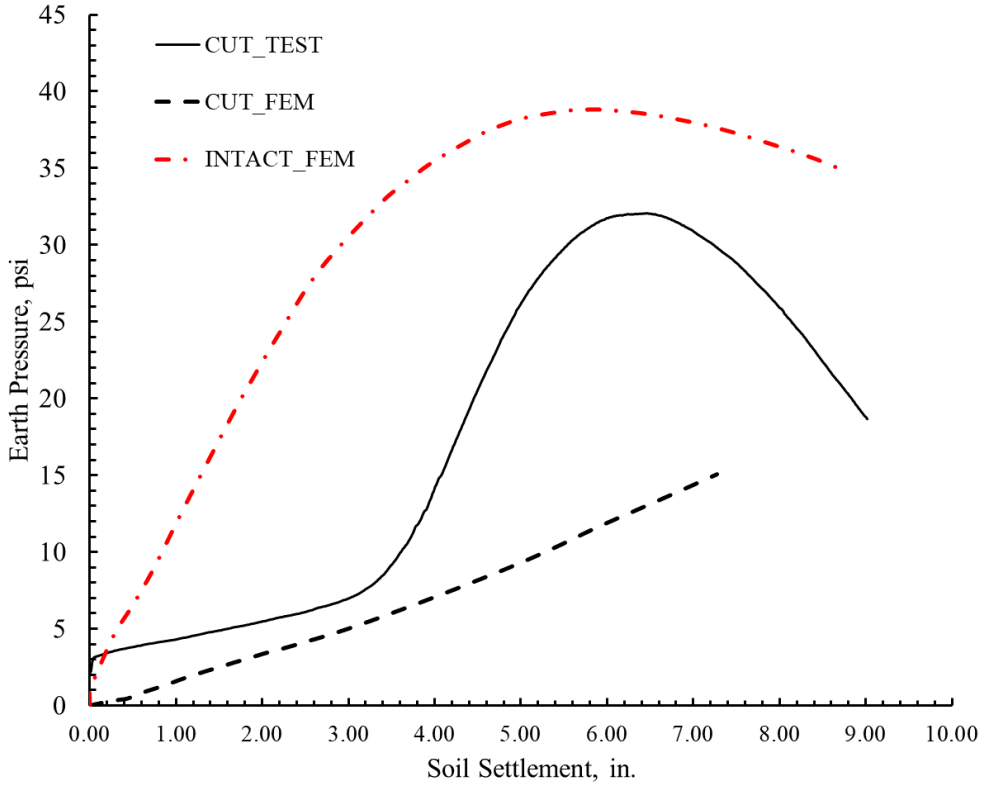

Figure 4-34 Earth pressure comparison

4.9 Results from Lined CMP

For the test of the CMP rehabilitated by spray-applied pipe liner, the process of the removal of the invert was changed. At first the mid-section of the invert was removed leaving 1 in. of the strip at the end of the CMP (Figure 3-38). With the 1 in. strip maintaining the ring stiffness in the CMP the liner was applied and after the liner was set the remaining end strip was removed as of results no movement in the soil or the pipe was observed. Thus, the collapse of the soil was prevented, and the same old soil model could be used to model the soil this time.

The material properties of the liner suggest that the liner is brittle with little plastic region (About 0.22% strain difference was seen in the tensile yielding and the breaking point). The liner is modeled using the simple elastic-plastic model and the plastic strain in the liner is considered as the crack in the liner. Thus, the appearance of the 1st crack in the experiment was related to the appearance of the first plastic strain in

the model. Overall, it was found that the model was close in predicting the 1st crack through the 1st plastic strain concept.

4.8.1 0.25-in. thick SAPL

The FE model for 0.25 in. liner compared well with the experimental results. In the test, it was observed that the first crack occurred right at the center of the CMP at the crown region. In the FEM model also, the 1st plastic strain was exactly seen in the center of the CMP at the crown region (Figure 4-35). The plastic strain seen the crown propagated longitudinally along the crown of CMP in the FE model which matches fairly with the propagation of the crack in the experimental results. (Figure 4-36).

The comparison of the other results is further discussed in this section:

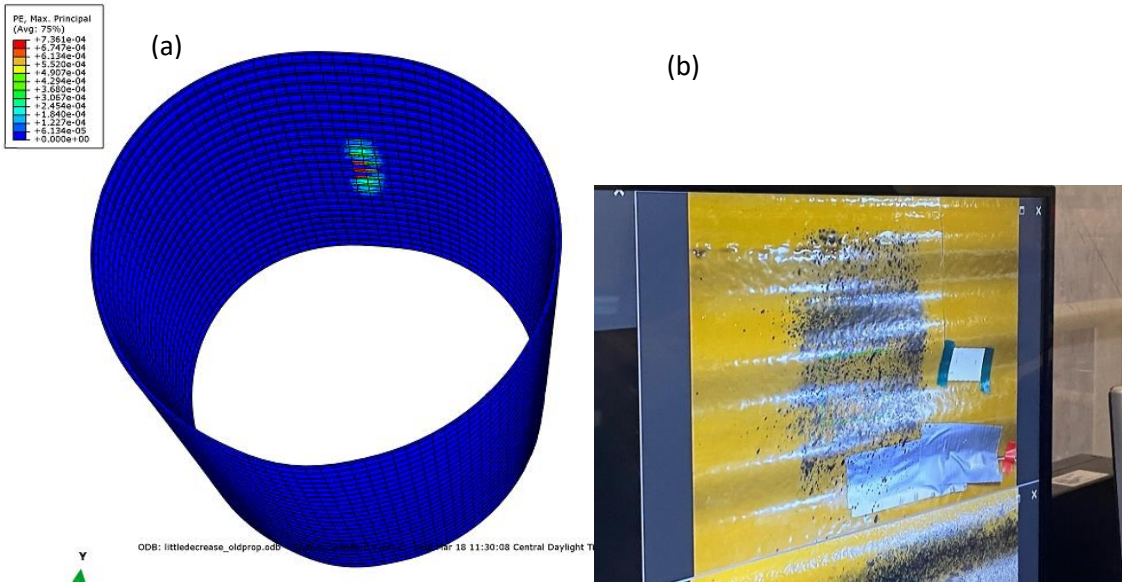

Figure 4-35 (a) 1st plastic strain in the CMP (b) 1st crack in the model for 0.25 in. thick liner (Source: CUIRE Laboratory)

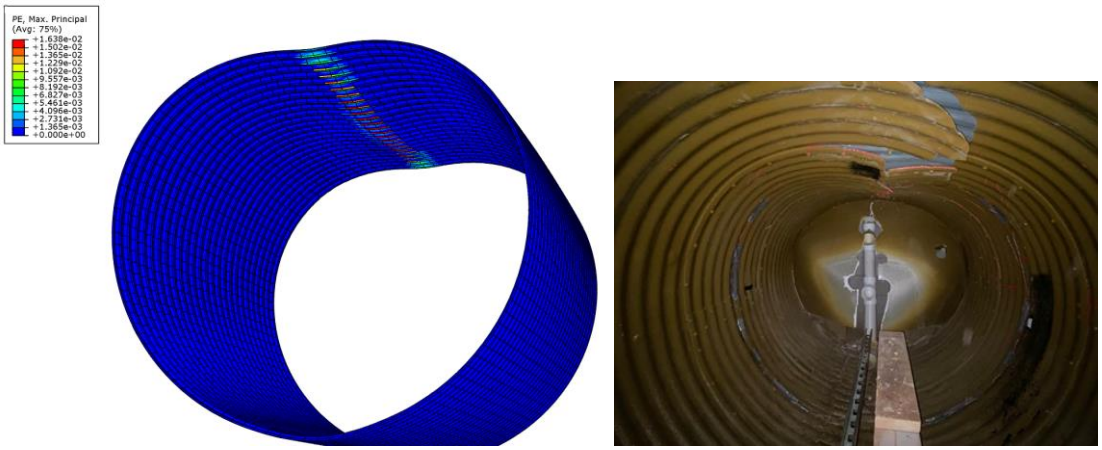

a b

Figure 4-36 (a) Plastic strain at the ultimate load in the FE model (b) Crack in the model at the end of the test for 0.25 in. thick liner (Source: CUIRE Laboratory)

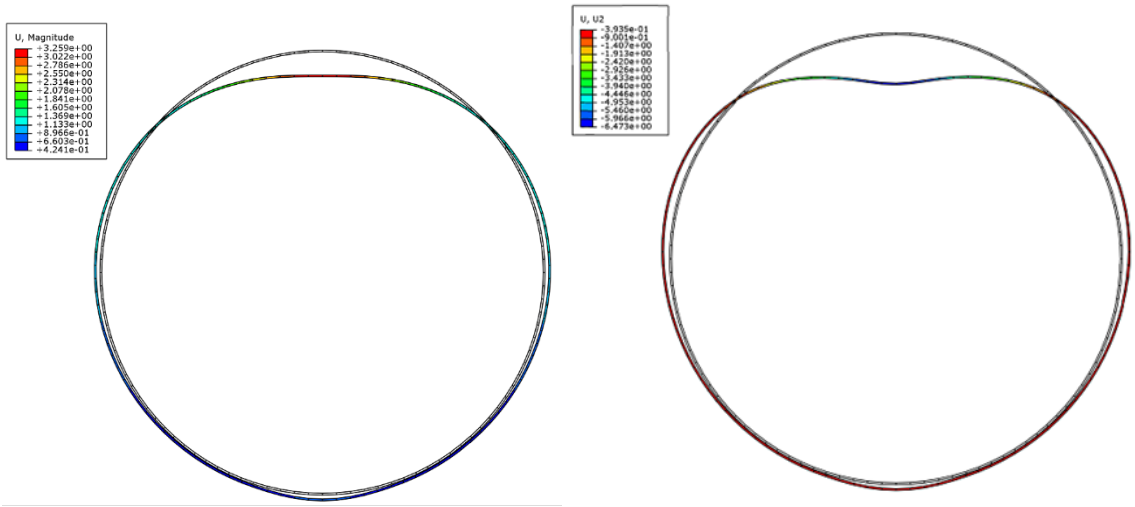

Figure 4-37 (left) Deformation of CMP at the time of the 1st plastic strain (right) Deformation of CMP at the ultimate load condition for 0.25 in. thick liner

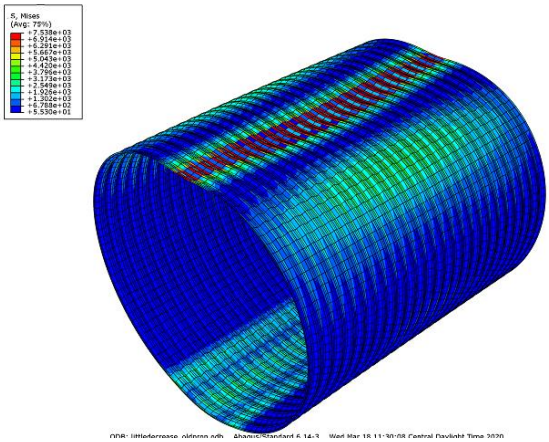

Figure 4-38 Stress Distribution in the pipe at the ultimate load conditions for 0.25 in. thick liner

1. Load Displacement Plots

The displacement of the CMP and the liner was monitored at the crown, spring line, and shoulder using the LVDTs in the experiment. So, for the comparison of the load-displacement curve, the load-displacement curve was plotted for the FE results for similar locations. (Figure 4-39, Figure 4-40, Figure 4-41). The comparison showed very similar results and the prediction of the crack load, ultimate load, and the displacement of the pipe was within the accuracy of 8 % (Table 4-12).

Initially, the stiffness of the liner in the test is more than the stiffness of the liner in the FEM model. This initial high stiffness from the experiment results compared to FE model could be attributed to the fact that the liner was attached to the wall initially due to the over spraying of the liner and which was not included in the FE model. The over spraying of the liner to the end wall caused the rehabilitated CMP to take more load than it could take. In the test, the first crack was observed at 40 kips of the load and it was indicated by a small drop in the load but no drop in the load was observed in the FE results. The FE results showed the first plastic strain at 43 kips of the load and this load at the appearance of first plastic strain in the model matches closely with the load at the appearance of the first crack from the experiment.. The displacement of the liner at the first crack load in the experiment and the first plastic strain also showed a discrepancy of 6% only.

Ultimately the liner pipe system took the ultimate load of 46 kips in the test which was predicted to the accuracy of 0.3% by the FE model.

Overall the FE model predicted the load and the displacement at the different locations with enough accuracy as shown in Table 4-12.

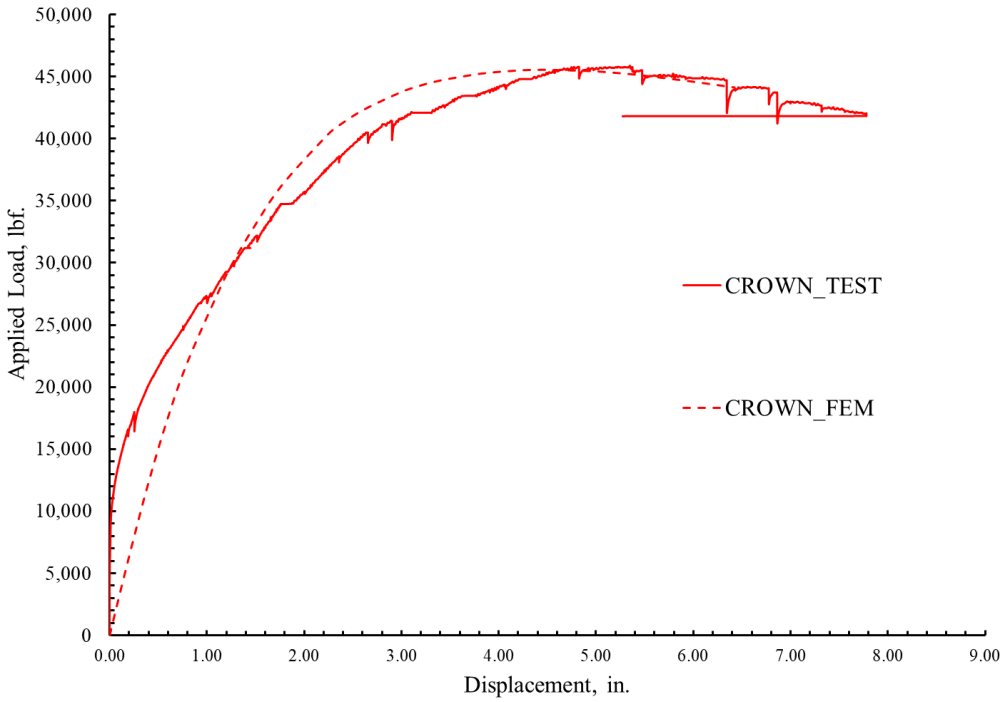

Figure 4-39 Comparison of the liner displacement at crown for 0.25 in. thick liner between Experiment and FEM results

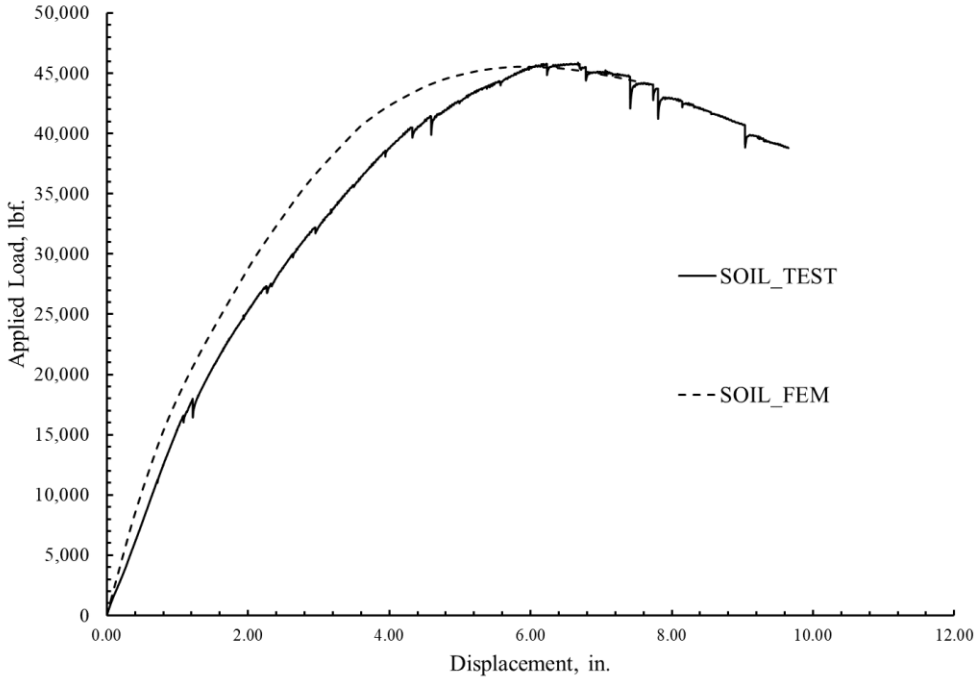

Figure 4-40 Comparison of the load and soil displacement for 0.25 in thick liner between Experiment and FEM results

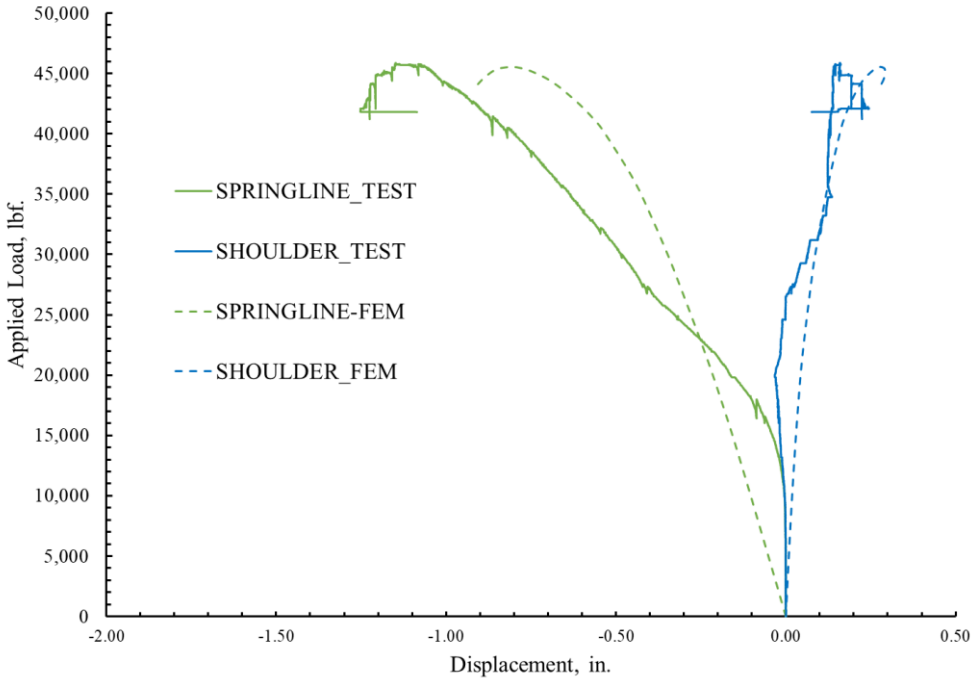

Figure 4-41 Comparison of the liner displacement at shoulder and springline for 0.25 in. thick liner between Experiment and FEM results

Description	1st plastic strain	1st Crack	Discrepancy Test vs. FEM (%)	Ultimate Load		Discrepancy Test vs. FEM (%)
	FEM	Test		FEM	Test	
Crown Displacement (in.)	3.13	2.92	6.7	4.92	5.23	5.92
Soil Displacement (in.)	4.86	4.64	4.7	6.0	6.49	7.5
Load (kips)	43.5	41.3	5.3	45.63	45.78	0.3
Springline disp. (in.)	0.68	0.86		0.85	1.14	

Table 4-12 Comparison of the load and displacement between the FE model and the Experimental results for 0.25 in. thick liner

2. Earth Pressure Distribution

Beside the load-displacement comparison, the comparison of the earth pressure obtained from the experiment and the FE model is also made. The comparison of the earth pressure is done for only the pressure obtained at the crown as the earth pressure at the spring line, and invert was measured low . The pressure plot showed a similar pattern of the curve for the experimental and the FE model results (Figure 4-42, Figure 4-43, Figure 4-44 The earth pressure at the time of the first crack and appearance of the first plastic strain of the liner is nearly equal. The earth pressure at the 1st crack is 36.42 psi (at 2.92 in. liner displacement in the experiment), while in the FE model at the time of 1st plastic strain the earth pressure was 36.16 psi (at 3.13 in. liner displacement). The ultimate crown pressure showed a discrepancy of about 7% between the experimental and FE model results.

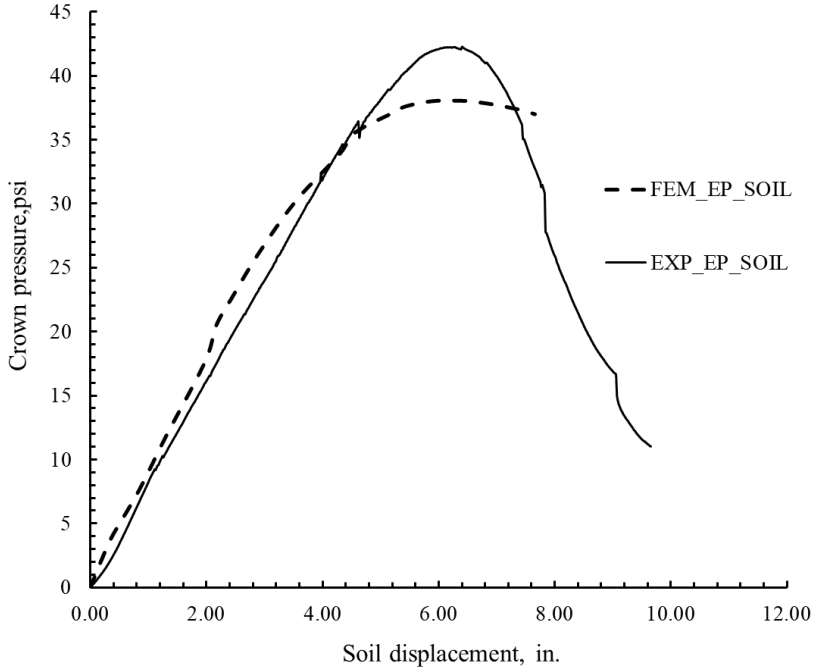

Figure 4-42 Comparison of the earth pressure at crown plotted against the soil displacement for 0.25 in thick liner

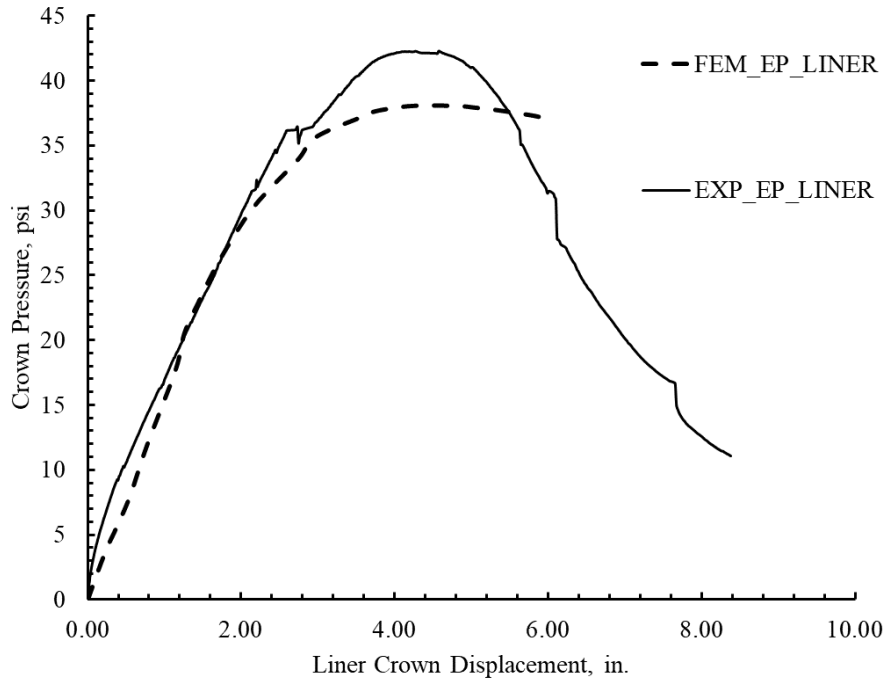

Figure 4-43 Comparison of the earth pressure at crown plotted against the liner displacement for 0.25 in. thick liner

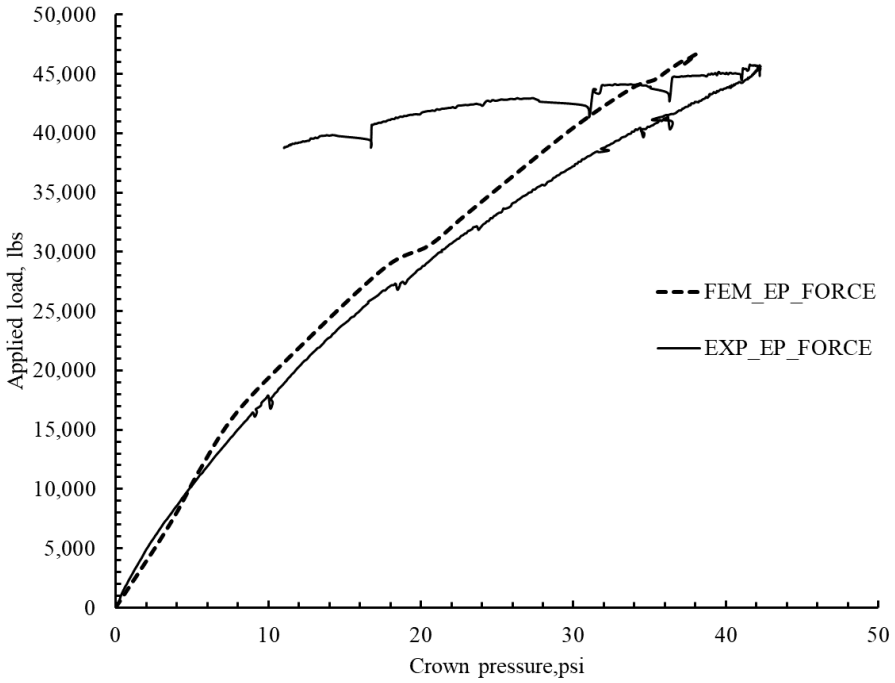

Figure 4-44 Comparison of the earth pressure at crown plotted against the applied load for 0.25 in. thick liner

3. Strains

Since the data logger was damaged for the testing of 0.25 in. liner and 0.5 in. liner, the data could not be fully recovered. With the only half of the data recovered, the comparison of the strains is made. Since the change in the strains in the spring line and near the invert was small, in the range of the 200-300 micro strains compared to the strains at the shoulder and the crown, the FE result comparison was made only for the strains at the crown and the shoulder. The obtained results were plotted against the soil displacement.

The strains at the crown, in which strain gauge was kept at the outside in the crest of the CMP, was overestimated compared to the experimental results. But the pattern of the strains was similar (Figure 4-45). While the strain recorded from the strain gage placed outside of the CMP in the crest in the shoulder was matched well to the strain recorded from the same place (Figure 4-46).

Although the comparison of the strains was fair for the strain gage kept on crest in the outside of the CMP, the strains that were recorded from the strain gage kept on the valley in inside of the liner did not show the fair comparison. The experimental results showed very low strains recorded at the crown and the shoulder (Table 4-13

Table 4-13) while the FE model showed otherwise. The pattern of the strains recorded from the strain gages kept at the crest in outside of the CMP and strain gages kept at the inner side of the valley in the liner showed a similar amount of strain with the opposite signs in the FE model while it was not the case in the experimental results.

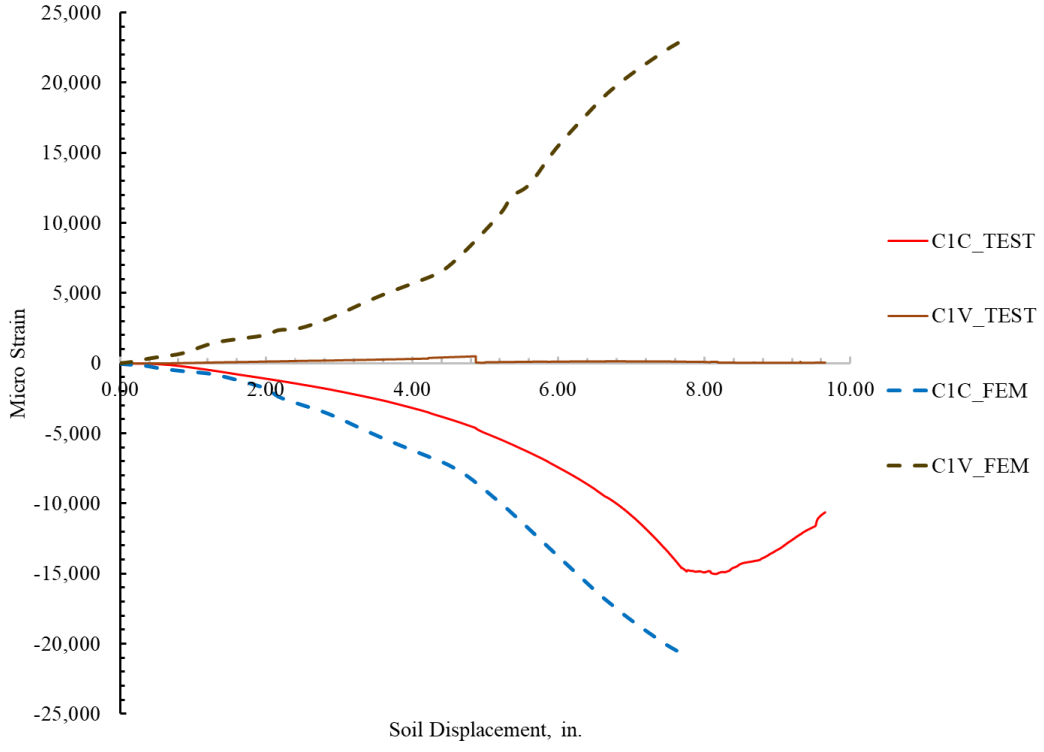

Figure 4-45 Comparison of the strains at the crown for 0.25 in. thick liner

(Source: CUIRE Laboratory)

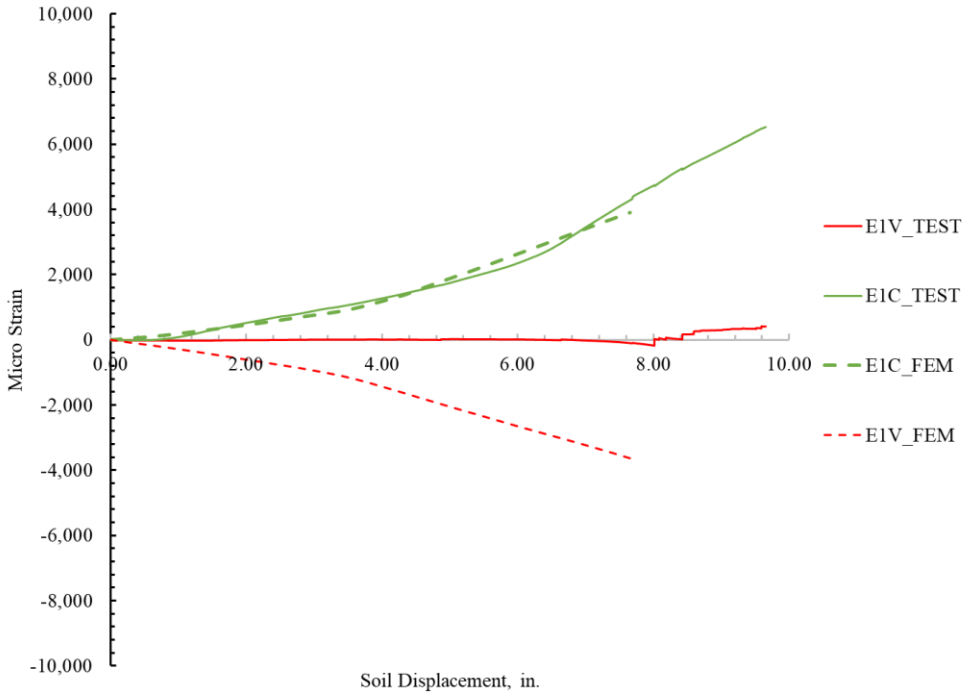

Figure 4-46 Comparison of the strain at the shoulder for 0.25 in. thick liner

(Source: CUIRE Laboratory)

Strain Comparison up to the 1st plastic strain (FEM) and 1st Crack (Test)		
Position	FEM (Micro strain)	Test (Micro strain)
C1C	-7235	-4530
C1V	6875	426
E1V	-1734	4
E1C	1503	1501

Table 4-13 Comparison of strains at 1st plastic strain and 1st crack condition for 0.25 in. thick liner

4.9.2 0.5-in. thick SAPL

The FE model for 0.5-in. thick SAPL also compared well with the experimental results. Similar to the test on 0.25-in. thick SAPL, in this test also it was observed that the first crack occurred right at the center of the CMP at the crown region. In the FEM model also the first plastic strain was exactly seen in the center

of the CMP at the crown region (Figure 4-47). The plastic strain propagated longitudinally along the crown in the FE model which was like the propagation of the crack in the experimental results.

The comparison of the other results is further discussed in this section:

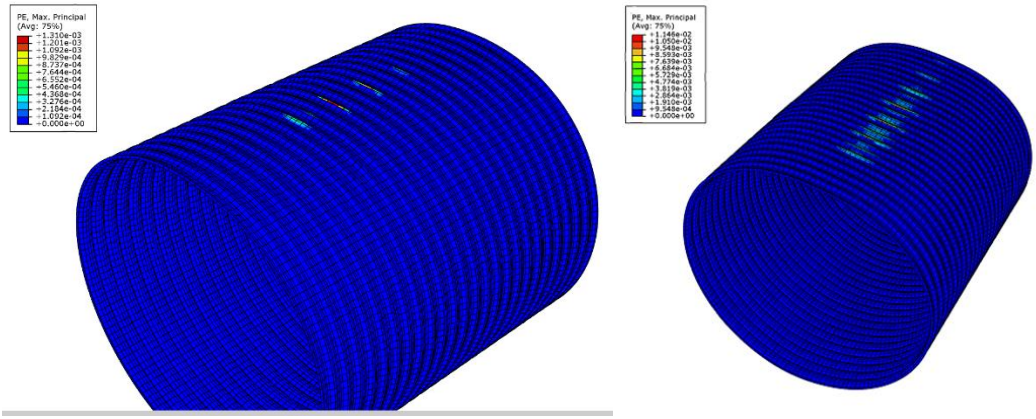

Figure 4-47(a) First plastic strain from FE model (b) First crack from the test for 0.5 in. thick liner

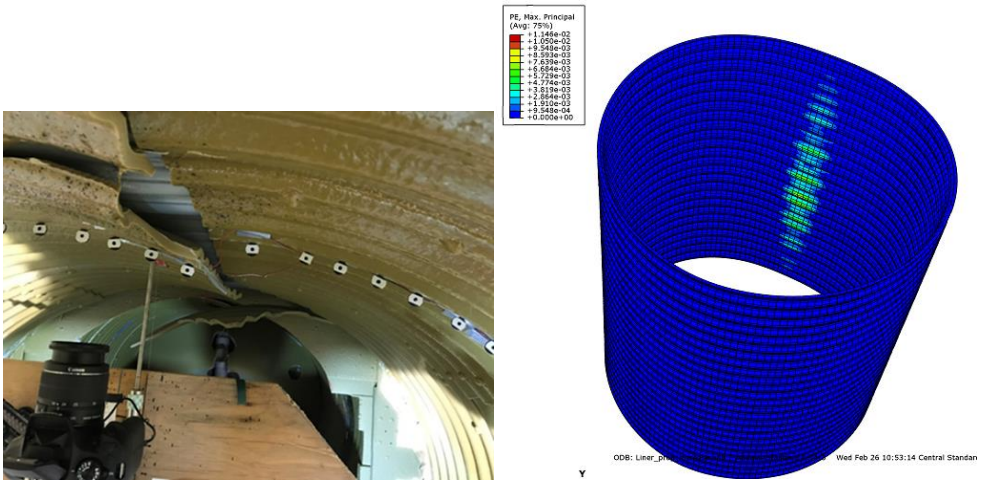

Figure 4-48 Plastic strain inside and outside of the CMP at the ultimate load conditions for 0.5 in. thick liner

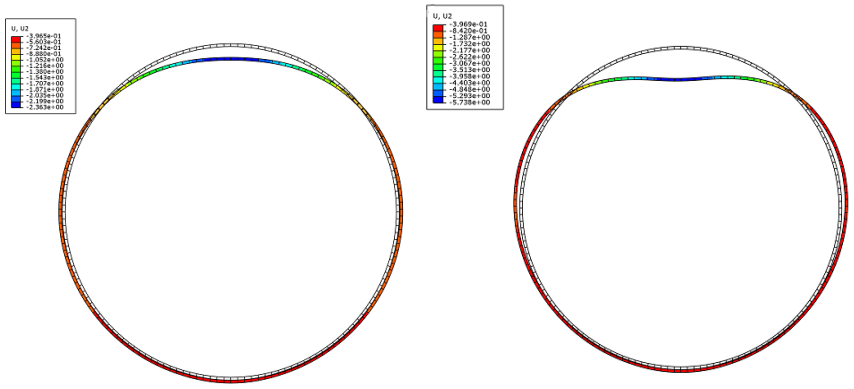

Figure 4-49 (a) Deformation of the Liner at the appearance of the first plastic strain (b) Deformation of the liner at the ultimate load for 0.5 in. thick liner

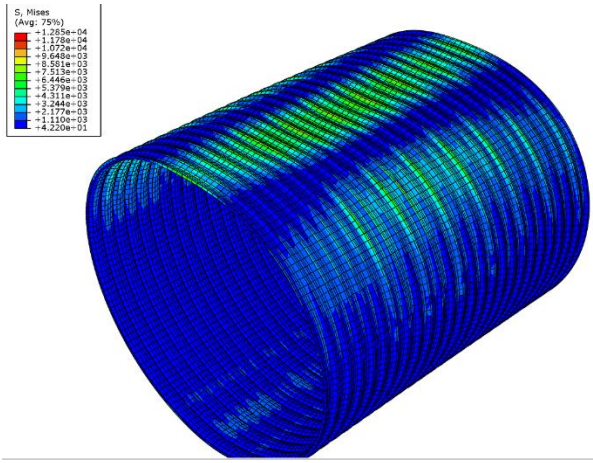

Figure 4-50 Von Mises stress in around the liner for 0.5 in. thick liner

1. Load Displacement Plots

For 0.5-in. thick SAPL similar to 0.25 in. thick SAPL, the load-displacement comparison was made for the displacement of the crown, spring line, and shoulder of the liner and the settlement of the soil. This FE model also showed close results with the experimental results. The prediction of the crack load, ultimate load, and the displacement of the pipe was within the accuracy of less than 2% for most of the cases (Table 4-14).

In this case also the initial stiffness of the liner in the test is more than the stiffness of the liner in the FEM model. For this case also the initial higher stiffness in the experiment could be attributed to the fact that the liner was attached to the wall initially due to the over spraying of the liner which causes the liner to take more load than it could take. As the liner got separated from the wall, which could be seen from the major drop of the load at 28 kips of the load, the test results and the FE model followed a similar trend. The first crack for this test occurred in around the 42 kips of the load with the drop in the load and the first plastic strain in the liner also occurred at the same load. Although the drop in the load was not observed in the FE model, the appearance of the plastic strain from the FE result had a close match with the occurrence of the crack in the liner from the experimental result. Ultimately the liner pipe system took the ultimate load of 52 kips in the test while the FE model took the ultimate load of 51 kips which was predicted with a

discrepancy of less than 4%. Overall, the FE model predicted the load and the displacement at a different location with enough accuracy.

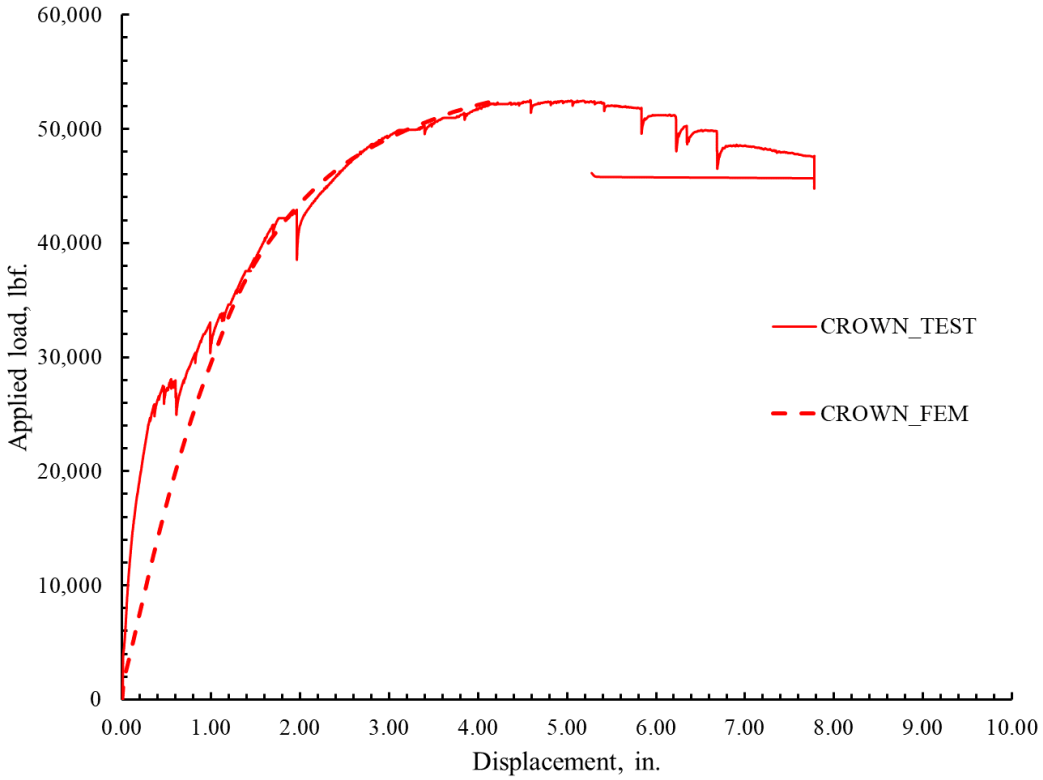

Figure 4-51 Comparison of load displacement plot for the 0.5 in. thick liner at crown

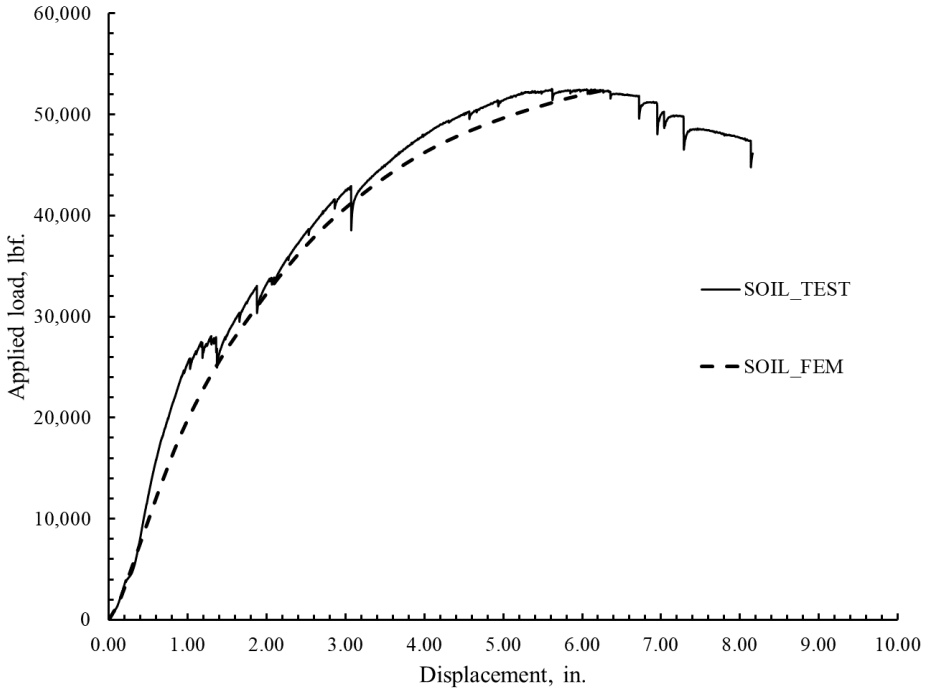

Figure 4-52 Comparison of load displacement of soil for the 0.5 in. thick liner

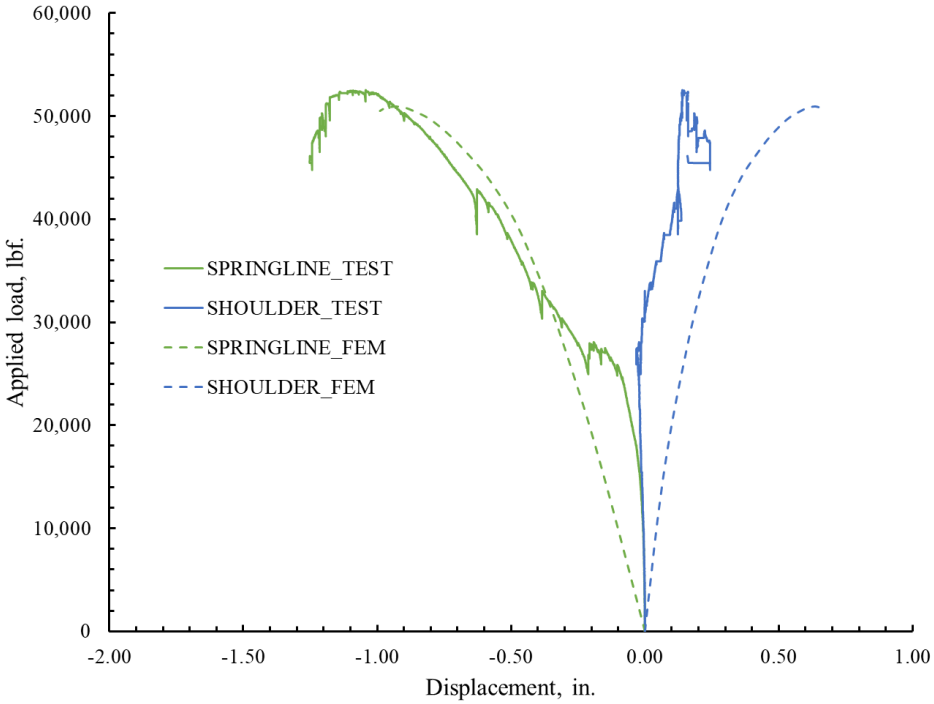

Figure 4-53 Comparison of load displacement plot for the 0.5 in. thick liner at shoulder and springline

Description	1st plastic strain	1st Crack	Discrepancy Test vs. FEM (%)	Ultimate Load		Discrepancy Test vs. FEM (%)
	FEM	Test		FEM	Test	
Crown Displacement (in.)	2.37	2.18	8.01	4.72	4.74	0.42
Soil Displacement (in.)	3.36	3.02	10.11	6.49	6.09	6.16
Load (kips)	42.30	42.59	0.68	50.15	52.24	4.0
Spring line disp. (in.)	0.54	0.60	10	0.98	1.15	10

Table 4-14 Comparison for the load-displacement plots from the FE model and Test for 0.5 in. thick liner

2. Earth Pressure Distribution

For this FE model also, only the pressure at the crown was compared with the experimental results. Upon comparing the crown earth pressure with different parameters such as soil displacement, liner displacement, and applied load, it was seen that the close match was obtained between the FE and test results (Figure 4-54, Figure 4-55, Figure 4-56). The ultimate pressure at the ultimate conditions is around 43 psi for both FEM and test results. The pressure at the time of the 1st crack on the test was around 27 psi while in the FEM the crown pressure at the time of 1st plastic strain was 28.5 psi which further suggests the 1st plastic strain and 1st crack will occur simultaneously.

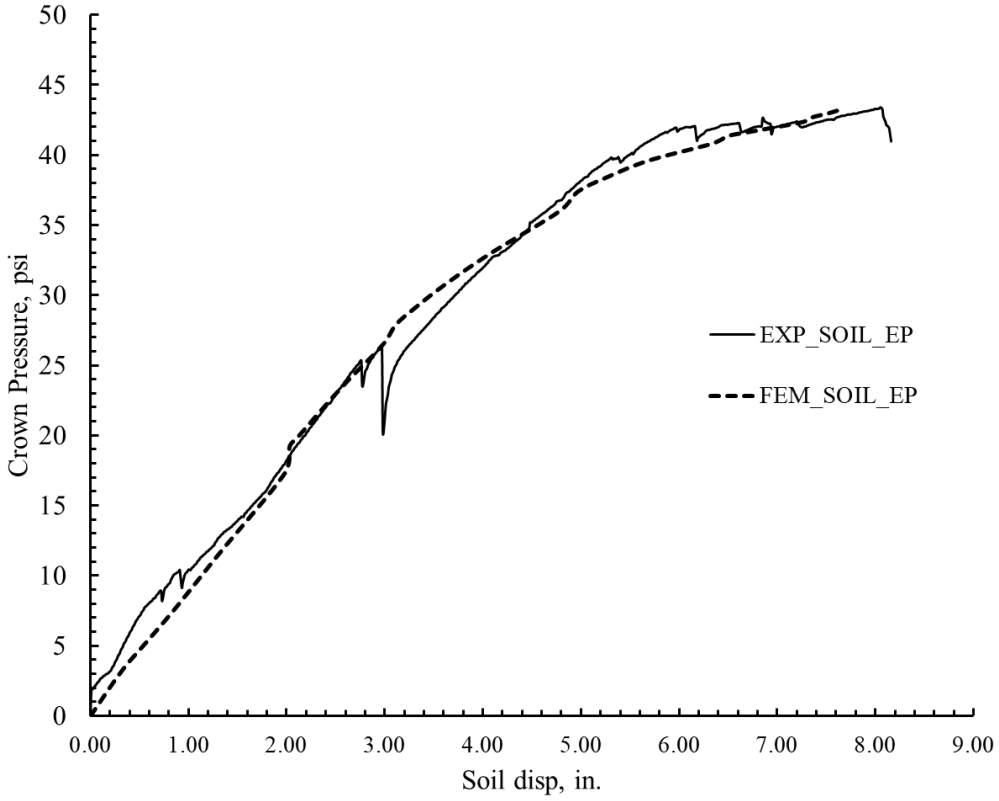

Figure 4-54 Comparison of the Earth pressure with soil disp., for 0.5 in. thick liner

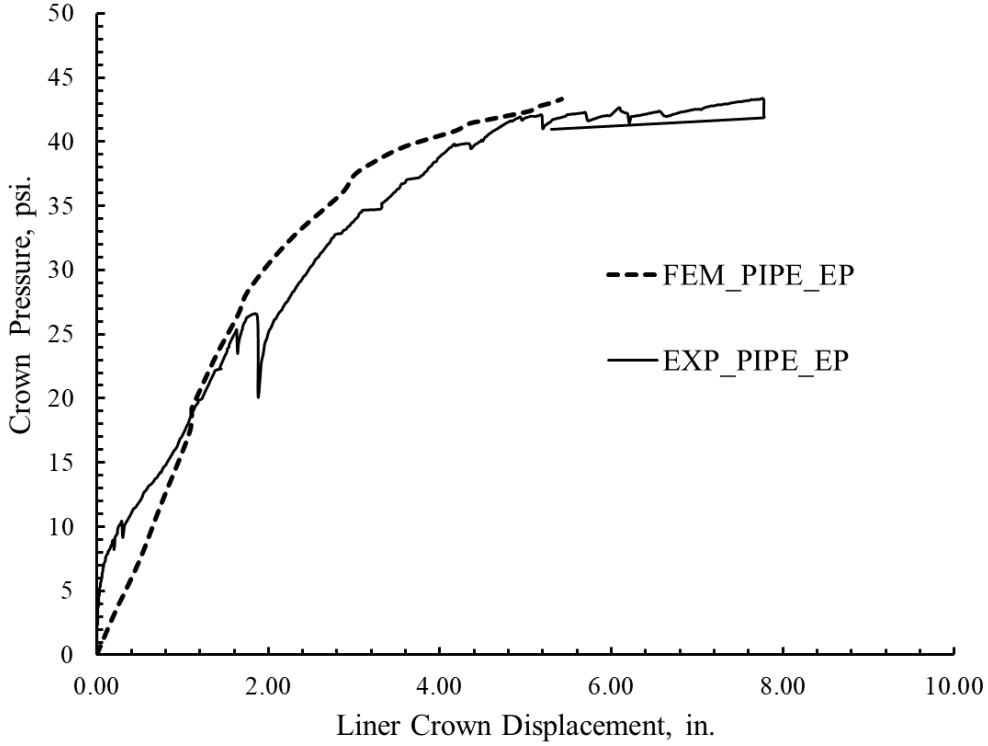

Figure 4-55 Comparison of the earth pressure with liner displacement at crown for 0.5 in. thick liner

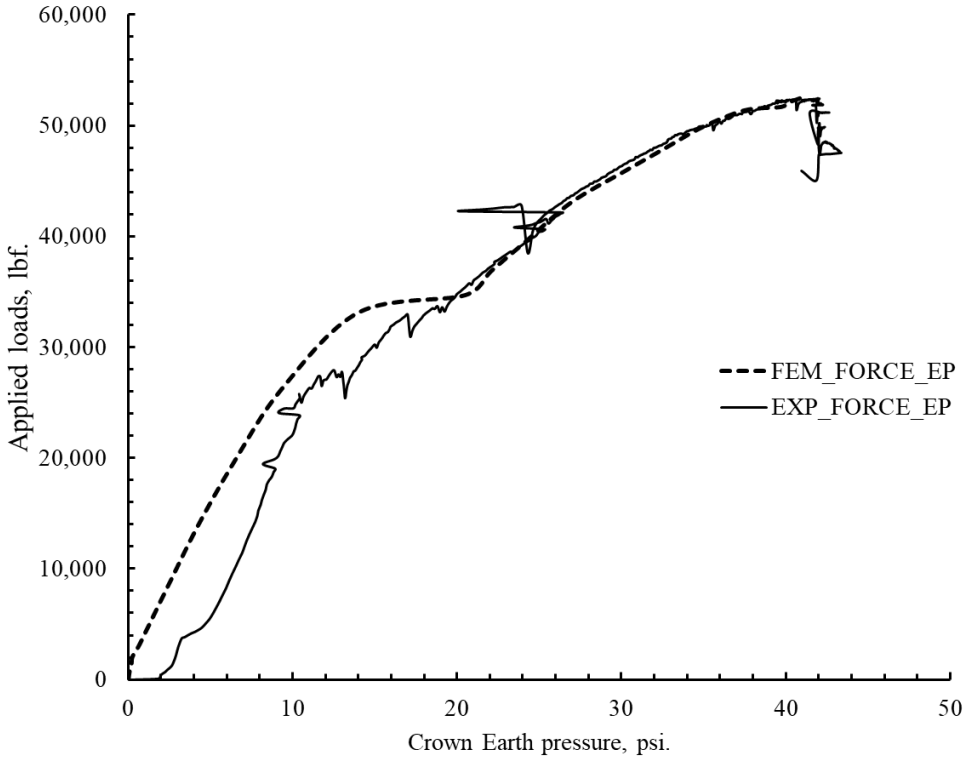

Figure 4-56 Comparison of the earth pressure with the applied load for 0.5 in. thick liner

3. Strains

The strains obtained from the test results for every strain gage were less but the FE results showed high strains at the crown and the shoulder. So, the comparison between the FE results and the experimental results is not shown in the graph. The graph only shows the strains obtained from the FE results. Like all other tests, the maximum strains were seen in the crown followed by shoulder.

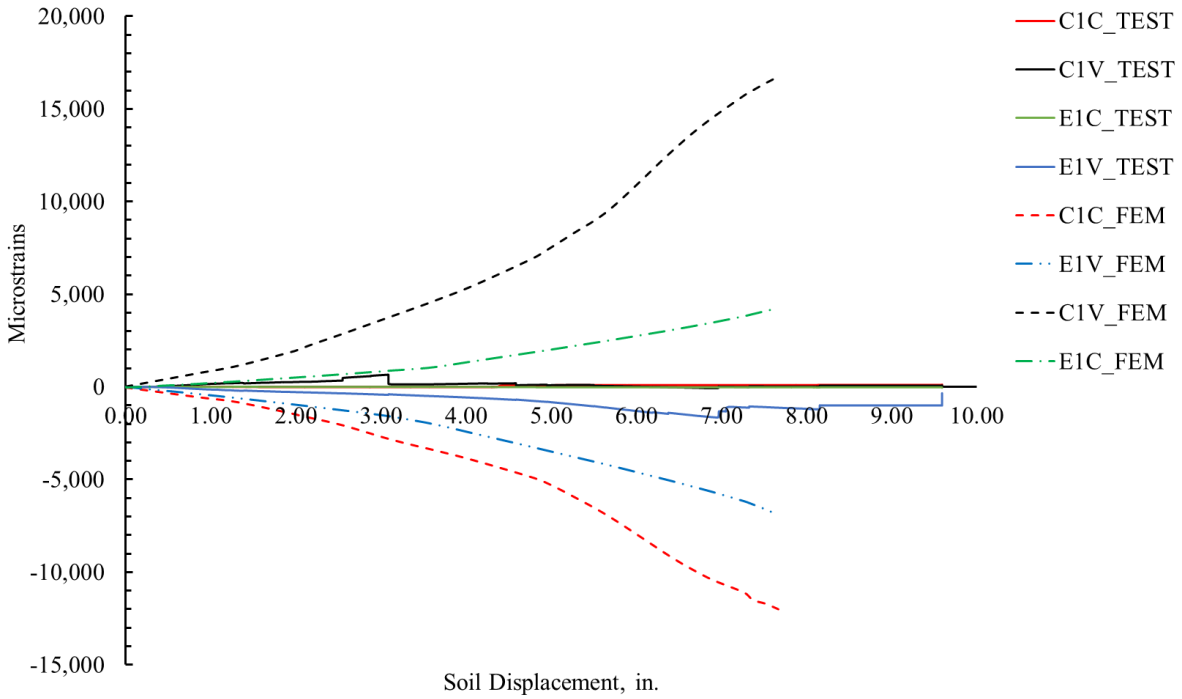

Figure 4-57 Comparison of the strains for 0.5 in. thick liner

Strain Comparison up to the 1st plastic strain (FEM) and 1st Crack (Test)		
Position	FEM (Micro strain)	Test (Micro strain)
C1C	-3083	-
C1V	4200	-
E1V	-2020	-
E1C	1065	-

Table 4-15 Strain at the 1st plastic strain in FE model for 0.5 in. thick liner

4.9.3 1-in. thick SAPL

The FE model for 1 in. thick SAPL also compares well with the experimental results. Like the test on 0.25 in. thick SAPL and 0.5 in. thick SAPL, in this test also it was observed that the first crack occurred right at the center of the CMP at the crown region. In the FEM model also the 1st plastic strain was exactly seen in the center of the CMP at crown region (Figure 4-58). After that in the FE model the plastic strain propagated along the centerline in the FEM which was like the experiment results (Figure 4-59). The pipe did not deflect much after the crack in the ultimate load conditions, unlike the other thickness liner.

The comparison of the other results is further discussed in this section:

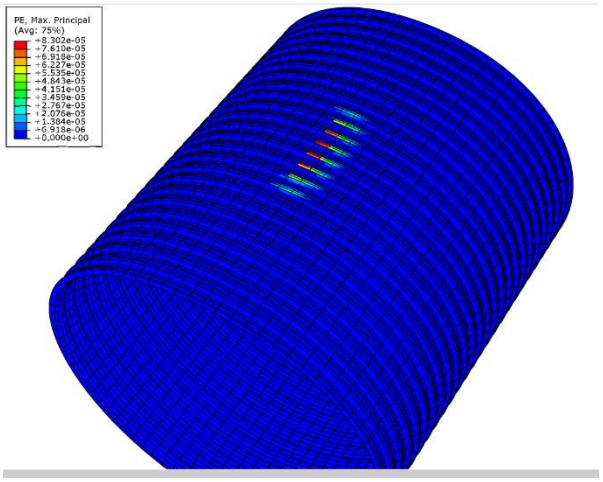

Figure 4-58 1st plastic strain in the liner for 1 in. thick liner

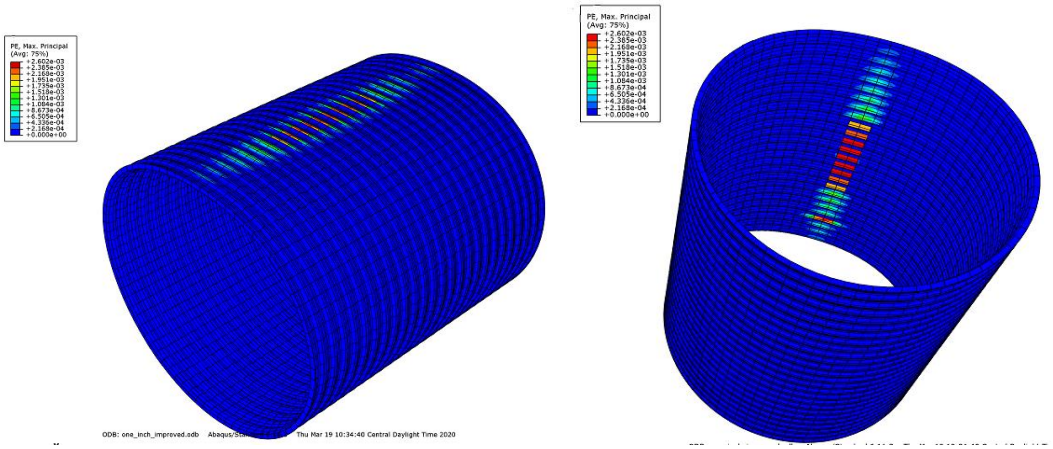

Figure 4-59 Plastic strain in the inside and outside the liner for 1 in. thick liner

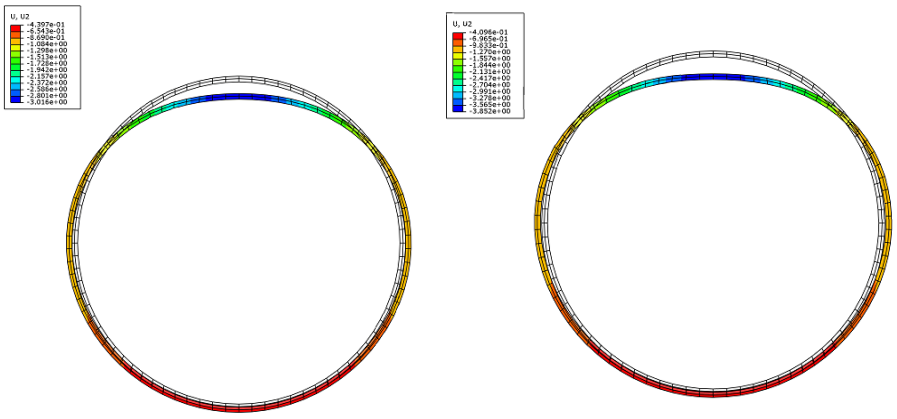

Figure 4-60 Deformation of the liner at(a) 1st plastic strain (b) at ultimate load conditions for 1 in. thick liner

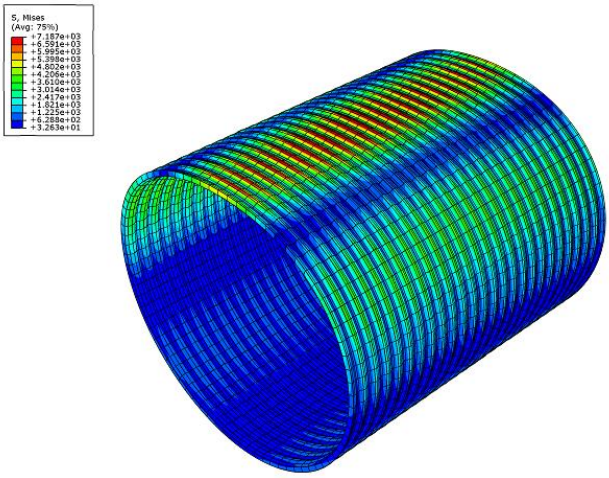

Figure 4-61 Von Mises stress around the liner at the ultimate load conditions for 1 in. thick liner

1. Load Displacement Plots

Similar to previous comparisons for 1 in. thick SAPL also the load-displacement comparison was made for the displacement of the crown, spring line, shoulder of the liner and settlement of the soil. This FE model also showed very similar results and the prediction of the crack load, ultimate load, and the displacement of the pipe was within the discrepancy of less than 2% for most of the cases (Table 4-16).

For this case also like the other cases, initially, the stiffness of the liner in the test is more than the stiffness of the liner in the FEM model. In this case in the test, due to the increased thickness in the liner, the attachment to the wall was also thicker and it only got separated at the time of the occurrence of the first crack in the experiment. During the 1st crack and complete separation of the liner from the wall, there was a huge drop in the load, but such was not observed in the FEM as FEM was modeled in the ideal case scenario i.e. no attachment to the end wall. The first crack was observed at the 66 kips of the load while the FEM predicted e first plastic strain at 67 kips of the load. Unlike others, in this case, a slight drop in the load was seen during the appearance of the 1st plastic strain in the FE model but the huge drop in the load was not observed.

Since due to the increase in the rigidity of the system the flattening of the curve at the ultimate load is not seen for this thickness liner. The FE model was implicit and could not predict the post-failure behavior of the system i.e. drop after the ultimate load. The ultimate load for this thickness FE model is obtained by displacing the soil until the FE analysis fails to converge. Thus, for this FE model, the soil was displaced by around 9.2 in. before the model failed to converge and the ultimate load at the point was 70.3 kips.

The model predicts the test results by around 10 % discrepancy for the 1st plastic strain and the 1st crack condition while the model predicts the ultimate load conditions with discrepancy of 7%.

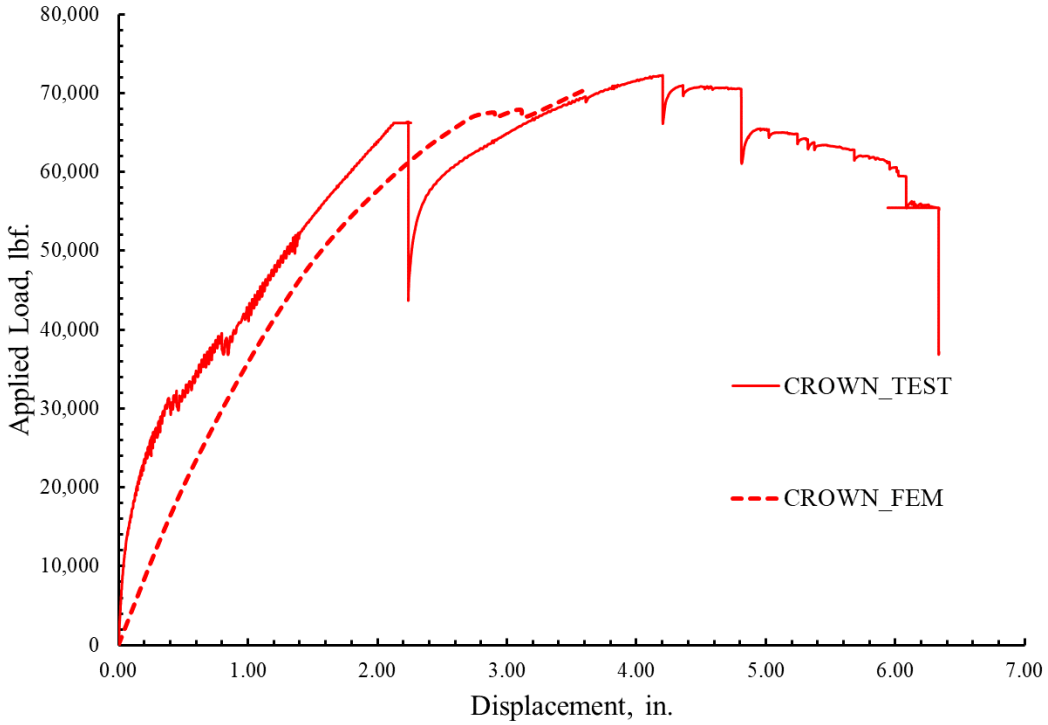

Figure 4-62 Load displacement comparison for FE and test results from crown for 1 in. thick liner

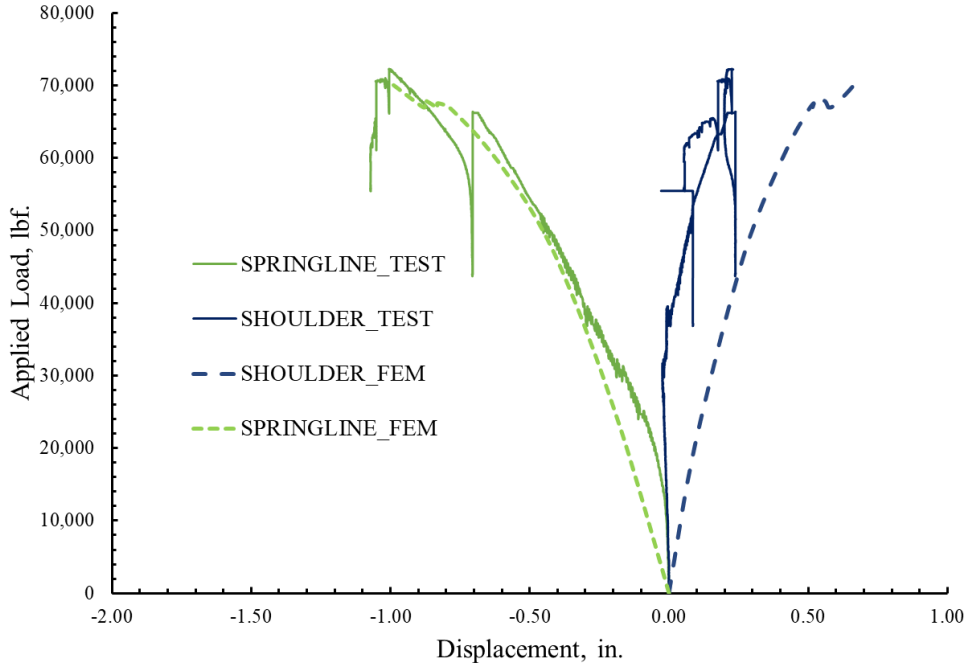

Figure 4-63 Load displacement comparison for FE and test results from spring line and shoulder for 1 in. thick liner

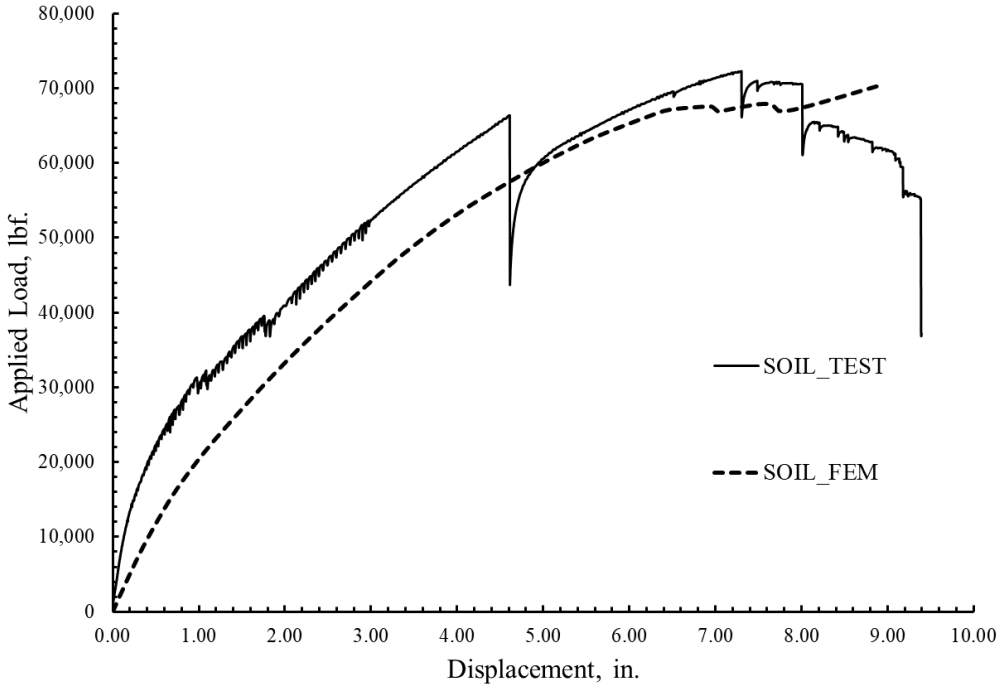

Figure 4-64 Load displacement comparison for FE and test results for soil displacement for 1 in. thick liner

Description	1st plastic strain	1st Crack	Discrepancy Test vs. FEM (%)	Ultimate Load		Discrepancy Test vs. FEM (%)
	FEM	Test		FEM	Test	
Crown Displacement (in.)	2.74	2.36	11.65	3.85	4.16	7.4
Soil Displacement (in.)	5.5	4.9	10.90	8.0	7.4	7.5
Load (kips)	67.10	66.26	1.25	70.27	72.17	2.7
Springline disp. (in.)	-0.82	-0.70	12.63	-0.99	-1.02	2.9

Table 4-16 Comparison of the test and FE model results for 1 in. thick liner

2. Earth Pressure Distribution

For this model also, only the pressure at the crown was compared with the experimental results. Upon comparing the crown earth pressure with different parameters such as soil displacement, liner displacement, and applied load, the pattern of the curve was well predicted. The pressure at the 1st plastic strain was predicted to be 3% less than the test value while the ultimate pressure was predicted 8% more than the test value (Table 4-17).

Location	Test		FEM	
	1st crack	Ultimate point	1st plastic strain	Ultimate point
Pressure (psi)	63.54	71.09	61.3	77
Liner Displacement (in.)	2.36	4.16	2.74	3.85

Table 4-17 Earth Pressure and corresponding liner displacement at crown for 1 in. thick liner

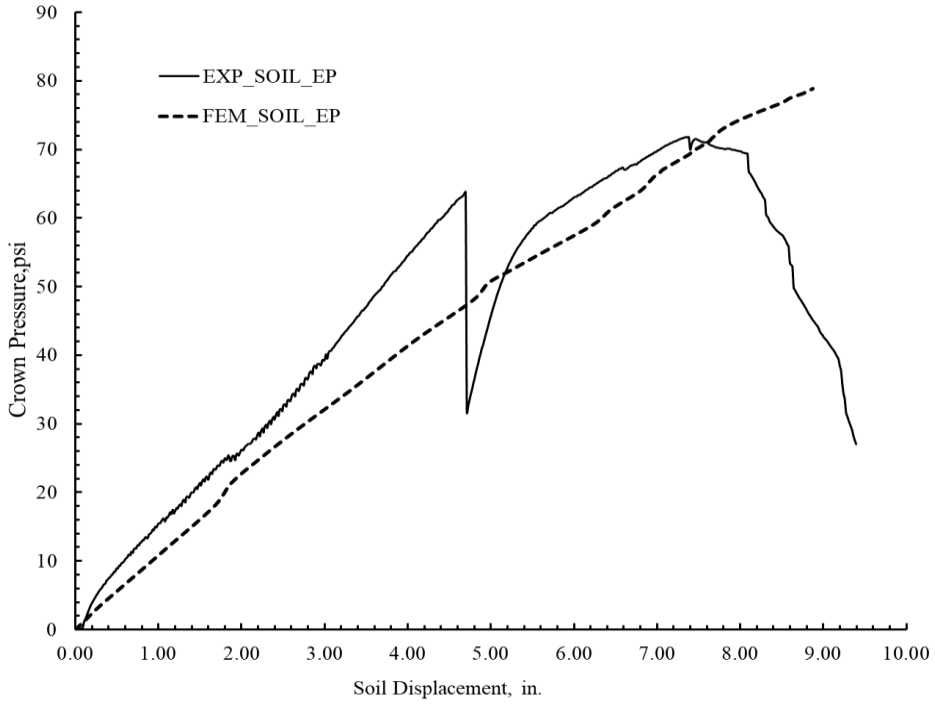

Figure 4-65 Comparison of the Earth pressure with soil disp., for 1 in. thick liner

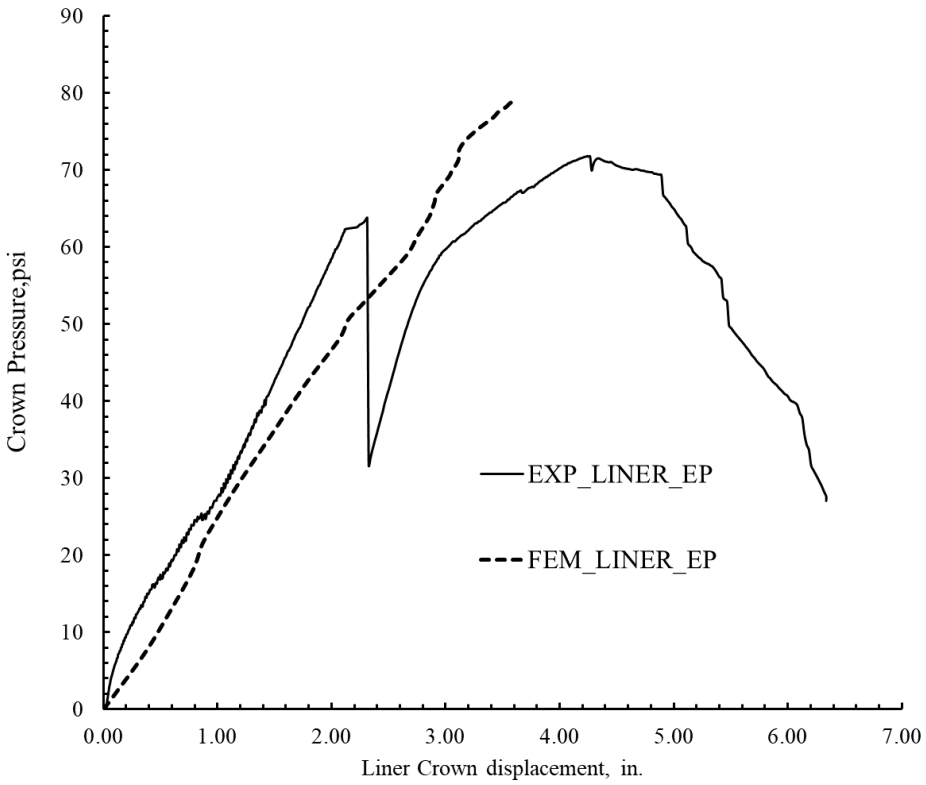

Figure 4-66 Comparison of the Earth pressure with liner's crown disp., for 1 in. thick liner

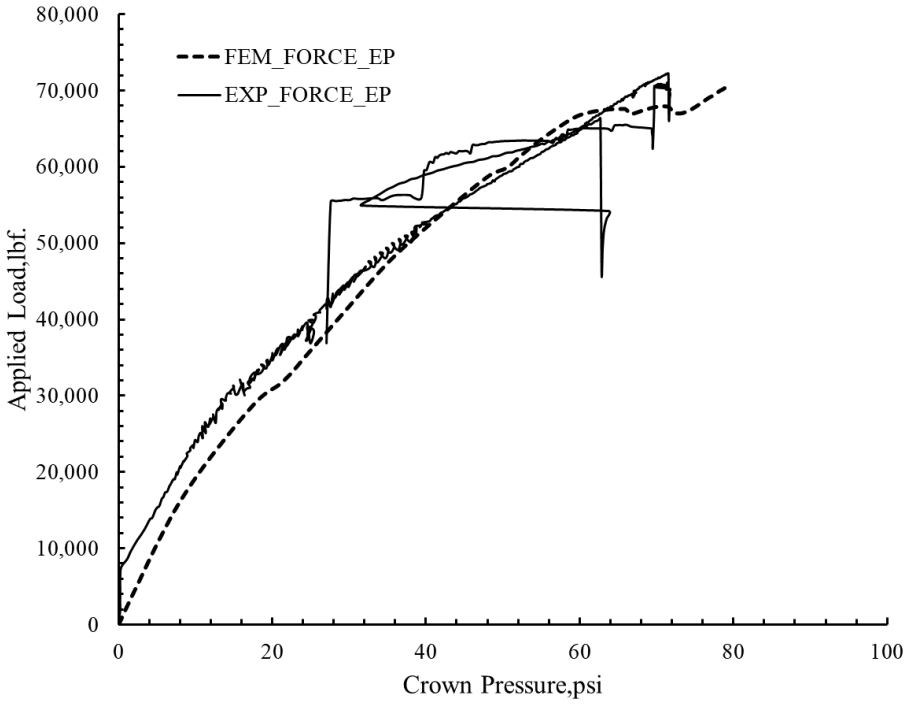

Figure 4-67 Comparison of the Earth pressure with applied load, for 1 in. thick liner

3. Strains Comparison

The strains plotted for this test matched nearly equal to the test results at the crown and the shoulder up to the 1st appearance of the crack in the test. After the 1st crack, the strain in the test showed a sudden surge in the strain gage placed on the outside part of the CMP on crest and strain gage placed on the inner side of the valley in the liner but the FEM results showed only the small change in slope. While the strain gage placed at the crown on the inside part of the liner got detached and the strain reading was zero thereafter.

In overall FEM predicted the strains very well before the appearance of the 1st crack in the test.

Strain Comparison up to the 1st plastic strain (FEM) and 1st Crack (Test)		
Position	FEM (Micro strain)	Test (Micro strain)
C1C	-3905	-3510
C1V	4301	3961
E1V	-2406	-2073
E1C	2107	1719

Table 4-18 Comparison of the strains for 1 in. thick liner

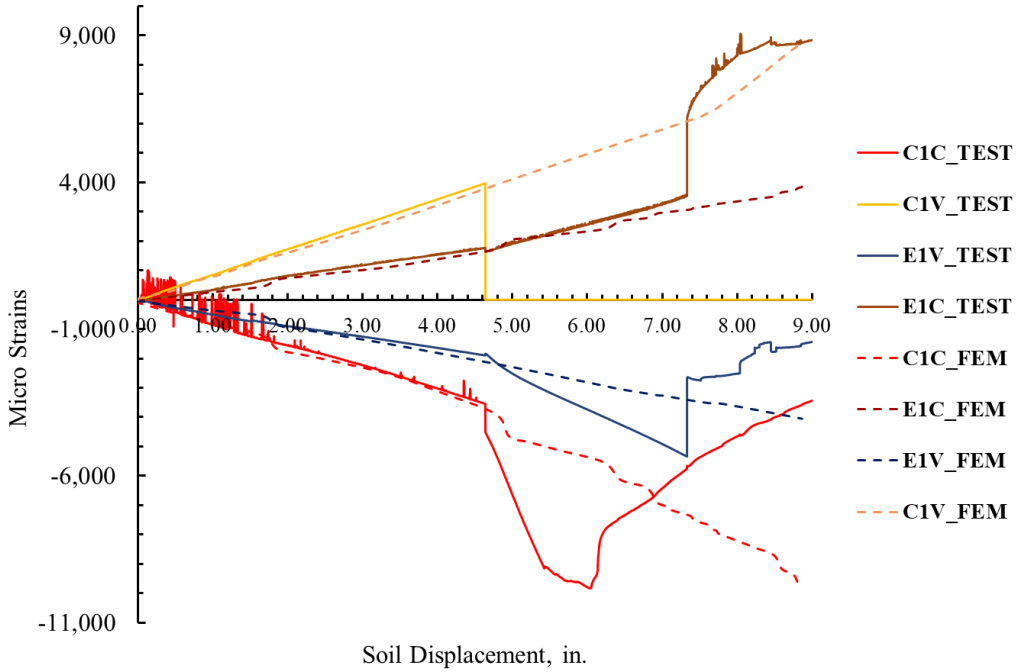

Figure 4-68 Comparison of the strains for 1 in. thick liner

Summary:

The FE analysis of the invert removed CMP rehabilitated by the Spray Applied Pipe Liner (SAPL) shows the close match between the FE and the test results. All the parameters used for comparison; the results are predicted with discrepancy of the less than 10%. Also, the assumption of the 1st plastic strain as the 1st crack, predicts the crack and the crack pattern in the CMP well. Form both the test and FEM results it is seen that the rigidity of the pipe is increased with the increase in the thickness of the liner. The drop in the load after the ultimate load is not predicted by the FE analysis as the FEM model was implicit and was not modeled for the -post-failure analysis of the liner. Although predicting the ultimate load for the thinner liner thickness was not a problem as the load-displacement curve first flatten and then only the drop was seen in test and the FEM was able to predict the flatten curve for 0.25 in. thick liner and 0.5 in. thick liner. But for 1 in. thick liner there was no flattening of the curve before the drop in the load, so the ultimate load is obtained by providing the ultimate displacement to the soil after which the FE model fails to converge.

4.8.4 Comparison of Liner Performance

1. Load Displacement Comparison

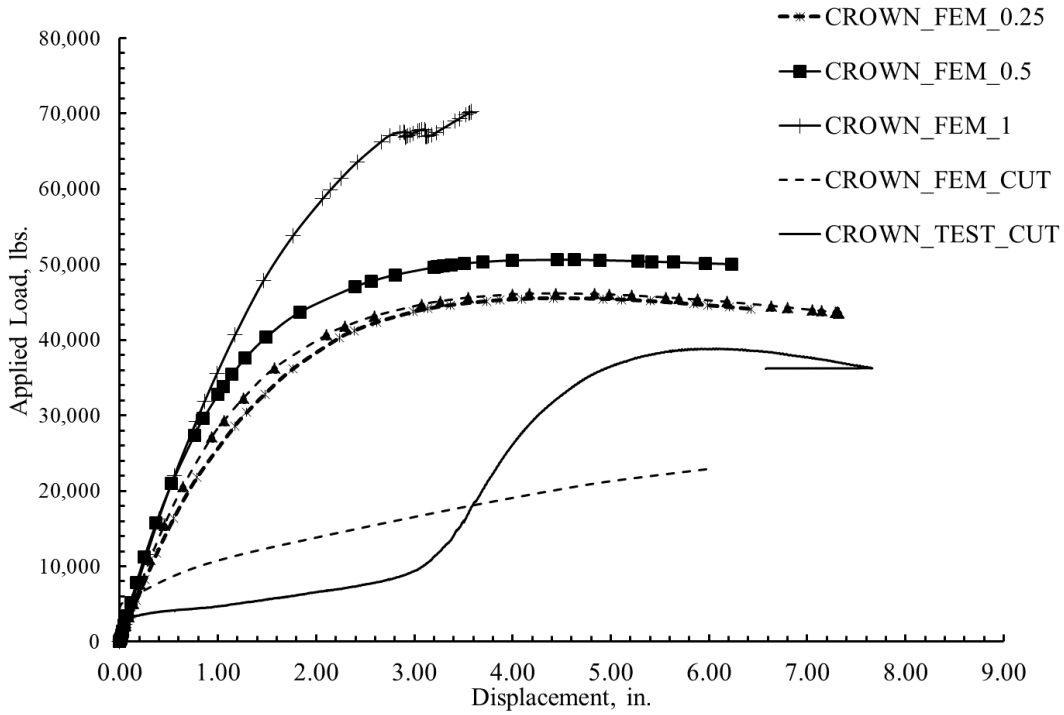

Figure 4-69 Comparison of the load displacement plot at the crown obtained from all the FE results

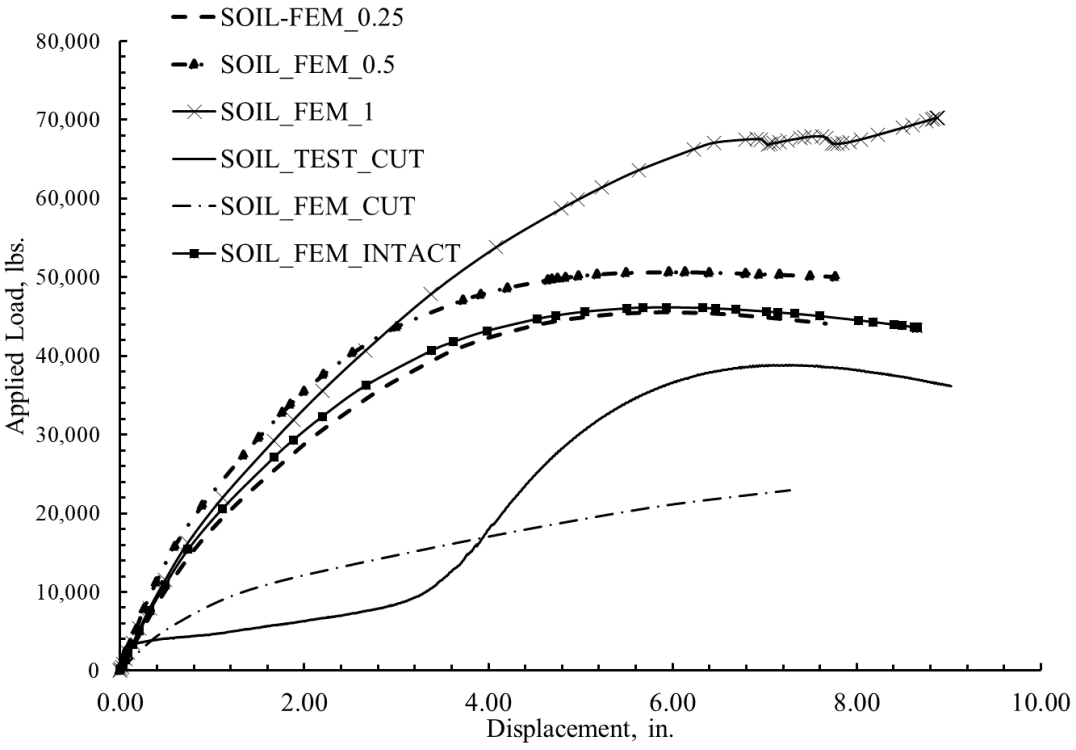

Figure 4-70 Comparison of the load displacement plot for the soil movement obtained from all the FE results

Description	Reduction in vertical diameter (in.)	Decrease in dia. (%)	Ultimate load (kips)	Increase/Decrease (%)
Intact Pipe	4.83	8.05	46.17	-
Invert Cut Pipe	6.01	10.01	22.93	-50.33
0.25 in. thick liner	4.92	8.20	45.63	-1.17
0.5 in. thick liner	4.72	7.8	50.63	+9.65
1 in. thick liner	3.57	5.95	70.27	+52.20

Table 4-19 Comparison of the reduction in the diameter and the ultimate load obtained from FEM

The overall comparison of the intact CMP, invert removed CMP and the renewed invert removed CMP is shown in Table 4-19. The comparison shows that the introduction of the liner will be able to bring back the structural capacity of the CMP whose inverts are removed. It is seen that the 0.25 in. the thick liner will restore the structural capacity of the CMP almost the same as the intact CMP. The 0.5 in. thick liner surpasses the ultimate structural load carried by the intact CMP by about 10% while for 1 in. thick liner the ultimate load in the similar burial configuration and loading condition is about 52% higher than the intact CMP.

Compared with the invert cut CMP which is equivalent to the complete loss of the invert, the renewal of the liner increases the CMP capacity almost to the intact CMP capacity with the application of only 0.25 in. thick liner.

Also considering the deflection limit criteria, it is seen that the invert cut CMP has been reduced by more than 10% vertically which is above the AASTHO'S deflection criteria at the ultimate load conditions. Among the rehabilitated pipe at the ultimate load condition only 1 in. thick liner was deflected by less than 5% vertically down. The other CMPs, intact and the lined CMP deflected by around 8%.

The H20 truck wheel is 10X20 in^2 and the designed service load for that wheel load is 16 kips without considering the factor of the safety. So, it is assumed that the for the double load pad size the design service load to be 32 kips. A comparison is made on the reduction in the vertical diameter of the CMP at 40 kips as shown in Table 4-20. The comparison shows, the decrease in the vertical diameter of the CMP is less than 5%, which is below the failure criteria limit established by AASTHO for the flexible pipes. Hence the liner is assumed to perform.

Description	Reduction in vertical diameter (in.)	Decrease in dia. (%)
Intact Pipe	2.1	3.5
Invert Cut Pipe	It could not take 40 kips of load	
0.25 in. thick liner	2.23	3.72
0.5 in. thick liner	1.49	2.48
1 in. thick liner	1.17	1.95

Table 4-20 Comparison of the reduction of the vertical diameter of the CMP at 40 kips of load

2. Earth Pressure Comparison

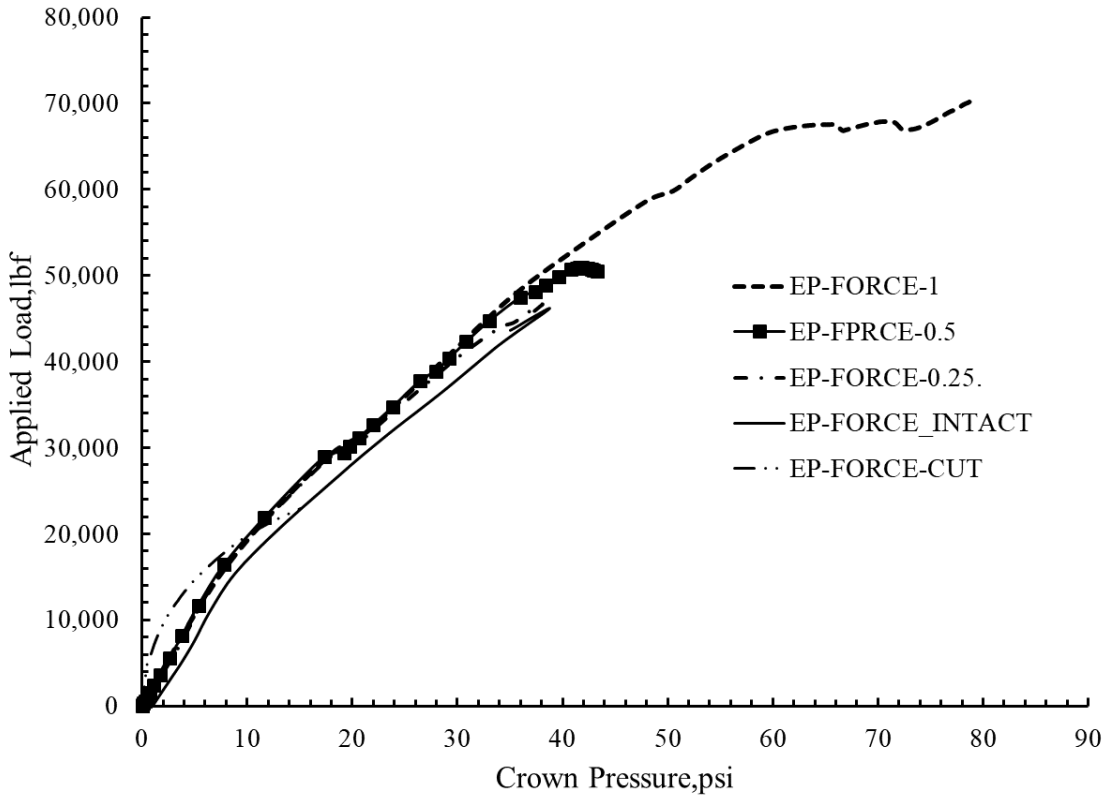

Figure 4-71 Comparison earth pressure at the crown with the applied load

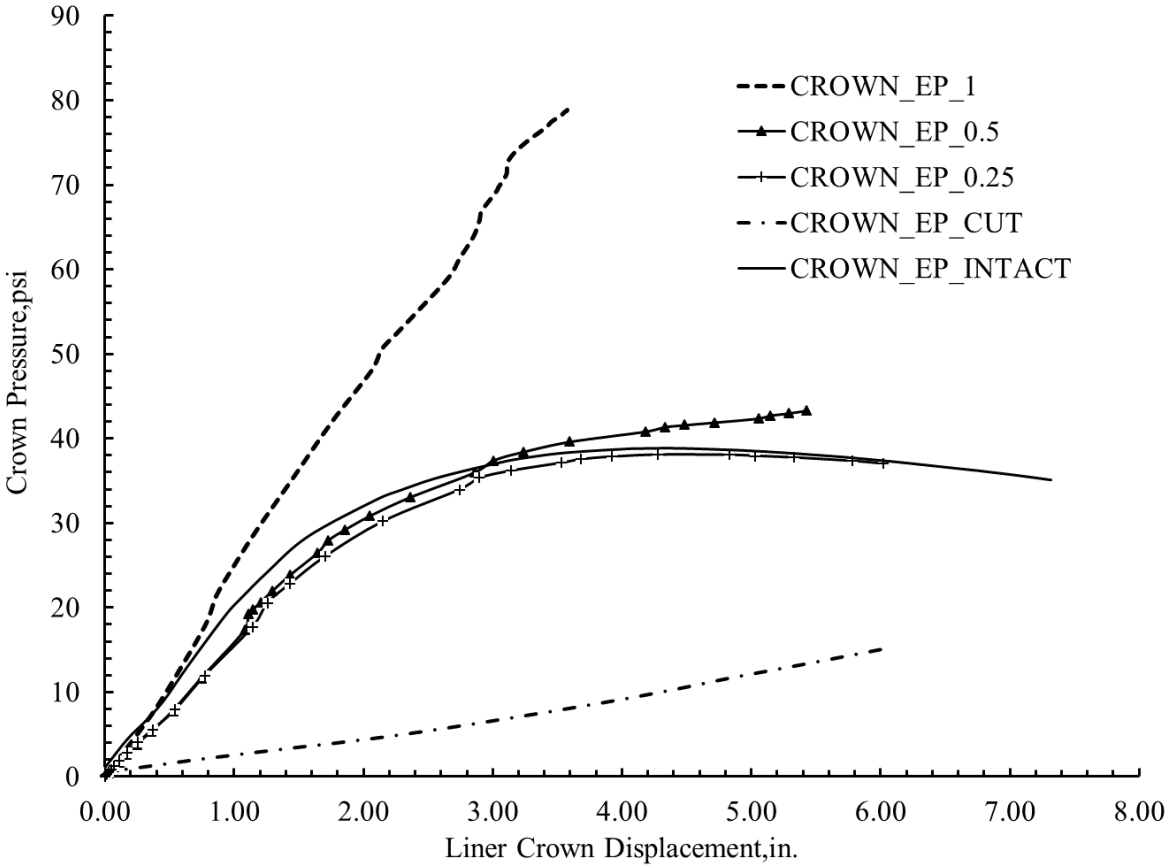

Figure 4-72 Comparison of earth pressure at the crown with the vertical displacement of the CMP

The comparison of the earth pressure at the crown with the applied force for the intact and rehabilitated CMPs shows that the earth pressure at the crown increases linearly with the applied force (Figure 4-71) in the FEM model. The comparison of the crown earth pressure and the deflection of the CMP showed a similar graph as in the applied load vs deflection of the CMP. Form the graph of the crown pressure vs. the deflection, Figure 4-72, in the CMP we can say that the 1 in. thick SAPL behaves as the rigid pipe while the behavior of the 0.25 in. and 0.5 in. thick CMP is more flexible.

5.0 Conclusions and Recommendations

5.1 Conclusions

The following conclusions are based on Finite Element analyses and comparison of the performance of the liners through FEM.

5.1.1 Finite Element Analysis Conclusion

1. Prediction of different parameters by the FE model showed reasonable accuracy for all cases except for the control test on invert cut CMP.
2. Intact pipe FEM results for load-displacement, earth pressure at the crown, strains, and bending moments compares well with the test results with a discrepancy of less than 5%.
3. For invert cut pipe FE model over predicts the load by about 145% before the invert edges meet. The FEM over-prediction may be due to its inability of soil model to replicate the collapse behavior of the soil during the invert removal process.
4. FE analysis of the liner predicts load -displacement, earth pressure curves, load at first crack, ultimate load, and strains well with less than 10% discrepancy.
5. FE analysis clearly shows the increase in the rigidity of the pipe with the increase in the thickness in the liner as we can see the reduction in the deformation of the liner at first plastic strain condition and ultimate load condition.
6. Prediction of the first crack with the first plastic strain matches the test results with less than 10% discrepancy.
7. From the FE analysis, it can be concluded that the FE model could be used for the parametric studies to better understand soil-CMP and liner performance.

5.1.2 Performance of the CMP after the application of the liner

1. The liner was able to increase the capacity of the invert removed CMP (whose capacity was decreased by more than 70% compared to the intact CMP) to more than 50% compared to the intact CMP capacity, when 1 in. thick liner was used.
2. The 0.25 in. thick liner was just enough for reestablishing the lost capacity of invert cut CMP.
3. The decrease in the vertical diameter of the rehabilitated CMP was less than 5% at 40 kips of load (double of the H20 load since we have used the double size of the H20 footprint) for all liner thicknesses. Hence the liner is assumed to perform well.
4. The increased rigidity due to the increase in liner thickness resulted in less deformation at the ultimate load.

5.2 Limitation of the FE model

1. The FE model was implicit and thus could not predict the load drop after the ultimate load.
2. Since the brittle polymeric material of the liner was modeled using the simple elastic-plastic model instead of crack models, a drop in load at first crack was not observed in the FE model.

5.3 Recommendation

1. To improve the FE model for the invert removed CMP, a different constitutive model of soil might achieve better results.
2. To understand and draw a concrete conclusion on the behavior of the liner, a series of parametric studies which include the different thickness is recommended in the future.
3. Since the behavior of the liner material is brittle, the crack model or damage plasticity model is recommended to get the crack and the drop-in load.
4. FE analysis with the varying depth and soil properties is also recommended to be done to understand the effect of the depth and different kinds of soil in the liner performance.

References

AASHTO. 2002. Standard Specifications for Highway Bridges. 17th ed. AASHTO.

ASTM. 2008. “ASTM D2412-11 - Standard Test Method for Determination of External Loading Characteristics of Plastic Pipe by Parallel-Plate Loading.” ASTM International. Vol. 08.04. https://doi.org/10.1520/D2412-11.2.

ASTM. 2015. “ASTM D2850-15 Standard Test Method for Unconsolidated-Undrained Triaxial Compression Test on Cohesive Soils.” ASTM International. Vol. D2850 − 15. https://doi.org/10.1520/D2850-15.2

ASTM. 2017. “ASTM D1633 Standard Test Methods for Compressive Strength of Molded Soil-Cement Cylinders.” ASTM International. https://doi.org/10.1520/D1633-00R07.combine.

ASTM. 2019. “ASTM C497-19 Standard Test Methods for Concrete Pipe , Concrete Box Section, Manhole Sections , or Tile.” ASTM International. https://doi.org/10.1520/C0497M-14.

American Concrete Pipe Association. (2009). *Highway Live Loads on Concrete Pipe.* American Concrete Pipe Assosciation.

Arizona DoT. (2014). *Arizona DOT turns to lining system for "No dig" culvert rehab.* Yuma District: Arizona DoT.

Arockiasamy, M., Chaalla, O., & Limpeteeprakarn, T. (2006). Full Scale Field Test on Flexible Pipes under Live Load Applications. *Journal of Peformance of constructed facilities*, 21-27.

Arulrajah, A., J.Piratheepan, M.M.Y.Ali, & Bo, M. (2012). Geotechnical Properties of the Recycled Concrete Aggregates in Pavement Subbase Applications. *ASTM*, 743-750.

Barbato, M., Bowman, M., & Herbin, A. (2010). *Performance Evaluation of the buried pipe installation.* Baton Rouge: Louisiana Department of Transportation and Development.

Campbell, A. (2018). *Three dimensional finite element modelling of the corroded corrugated metal pipe culverts.* Nova Scotia: Dalhousie University.

Campbell, A. R. (2018). *Three Dimensional Finite Element Modeling of corroded Corrugated Metal Pipe.* Halifax, Nova Scotia: Dalhousie University.

Chimauriya, H. R. (2019). *Laboratory Test and Finite Element Modeling of the Invert removed corrugated steel culvert buried under the shallow cover.* Arlington: University of Texas at Arlington.

Chimauriya, H. R. (2019). *Laboratory test and finite element modeling of the invert removed corrugated steel culvert buried under shallow cover.* Arlington: UTA.

Colorado DOT. (2014, June 5). CDOT HWY 52 CMP Rehabilitation. Hudson, Colorado, USA.

CUIRE. (2012). *Testing and Evaluation of statically loaded large diameter steel pipe with native backfill.* Arlington: Tarrant Regional Water Districy (TWRD).

CUIRE. (2018). *Structural Design Methodology for Spray Applied Pipe Liners in Gravity Storm Water Conveyance Conduits-3rd Quarterly Progress Report* . Ohio: ODOT.

Darabnoush Tehrani, A., Kohankar Kouchesfehani, Z., Najafi, M., & Kambell, N. (2019). Evaluation of filling the vallyes of corrugated metal pipes by trenchless spray applied pipe linings. *Pipelines, American Society of Civil Engineers*.

Darabnoush Tehrani, A., Kouchesfehani Kohankar, Z., Chimauriya Raj, H., Raut, S., Najafi, M., & Yu, X. (2020). Structural Evaluation of the Invert -Cut Circular and Arch Shape Corrugated Steel Pipes through Laboratory Testing. *Canadian Journal of Civil Engineering*.

El-Sawy, K. (2003). Three dimensional modeling of the soil-steel culverts under the effect of the truckloads. *Thin walled structures*, 747-768.

Elshmi, T. M. (2011). *Three dimensional non-linear analysis of deep corrugated steel culverts.* Ontario: Queen's University.

Elshmi, T. M., & Moore, I. D. (2014). Modeling the effects of the backfilling and soil compaction beside shallow buried pipes. *Journal of Pipeline system engineering*, 04013004(1-7).

Fuerst, P. R., & Robertson J., S. (2013). *Method of prediction of the flexible pipes.* U.S. Deparment of the Interior Bureau of Reclamation.

G. Katona, M. (2018). Culvert and Soil Structure Interaction. *Transportation Research Circular E-C230*, 13-21.

Garcia, D. B., & Moore, I. D. (2015). Pereformance of deteriorated corrugated steel culverts rehabilated with sprayed on cementitious liners subjected to surface loads. *Tunneling and Underground Space Technology*, 222-232.

Hartley, N. (2014). *Culvert Rehabilitation Guidance.* Maine: State of Maine Department of Transportation.

Katona, M. G. (2018). History of the Soil-Structure Interaction Models for the Buried Culverts. *Transportation Research Circular* (pp. 13-20). Transportation Research Board.

Mai, V. T., Hoult, N. A., & Moore, I. D. (2013). Effect of deterioration on the performance of the corrugated steel culverts. *Journal of Geotech, GeoEnvironment Engineering*, 04013007(1-11).

Mandli, C. (2017). *CIPP Lining Methods and Project.* Pennsylvania: Cleaner.

Masada, T. (2017). *Structural Benefit of the concrete paving of steel culverts inverts.* Ohio: Ohio Deparment of Transportation.

Matthews, J. C., Simicevic, J., & Kestler, M. A. (2012). *Decision Analysis guide for corrugated metal culvert rehabilitation and replacement using trenchless technology.* United States Department of Agriculture.

Meegoda, J. N. (2009). *Corrugated steel culvert pipe deterioration.* NewJersey: New Jersey DOT and FHWA.

Mohommad, N. (2016). *Pipeline Infrastructure renewal and asset management.* McGraw Hill Professional.

Muhannad, T. S. (2002). *The structural performance of the flexible pipes.* Ames,Iowa: Iowa State University.

Najafi, M. (2013). *Trenchless technology: Planning, equipment and Methods.* Chicago: McGraw Hill Professional.

NCHRP Synthesis 474. (1998). *Service life of culverts.* The national academic press.

Paredes, M. (2018). *Evaluation of spraywall structural coating.* Austin: NTPEP.

Regier, C., Moore, D. I., & Hoult, N. A. (2018). Remaining Strength of Deteriorated Corrugated Steel Culverts. *Journal of pipeline system engineering practice*, 04018002(1-15).

Rinker Materials. (1994, January). Info Series-Corrugated Metal pipe.

Sargand, S. M., Khoury, I., & Hussein, H. H. (2018). Load capacity of corrugated steel pipe with extreme corrosion under shallow cover. *Journal of Performance Construction* , 04018050(1-10).

Siavkumar Babu, G. A. (2010). Relaiability Analysis of Buried Flexible Pipe-Soil Systems. *Journal of Pipeline Systems Engineering and Practice*, 33-41.

SIMULIA. (2014). *ABAQUS User's Manual 6.11.* Dassaults System.

Sprayroq. (2020, 05 04). *Sprayroq.* Retrieved from Sprayroq: http://www.sprayroq.com

Taher, M. E., & Moore, I. D. (2011). Effect of wall corrosion and backfill erosion on the strength og deteriorated metal culverts. *International No-Dig 2011Conference* (pp. 3C-5-(1-10)). Berlin: International Society for Trenchless Technology.

Tenbusch, A. F., & Dorwart, B. (2009). *Failing Culverts- Geotechnical Perspective.* Tenbusch and Brierley Associates .

Webb, M. (1995). *Field studies of buried pipe behaviour during backfilling.* Amherst: University of Massachusets .

Winconsin DOT. (2018). *Culvert and Storm Sewer Rehabilitation and Replacement.* Wisconsin DoT.

Winconsin Transportation Bulletin. (2015). *Culverets-Proper use and installation.* Winconsin: Winconsin DOT.